Proceedings
of the
Seventeenth
International Tissue Elasticity Conference™

"In the cloud"
September 13 – 15, 2020

PROCEEDINGS

of the

Seventeenth International Tissue Elasticity Conference™

Virtual, hosted online by the Institute of Cancer Research
September 13-15, 2020

Table of Contents

QUESTIONS OR COMMENTS ARE WELCOME AT ANY TIME AT <secretariat@elasticityconference.org>

Some abstracts may have been edited by the reviewers for clarity of presentation.

Original Cover Photo by JC Bamber

FOREWORD

Dear Conference Delegate:

Welcome to the Seventeenth International Tissue Elasticity Conference™ (ITEC™), our first virtual conference. The months preceding ITEC 2020 have been the strangest ever, with the COVID-19 pandemic sweeping the world, many countries in "lockdown" (a new word in our vocabulary), travel severely inhibited, and life disrupted with, for example, working from home, closure of laboratories, preparing and delivering online courses, home schooling for children and the shielding of the vulnerable. This led to the postponement of ITEC from the planned date in the spring and, for a while, the decision hanging in the balance of whether to cancel ITEC 2020 entirely. We waited until an exceptionally late deadline to allow abstract submission, knowing that the disruption experienced by many would have made it difficult for them to have their work ready this year. Despite these difficulties, and thanks to all of you who have submitted abstracts, we are delighted to be able to run the conference.

Although it is relatively easy to attend a virtual conference, there are more opportunities than usual for delays in the sessions due to technical problems. Please, therefore, take advantage of the drop-in facility that we have provided to speakers to test their audio and visual connections and presentations. One of the greatest disadvantages of not being together physically, is the difficulty of exchanging information and enjoying each other's company. I therefore encourage you to take advantage of the many group sessions that we have scheduled in the program over refreshments and meals, and in the evenings. It is our hope that these will provide the time and opportunity for the friendly discussions and networking, for which ITEC is well known.

When Jonathan Ophir and Kevin Parker conceived this conference series they expressed the purpose as "to advance the field of measurement and imaging of the elastic attributes of soft tissues through tutorials and scientific presentations of the state of the art in the field, within a unique and unified forum that would bring together researchers from several countries and ultimately contribute to the rapid development and clinical introduction of this new medical imaging technology". Nineteen years on, there is now wide medical acceptance of the first generation of clinical elastography systems and a long history of scientific discovery and technical innovation. In the past, ITEC tended to emphasise ultrasound as the underlying imaging modality for extracting biomechanical information. This year, our abstract submission forms were enhanced to reflect the reality that tissue elasticity measurement and imaging is a truly multimodal field that spans resolutions from subcellular to the macroscopic, with applications that include fundamental mechanobiology, preclinical research and clinical applications. Our 2020 program reflects this, making ITEC an exceptional opportunity for cross-disciplinary exchange of ideas and knowledge.

We are deeply saddened by the death of our dear friend and colleague Karen Ophir, shown here, who passed away on 5th August 2020. Karen and her husband Jonathan, who died in 2017, were founding members of ITEC, leaders in the field of ultrasound strain imaging, and coined the term elastography. For ITEC, Karen handled meticulously all the administration for 11 years, including taking personal care of each delegate and exhibitor, and editing the conference book. Today, we still use her methods and templates, and we try to emulate her personal approach. Karen is survived by her son Alex, daughter-in-law Angela and their three children, Marcus, Evan and Cohen. They are in our thoughts and prayers.

Many volunteers and colleagues have helped to bring about this conference, especially our conference secretary, Cheryl Taylor. Please join me in thanking Cheryl for working tirelessly, once again, to make the conference a success. It is a pleasure also to acknowledge contributions from other staff at the Institute of Cancer Research, especially Nigel Bush for providing audio-visual support to delegates, Jo Hows, Alan Hill and Liam Blake for assistance in legal and financial matters, and Richard Buckner, T'Laina Johnson and James Alexander for helping to set up webinars. We are particularly grateful to Stefan Catheline for presenting a tutorial on Passive Elastography, and express huge thanks to all helpers, reviewers, session chairs, award judges and contributors, without whom the conference could not maintain the high standards for which it has become known.

ITEC must evolve if it is to serve the needs of researchers and practitioners of elastometry and elastography. We would be hugely grateful if you would complete the feedback forms in these Proceedings or, if you prefer, speak directly to me or Cheryl.

May your research be inspired by the presentations and discussions during the Seventeenth ITEC, and may you make new friends, establish productive collaborations and renew old acquaintances.

Jeffrey Bamber
General Conference Organizer, ITEC
Online, September 13-16, 2020

CONFERENCE–AT–A–GLANCE

Seventeenth International Tissue Elasticity Conference™
Virtual, hosted online by the Institute of Cancer Research
September 13–15, 2020, EDT (EST+1)

Sunday, September 13 9:00A – 7:30P

9:00A – 12:00P Set Up: Oral Presenters test presentations
9:00A – 5:00P *Registration Desk Open*
2:00P – 5:30P Session EEX: Equipment Exhibit (during breaks & Reception)
2:30P – 3:45P Session SAS-1: Oral Presentations of Finalists for Student Awards Session
3:45P – 4:15P *Group Coffee Break*
4:15P – 5:30P Session SAS-2: Oral Presentations of Finalists for Student Awards Session
5:30P – 7:30P *Group Chat/meet the professor*

Monday, September 14 8:30A – 7:05P

8:30A – 5:30P *Registration Desk Open*
8:30A – 4:30P Session EEX: Equipment Exhibit
8:45A – 9:00A *Opening Remarks*
9:00A – 10:00A Session TUT: Tutorial
10:00A – 11:15A Session USE-1: Ultrasound Elasticity Imaging - I
11:15A – 11:45A *Group Coffee Break*
11:45A – 12:40P Session MPT: Mechanical Properties of Tissues
12:40P – 2:00P *Group Lunch*
2:00P – 3:35P Session MRE: Magnetic Resonance Elasticity Imaging
3:35P – 4:05P *Group Coffee Break*
4:05P – 4:40P Session MEI: Multi-modality Elasticity Imaging
4:45P – 5:00P Session INS: Instrumentation including Phantoms
5:05P – 7:05P *Group Chat/meet the professor*

Tuesday, September 15 8:30A – 7:30P

8:30A – 5:30P *Registration Desk Open*
8:45A – 5:30P Session EEX: Equipment Exhibit
9:00A – 9:40A Session OEI: Optical Elasticity Imaging
9:40A – 10:00A Session MMI: Micro-elasticity Measurement or Imaging
10:00A – 10:55A Session SIP: Signal and Image Processing
10:55A – 11:25A *Group Coffee Break*
11:25A – 12:05P Session MIP: Methods for Imaging Elastic Tissue Properties
12:05P – 12:40P Session MSE: Musculoskeletal Elasticity
12:40P – 2:00P *Group Lunch*
2:00P – 3:15P Session USE-2: Ultrasound Elasticity Imaging - II
3:15P – 3:45P Group Coffee Break
3:45P – 5:00P Session USE-3: Ultrasound Elasticity Imaging - III
5:00P – 5:15P *Group Photo*
5:15P – 7:30P *Group Chat/meet the professor*

PROGRAM

Seventeenth International Tissue Elasticity Conference™

Virtual, hosted online by the Institute of Cancer Research

September 13-15, 2020

Sunday, September 13 9:00A – 7:30P, EDT (EST+1)

9:00A – 12:00P Presentation & Exhibit Set Up
Oral Presenters test presentations

9:00A – 5:00P
Registration Desk Open

2:00A – 5:30P Session EEX: Equipment Exhibit

Sunday 2:30P – 3:45P
Session SAS: Oral Presentations of Finalists for Student Awards Session

Chair: JC Bamber, UK

Page No.

2:30P – 2:45P

005 EX-VIVO STUDY OF MYOCARDIAL DEFORMATION IMAGING USING MULTI-PERSPECTIVE ULTRAFAST ULTRASOUND.. 16

Peilu Liu[1], Hein de Hoop[1], Marloes Sjoerdsma[1], Hans-Martin Schwab[1], Richard Lopata[1].*

[1]Eindhoven University of Technology, Eindhoven, North Brabant, THE NETHERLANDS.

2:50P – 3:05P

009 DEMONSTRATION OF ULTRASONIC ROTATIONAL 3D SWE INDUCED COMPLEX SHEAR WAVE PATTERNS IN SKELETAL MUSCLE IN VIVO. 17

AE Knight[1], CA Trutna[1], LD Hobson-Webb[2], NC Rouze[1], ML Palmeri[1], AF Caenen[3,4], KR Nightingale[1]*

[1]Duke University, Durham, NC, USA; [2]Duke University Health System, Durham, NC, USA; [3]Ghent University, Ghent, BELGIUM; [4]Catholic University of Leuven, Leuven, BELGIUM.

3:10P – 3:25P

019 3D MULTIFREQUENCY LIVER SHEAR WAVE ABSOLUTE VIBRO-ELASTOGRAPHY WITH AN XMATRIX ARRAY – PRELIMINARY IN-VIVO VALIDATION. 18

Qi Zeng[1], Mohammad Honarvar[1], Julio Lobo[1], Caitlin Schneider[1], Gerard Harrison[2], Changhong Hu[2],*

[1]Duke University, Durham, NC, USA; [2]Duke University Health System, Durham, NC, USA; [3]Ghent University, Ghent, BELGIUM; [4]Catholic University of Leuven, Leuven, BELGIUM.

3:30P – 3:45P

024 DETECTION OF CEREBRAL STIFFNESS BEFORE AND AFTER LUMBAR PUNCTURE BY NONINVASIVE TIME-HARMONIC ULTRASOUND ELASTOGRAPHY. 19

B Kreft[1], M Shahryari[1], J Braun[1], I Sack[1], K-J Streitberger[1], H Tzschätzsch[1].*

[1] Charité – Universitätsmedizin, Berlin, Berlin, GERMANY.

3:45P – 4:15P
GROUP COFFEE BREAK

(Session SAS-1 continues on next page)

(Session SAS-1 continued from previous page)

Sunday 4:15P – 5:30P
Session SAS: Oral Presentations of Finalists for Student Awards Session

Chair: H Rivaz, USA

Page No.

4:15P – 4:30P

025 DESIGN OF A "SMART" GRASPER ROBOT FOR TISSUE CLASSIFICATION. 20

Y. Sosnovskaya[1], J. M. Jaime[1], W. Premvuti[1], B. Hannaford[1].*
[1]University of Washington, Seattle, WA, USA.

4:35P – 4:50P

030 THREE-DIMENSIONAL IMAGING OF CELL AND EXTRACELLULAR MATRIX ELASTICITY USING QUANTITATIVE MICRO-ELASTOGRAPHY. 21

Matt S. Hepburn, [1,2] Jiayue Li,[1,2,4] Alireza Mowla,[1,2] Yu Suk Choi[3] and Brendan F. Kennedy[1,2,4]*
[1]BRITElab, Harry Perkins Institute of Medical Research, QEII Medical Centre, Nedlands, Western Australia, Australia and Centre for Medical Research, The University of Western Australia, Crawley, Western Australia
[2]Department of Electrical, Electronic & Computer Engineering, School of Engineering, The University of Western Australia, Perth, Western Australia
[3]School of Human Sciences, The University of Western Australia, 35 Stirling Highway, Crawley, Western Australia
[4]Australian Research Council Centre for Personalised Therapeutics Technologies, Australia

4:55P – 5:10P

031 CAMERA-BASED OPTICAL PALPATION TOWARDS *IN VIVO* BREAST CANCER ASSESSMENT. 22

RW Sanderson[1,2,], Q Fang[1,2], A Curatolo[1,2,3], W Adams[1,2], DD Lakhiani[1,2], HM Ismail[1,2], KY Foo[1,2], BF Dessauvagie[2,4], B Latham[4,5], C Yeomans[4], CM Saunders[2,6,7] and BF Kennedy[1,2,8].*
[1]BRITElab, Harry Perkins Institute of Medical Research, QEII Medical Centre, Nedlands and Centre for Medical Research, The University of Western Australia, Perth, Western Australia, 6009, AUSTRALIA;
[2]Department of Electrical, Electronic & Computer Engineering, School of Engineering, The University of Western Australia, Crawley, Western Australia, 6009, AUSTRALIA;
[3]Currently with Visual Optics and Biophotonics Group, Instituto de Óptica "Daza de Valdés", Consejo Superior de Investigaciones Cientificas (IO, CSIC), C/Serrano, 121, Madrid, SPAIN;
[4]PathWest, Fiona Stanley Hospital, 11 Robin Warren Drive, Murdoch, Western Australia, 6150, AUSTRALIA;
[5]Division of Pathology and Laboratory medicine, Medical School, The University of Western Australia, Crawley, Western Australia, 6009, AUSTRALIA;
[6]The University of Notre Dame, Fremantle, Western Australia, 6160, AUSTRALIA;
[7]Division of Surgery, Medical School, The University of Western Australia, Crawley, Western Australia, 6009, AUSTRALIA;
[8]Breast Centre, Fiona Stanley Hospital, 11 Robin Warren Drive, Murdoch, Western Australia, 6150, AUSTRALIA;
[9]Breast Clinic, Royal Perth Hospital, 197 Wellington Street, Perth, Western Australia, 6000, AUSTRALIA;
[10]Australian Research Council Centre for Personalised Therapeutics Technologies, AUSTRALIA.

5:15P – 5:30P

032 Hb-OCE: CORNEAL BIOMECHANICAL RESPONSE TO HEARTBEAT PULSATION. 23

Achuth Nair[1], Manmohan Singh[1], Salavat Aglyamov[1], and Kirill V. Larin[1],*
[1]University of Houston, Houston, TX, USA.

5:30P – 7:30P

GROUP CHAT / MEET THE PROFESSOR

8:30A – 5:30P
Registration Desk Open
8:30A – 4:30P Session EEX: Equipment Exhibit

Monday 8:45A – 9:00A
OPENING REMARKS
JC Bamber

Monday 9:00A – 10:00A
Session TUT: Tutorial
Chair: JC Bamber, UK

Page No.

9:00A – 9:40A
007 WHAT TO EXPECT FROM PASSIVE ELASTOGRAPHY? 24
Stefan Catheline*
University of Lyon, INSERM LabTau U1032, Lyon, FRANCE.

9:40A – 9:55A DISCUSSION

Monday 10:00A – 11:15A
Session USE-1: Ultrasound Elasticity Imaging - I
Chair: S Aglyamov, USA

Page No.

10:00A – 10:15A
033 HIFU LESION DETECTION IN PROSTATE CANCER USING PASSIVE ELASTOGRAPHY BASED ON CONVENTIONAL B-MODE IMAGES. 25
T Payen[1], S Crouzet[1], N Guillen[2], JY Chapelon[1], C Lafon[1], S Catheline[1].*
[1]LabTau, U1032 INSERM, Lyon, France ; [2]EDAP-TMS, Vaulx-en-Velin, France.

10:20A – 10:35A
004 COMPARISON OF PLANE WAVE IMAGING AND FOCUSED SINGLE LINE TRANSMIT ECHOGRAPHY FOR DETERMINATION OF THE PULSE WAVE VELOCITY IN VIVO. 26
Melissa GM van de Steeg[1,2], Stein Fekkes[1], Anne ECM Saris[1], Hendrik HG Hansen[1], Chris L de Korte[1]. [1]Radboud university medical center, Nijmegen, THE NETHERLANDS; [2]Catharina Hospital, Eindhoven, THE NETHERLANDS.*

10:40A – 10:55A
039 ULTRASOUND VIBRATIONAL SHEAR WAVE ELASTOGRAPHY IN PRECLINICAL HUMAN XENOGRAFT TUMOR MODELS. 27
J Civale[1], JC Bamber[1], EJ Harris[1].*
[1]The Institute of Cancer Research, London, UNITED KINGDOM.

11:00A – 11:15A

040 SHEAR WAVE SPEED ESTIMATION WITH A DIRECTIONAL DETECTOR IN PRECLINICAL HUMAN XENOGRAFT TUMOR MODEL. 28
J Civale[1], JC Bamber[1], EJ Harris[1].*
[1]The Institute of Cancer Research, London, UNITED KINGDOM.

11:15A – 11:45A
GROUP COFFEE BREAK

Monday 11:45A – 12:40P

Session MPT: Mechanical Properties in Tissues

Chair: E Harris, UK

Page No.

11:45A – 12:00P

034 INCORPORATING SECOND ORDER REGULARIZATION IN ULTRASOUND ELASTOGRAPHY. 29
Md Ashikuzzaman[1], Ali Sadeghi-Naini[2], Abbas Samani[3], Hassan Rivaz[1]*
[1]Concordia University, Montreal, QC, CANADA; [2]York University, Toronto, ON, CANADA; [3]The University of WEDTern Ontario, London, ON, CANADA.

12:05P – 12:20P

035 BIOMECHANICAL AND STRUCTURAL CHARACTERIZATION OF PERIPHERAL NERVE TISSUE DURING DEVELOPMENT. 30
G Rosso[1,2], J Guck[1].*
[1]Max Planck Institute for the Science of Light & Max-Planck-Zentrum für Physik und Medizin, Erlangen, GERMANY; [2]Institute of Physiology II, University of Münster, Münster, GERMANY.

12:25P – 12:40P

036 TOWARDS UNDERSTANDING THE MECHANICAL FINGERPRINT OF REGENERATING SPINAL CORD TISSUE. 31
S Möllmert[1], M Kharlamova[2], R Schlüßler[3], J Guck [1].*
[1]Max Planck Institute for the Science of Light and Max-Planck-Zentrum für Physik und Medizin, Erlangen, GERMANY; [2]Universität Tübingen, Tübingen, GERMANY; [3]Technische Universität Dresden, Dresden, GERMANY.

12:40P – 2:00P

GROUP LUNCH

Monday 2:00P – 3:35P
Session MRE: Magnetic Resonance Elasticity Imaging

Chair: S Catheline

Page No.

2:00P – 2:15P

008 SUPER-RESOLUTION MAGNETIC RESONANCE ELASTOGRAPHY OF THE HUMAN BRAIN USING MULTIPLE FREQUENCIES. 32
AT Anderson[1,2], AM Cerjanic[1], BP Sutton[1], EEW Van Houten[3].*
[1]University of Illinois at Urbana-Champaign, Urbana, IL, USA; [2]Carle Foundation Hospital, Urbana, IL, USA; [3]Université de Sherbrooke, Sherbrooke, QC, CANADA.

2:20P – 2:35P

013 A SHEAR-ONLY SELECTIVE WAVE FIELD FILTER FOR IMPROVED SHEAR MODULUS ESTIMATION IN ELASTOGRAPHY. 33
T Deruelle[1], S. Catheline[1], O. Rouvière[2], R Souchon[1].*
[1]INSERM, Université Lyon 1, Lyon, FRANCE ; [2]Hospices Civils de Lyon, Lyon, FRANCE.

2:40P – 2:55P

020 ANATOMY GUIDED TOTAL VARIATION FOR ELASTICITY RECONSTRUCTION WITH BI-CONVEX ALTERNATING DIRECTION METHOD OF MULTIPLIERS. 34
SK Mohammed[1], M Honarvar[1], P Kozlowski[2], SE Salcudean[1].*
[1] University of British Columbia, Vancouver, BC, Canada; [2] University of British Columbia, Vancouver, BC, Canada.

(Session MRE continues on next page)

(Session MRE continued from previous page)

3:00P – 3:15P

026 AXIAL AND TORSIONAL ACTUATION FOR MAGNETIC RESONANCE ELASTOGRAPHY OF ANISOTROPIC SAMPLES. 35

Martina Guidetti[1], Chiara Gambacorta[1], Dieter Klatt[1], Thomas J. Royston[1].*
[1]University of Illinois at Chicago, Chicago, Illinois, USA.

3:20P – 3:35P

028 MULTIFREQUENCY MR ELASTOGRAPHY REVEALS DIFFERENCES IN MURINE CORTICAL AND HIPPOCAMPAL MECHANICAL HETEROGENEITY. 36

Shreyan Majumdar[1], Dieter Klatt[1].*
[1]University of Illinois at Chicago, Chicago, Illinois, USA.

3:35P – 4:05P

GROUP COFFEE BREAK

Monday 4:05P – 4:40P
Session MEI: Multi-modality Elasticity Imaging

Chair: H Rivaz, USA

Page No.

4:05P – 4:20P

021 A COMPREHENSIVE LIVER VISCOELASTIC CHARACTERIZATION; ASSESSMENT OF SHEAR WAVE (GROUP AND PHASE) VELOCITY, ATTENUATION, DISPERSION, AND THEIR RELATIONSHIP UNDER A POWER LAW MODEL. 37

J Ormachea[1], KJ Parker[1].*
[1]University of RochEDTer, RochEDTer, NY, USA.

4:25P – 4:40P

038 ULTRASOUND ECHO AND PHOTOACOUSTIC VECTORAL DOPPLER IMAGING FOR HUMAN IN VIVO SOFT TISSUE AND BLOOD. 38

Chikayoshi Sumi1[1], Ryo Nakagawa[1], Kanta Ueno[1]*
[1]Sophia University, 7-1, Kioi-cho, Chiyoda-ku, Tokyo, JAPAN.

Monday 4:45P – 5:00P
Session INS: Instrumentation including Phantoms

Chair: H Rivaz, USA

Page No.

4:45P – 5:00P

023 A DISPERSIVE ELASTOGRAPHY PHANTOM WITH VISCOELASTIC PROPERTIES SIMILAR TO HEALTHY LIVER. 39

Anna Morr[1], Helge Herthum[1], Felix Schrank[1], Steffen Görner[1], Jürgen Braun[2], Ingolf Sack[1], Heiko Tzschätzsch[1].*
[1]Department of Radiology, Charité – Universitätsmedizin Berlin, Berlin, GERMANY;
[2]Institut of Medical Informatics, Charité – Universitätsmedizin Berlin, Berlin, GERMANY.

5:05P – 7:05P

GROUP CHAT / MEET THE PROFESSOR

Tuesday, September 15 8:30A – 7:30P, EDT (EST+1)

8:30A – 5:30P
Registration Desk Open
8:45A – 5:30P **Session EEX: Equipment Exhibit**

Tuesday 9:00A – 9:40A
Session OEI: Optical Elasticity Imaging
Chair: B Kennedy, AUSTRALIA

Page No.

9:00A – 9:15A

010 OPTICAL COHERENCE ELASTOGRAPHY AND BRILLOUIN SPECTROSCOPY FOR BIOMECHANICAL MAPPING OF TISSUES. 40
*KV Larin.**
University of Houston, Houston, TX, USA.

9:20A – 9:35A

029 WAVE-BASED OPTICAL COHERENCE ELASTOGRAPHY OF THE ANTERIOR EYE: EXPLORING THE BIOMECHANICS OF LIMBUS. 41
Fernando Zvietcovich[1], Achuth Nair[1], Manmohan Singh[1], Salavat R. Aglyamov[2], Michael D. Twa[3], and Kirill V. Larin[1]*
[1]Department of Biomedical Engineering, [2]Department of Mechanical Engineering, [3]College of Optometry, University of Houston, Houston, Texas, USA.

Tuesday 9:40A – 10:00A
Session MMI: Micro-elasticity Measurement or Imaging
Chair: B Kennedy, AUSTRALIA

Page No.

9:40A – 9:55A

001 COMPLEX ELASTIC WAVE PROPAGATION IN MICRO-ELASTOGRAPHY. 42
Gabrielle Laloy-Borgna[1], Ali Zorgani[1], Pol Grasland-Mongrain[2], Stefan Catheline[1].*
[1]LabTAU, INSERM, Centre Léon Bérard, Université Lyon 1, Lyon, FRANCE;
[2]Laboratoire de Physique, Ecole Normale Supérieure de Lyon, CNRS UMR5672, Lyon, FRANCE.

Tuesday 10:00A – 10:55A
Session SIP: Signal and Image Processing
Chair: K Larin, USA

Page No.

10:00A – 10:15A

015 ULTRASOUND IMAGE REGISTRATION USING MOMENTUM EQUATION CONSTRAINTS. 43
OA Babaniyi[1], MS Richards[1].*
[1]RochEDTer Institute of Technology, RochEDTer, NY, USA.

10:20A – 10:35A

017 FRAME RATE OPTIMIZATION OF ELECTROMECHANICAL WAVE IMAGING FOR THE MEASUREMENT OF ELECTROMECHANICAL ACTIVATION DURING SINUS RHYTHM. 44
M Tourni[1], L Melki[1], R Weber[1], EE Konofagou[1].*
[1]Columbia University, New York, NY, USA;

10:40A – 10:55A

037 ULTRASONIC VECTORAL OBSERVATION OF LOW FREQUENCY MECHANICAL WAVE PROPAGATION AND INVERSE PROBLEM APPROACH ON SOFT TISSUE PHANTOM. 45
Chikayoshi Sumi1[1], Yusuke Kobayashi[1]*
[1]Sophia University, 7-1, Kioi-cho, Chiyoda-ku, Tokyo 102-8554, JAPAN.

10:55A – 11:25A
GROUP COFFEE BREAK

Tuesday 11:25A – 12:05P
Session MIP: Methods for Imaging Elastic Tissue Properties

Chair: R Souchon, FRANCE

Page No.

11:25A – 11:40A

002 REAL-TIME AND HIGH QUALITY ULTRASOUND ELASTOGRAPHY USING CONVOLUTIONAL NEURAL NETWORK BY INCORPORATING ANALYTIC SIGNAL. 46
A K.Z Tehrani[1], M Amiri[1], H Rivaz[1]*
[1]Concordia University, Montreal, QC, CANADA.

11:45A – 12:00P

006 MULTIPERSPECTIVE 2-D ULTRASOUND STRAIN IMAGING OF PORCINE AORTAS IN AN ABDOMEN PHANTOM. 47
Hein de Hoop[1], Niels Petterson[1], Marc van Sambeek[1,2], Frans van de Vosse[1], Richard Lopata[1.]*
[1]Eindhoven University of Technology, Eindhoven, North Brabant, The Netherlands; [2]Catharina Hospital Eindhoven, Eindhoven, THE NETHERLANDS.

Tuesday 12:05P – 12:40P
Session MSE: Musculoskeletal Elasticity

Chair: R Souchon, FRANCE

Page No.

12:05P – 12:20P

041 DESIGN OF AN ULTRASOUND PROBE HOLDER TO SECURE THE PROBE FOR REAL TIME IMAGE CAPTURE DURING DYNAMIC LOADING OF THE HUMAN ACHILLES TENDON; VALIDATION STUDY. 48
Gamalendira Shivapatham [1], Wing Keung Cheung [1], Dylan Morrissey [1], Jeffrey C. Bamber [2], Hazel R.C. Screen[1].*
[1]Queen Mary University of London, London, UK; [2] Institute of Cancer Research and Royal Marsden NHS Foundation Trust, London, UK.

12:25P – 12:40P

042 TOWARDS THE DEVELOPMENT OF SPECKLE TRACKING FOR VISUALIZING SLIP PLANES IN THE HUMAN ACHILLES TENDON DURING DYNAMIC LOADING; PRELIMINARY RESULTS. 49
Gamalendira Shivapatham [1], Wing Keung Cheung [1], Dylan Morrissey [1], Hazel R.C. Screen[1,] Jeffrey C. Bamber [2].*
[1]Queen Mary University of London, London, UK; [2] Institute of Cancer Research and Royal Marsden NHS Foundation Trust, London, UK.

12:40P – 2:00P
GROUP LUNCH

Tuesday 2:00P – 3:15P
Session USE–2: Ultrasound Elasticity Imaging – II

Chair: E Harris, UK

Page No.

2:00P – 2:15P

012 SAFETY ANALYSIS OF SHEAR WAVE ELASTOGRAPHY FOR DYNAMIC CAROTID PLAQUE ELASTICITY ASSESSMENT. 50
AD Rog[1,2], JT Pruijssen[1], JMK de Bakker[1], CL de Korte[1,3], HHG Hansen[1].*
[1]Radboud University Medical Center, Nijmegen, THE NETHERLANDS; [2]Elisabeth-TweEDTeden Ziekenhuis, Tilburg, THE NETHERLANDS; [3]University of Twente, Enschede, THE NETHERLANDS.

(Session USE–2 continues on next page)

(Session USE–2 continued from previous page)

2:15P – 2:35P

022 ESTIMATION OF SHEAR WAVE ATTENUATION USING THE REVERBERANT SHEAR WAVE ELASTOGRAPHY (R-SWE) APPROACH. 51

J Ormachea[1], Richard G. Barr [2], KJ Parker[1].*
[1]University of RochEDTer, RochEDTer, NY, USA. [2]Northeastern Ohio Medical University and Southwoods Imaging, Youngstown, OH, USA.

2:40P – 2:55P

016 HIGH FRAME RATE PULSE WAVE IMAGING IN STROKE PATIENTS IN VIVO. 52

Grigorios M. Karageorgos[1], Changhee Lee[1], Salah Mahmoudi[1], Rachel Weber[1], Randolph Marshall[2], Joshua Z. Willey[2], Eliza Miller[2] and Elisa E. Konofagou[1,3].*
[1] Department of Biomedical Engineering, Columbia University, New York, USA;
[2] Department of Neurology, Columbia University Medical Center, New York, USA;
[3] Department of Radiology, Columbia University Medical Center, New York, USA.

3:00P – 3:15P

011 MULTI-PLANE ULTRASOUND ELASTOGRAPHY OF HEALTHY ABDOMINAL AORTAS IN VIVO. 53

Larissa C. Jansen[1,2], Hans-Martin Schwab[1], Marc R.H.M. van Sambeek[1,2], Frans N. van de Vosse[1], Richard G.P. Lopata[1].*
[1]Eindhoven University of Technology, Eindhoven, Noord-Brabant, THE NETHERLANDS;
[2]Catharina Ziekenhuis Eindhoven, Eindhoven, Noord-Brabant, THE NETHERLANDS.

3:15P – 3:45P

GROUP COFFEE BREAK

Tuesday 3:45P – 5:00P

Session USE–3: Ultrasound Elasticity Imaging – III

Chair: J Bamber, UK

Page No.

3:45P – 4:00P

003 ROBUST DATA FUNCTION IN GLOBAL ULTRASOUND ELASTOGRAPHY. 54

Md Ashikuzzaman[1], Hassan Rivaz[1]*
[1]Concordia University, Montreal, QC, CANADA.

4:05P – 4:20P

014 LIVER ELASTOGRAPHY REVISITED: CAN PORO-ELASTIC THEORY EXPLAIN IN VIVO DISPERSION? 55

Johannes Aichele[1□], Stefan Catheline[1].
[1]INSERM - University of Lyon, Lyon, FRANCE.

4:25P – 4:40P

018 AMPLITUDE-MODULATION FREQUENCY OPTIMIZATION FOR HARMONIC MOTION IMAGING (HMI). 56

N Saharkhiz[1], HAS Kamimura[1], MM Hossain[1], EE Konofagou[1].*
[1]Columbia University, New York, NY, USA; [2]Columbia University Medical Center, New York, NY, USA.

Tuesday 5:00P – 5:15P

Group Photo

5:15P – 7:30P

GROUP CHAT / MEET THE PROFESSOR

Verasonics, Inc.
Redmond, WA, USA.

AUTHOR INDEX

ABSTRACTS

Seventeenth International Tissue Elasticity Conference

Virtual, hosted online at the Institute of Cancer Research September 13-15, 2020

005 **EX-VIVO STUDY OF MYOCARDIAL DEFORMATION IMAGING USING MULTI-PERSPECTIVE ULTRAFAST ULTRASOUND.**

Peilu Liu[1], Hein de Hoop[1], Marloes Sjoerdsma[1], Hans-Martin Schwab[1], Richard Lopata[1]*
[1]Eindhoven University of Technology, Eindhoven, North Brabant, the Netherlands

Background: Speckle tracking echocardiography (STE) has proven to be more robust than tissue Doppler imaging (TDI) to estimate myocardial deformation, given it can be performed on 2D B-mode images [1]. A single probe implementation of STE, however, can only measure the strain accurately when the direction of myocardial deformation is parallel to the axial direction [2]. Because of the complexity of the heart and the irregularity of myocardial deformation, it is difficult to measure all the strains precisely when only using one probe, even at a high frame rate.

Aims: Therefore, we proposed a multi-probe 2D ultrasound (US) cardiac strain imaging system followed by a novel method to automatically compound strain data acquired simultaneously from the dual transducers. The aim is to improve the measurement of myocardial deformation in all directions within a 2D image plane.

Methods: In an ex-vivo beating porcine heart experiment (PhysioHeart, LifeTec, NL), parasternal long axis, short axis and four-chamber apical views of the left ventricle were acquired with two phased array probes (P4-2V, Verasonics). The dual probes were attached to an arch that ensures they were exactly in the same imaging plane, and allows to adjust the relative angle between the probes. For the long view imaging plane, probe 1 was positioned at four-chamber apical view and probe 2 was rotated in steps of 15˚ from parasternal long axis view to apical view. For the short view imaging plane, probe 1 was positioned to acquire the parasternal short axis view while the second probe was rotated every 15˚ from 30˚ to 75˚ with respect to the first probe. All US data were acquired at a frame rate of 170 FPS, using spherical wave imaging under 11 angles (Fig. 1). RF-based strain imaging was performed using the same segmentation mesh for both datasets after automatic registration of the dual probe image sets. Global and regional strains of the two probes were calculated respectively. A strain compounding mask was created to automatically fuse the optimal strain data from both probes.

Results: In the short axis view, compounded radial (RS) circumferential (CS) strains have all been improved in every different relative angle compared to single probes. For the largest angle (75˚), mean drift error MDE (RS: - 38.7%, CS: -35.3%) and strain variability (SV) (RS: -36.8%, CS: -37.1%) drop significantly, and strain curves reveal less noise for each region. Long axis view strains show similar results.

Conclusions: We introduced a multi-probe 2D ultrafast US strain compounding system, which can improve all the strains estimation in the imaging plane. Future work will include 3D multi-probe imaging and first-in-men studies.

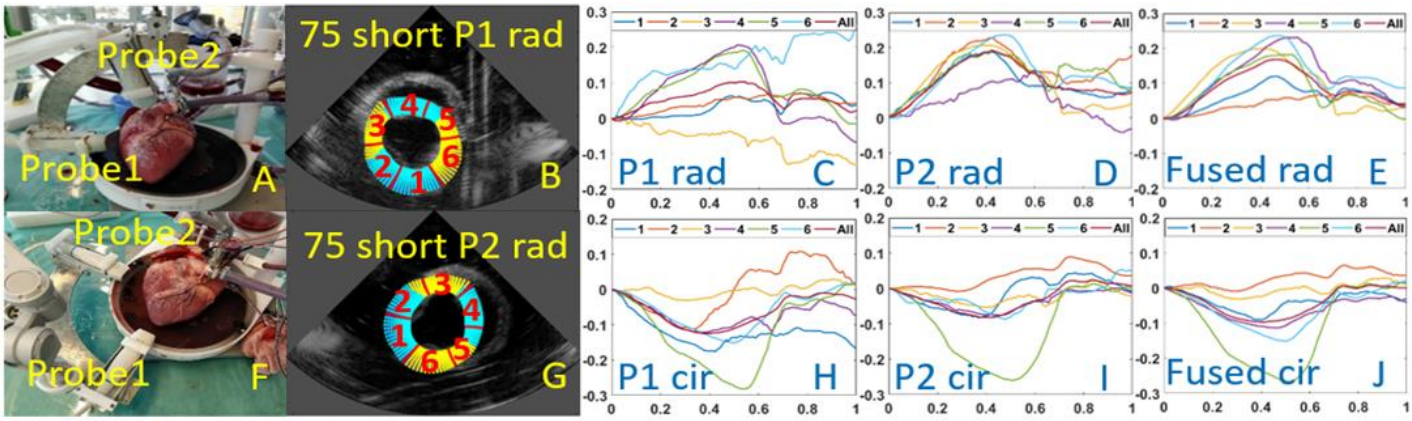

Fig.1: (A)(F) Physioheart experiment and dual probe setup of short axis view and long axis view respectively; (B)(G) Masks of radial strain with 75˚ relative angle in short axis view of the two probes respectively (cyan and yellow mean strain taken from Probe 1 and Probe 2 respectively); (C)(D)(E) Global and regional radial strain curves with 75 relative angle of the two probes in short axis view; (H)(I)(J) Global and regional circumferential strain curves with 75 relative angle of the two probes in short axis view.

Acknowledgements: This work is part of the MUSE project, which has received funding from the European Research Council (ERC) under the European Union's Horizon 2020 research and innovation program (ERC starting grant 757958).

References:

[1]. Shah, A.M. *Circulation* 125.2 (2012): e244-e248.
[2]. Hansen, H.H.G. *Med. Imaging IEEE Trans. On* 28, 872-880 (2009).

* *indicates Presenter*

009 **DEMONSTRATION OF ULTRASONIC ROTATIONAL 3D SWE INDUCED COMPLEX SHEAR WAVE PATTERNS IN SKELETAL MUSCLE *IN VIVO*.**

AE Knight[1], CA Trutna[1], LD Hobson-Webb[2], NC Rouze[1], ML Palmeri[1], AF Caenen[3,4], KR Nightingale[1]*

[1]Duke University, Department of Biomedical Engineering, 1427 FCIEMAS 101 Science Drive, Durham, NC USA; [2]Duke University Health System, Department of Medicine, Division of Neurology, Durham, NC, USA; [3]IBiTech-bioMMeda, Ghent University, Ghent, Belgium; [4]Cardiovascular Imaging and Dynamics, Catholic University of Leuven, Leuven, Belgium

Background: When existing methods of 2D shear wave elastography (SWE) are employed to evaluate the biomechanical properties of skeletal muscle, they are challenged by 2D planar imaging, assumptions of material isotropy, and limitations with fiber alignment in the imaging plane. Our group has demonstrated in simulation [1] and in stretched PVA phantoms [2] that in a transversely isotropic material aligned at a 45 degree tilt relative to the push axis, multiple shear wave modes can be excited, representing the shear vertical (SV) and shear horizontal (SH) modes, which would allow for full characterization of transversely isotropic material characteristics [1], [2]. To our knowledge, the presence of both the SV and SH modes has not been measured *in vivo* with ultrasonic SWE.

Aims: This work aims to demonstrate the presence of complex shear wave patterns, likely the SV and SH modes, *in vivo* in the vastus lateralis muscle.

Methods: Using a Verasonics scanner and L74 transducer pushing at 4 MHz at a depth of 20 mm, 36 acquisitions were taken in the vastus lateralis muscle *in vivo* by rotating the transducer around its central axis in 5° increments to reconstruct a 3D volume. From the synthesized 3D SWE volume through time, the coronal plane was extracted, and speeds were estimated at all rotation angles. These speeds were fit to an ellipse, with major and minor axes indicating the shear wave speed along and across the fibers.

Results: Preliminary results in a single subject are shown in Figure 1. Figure 1a shows an approximation of the experimental set up, demonstrating the angle between the transducer push (F) and the fiber orientation (A). Figure 1b shows a B-mode in the vastus lateralis, demonstrating the 11 degree tilt of the fibers in the sagittal plane (blue arrow). Figure 1c shows the particle speeds at 2 ms in the coronal plane, while Figure 1d shows the calculated group speeds at each angle. Speeds in black in Figure 1d show the main ellipse, while the values in cyan show the faster speeds outside the ellipse. Figure 1e shows an example of a space time plot of the particle velocities at the angle of 150°, aligning with the yellow arrow in Figure. 1c and d. The speeds along and across the fibers were 3.15±0.41 m/s and 1.35±0.12 m/s respectively (Figure 1d), and the ellipse fitting found a rotation angle of 8° in the coronal plane. Interestingly, at multiple angles (25-40°, 150-170°, 205-225°, and 330-350°), we observed two shear wave trajectories in Figure 1c, 1d, and 1e: a slower wave which aligned with the main ellipse (1.98±0.21 m/s), and a faster wave than the main ellipse (4.15±0.63 m/s).

Conclusions: This wave behavior is consistent with the shear splitting predicted in TI material simulations with angled excitations [1], suggesting that both the SH and SV modes may have been excited in these experiments.

Acknowledgements: We would like to thank NIH grants R01-EB022106, R01-CA142824, and DOD PCRP grant W81XWH-16-1-0653

References: [1] N. C. Rouze, M. H. Wang, M. L. Palmeri, and K. R. Nightingale, "Finite element modeling of impulsive excitation and shear wave propagation in an incompressible, transversely isotropic medium.," J. Biomech., pp. 1–8, Sep. 2013.

[2] A. Caenen, A. E. Knight, N. C. Rouze, N. B. Bottenus, P. Segers, and K. R. Nightingale, "Measuring elastic nonlinearity in a soft solid using a tilted acoustic radiation force for shear wave excitation," 2019 IEEE Int. Ultrason. Symp., pp. 9–11, 2019.

[3] N. C. Rouze, M. L. Palmeri, and K. R. Nightingale, "Tractable calculation of the Greens tensor for shear wave propagation in an incompressible, transversely isotropic material," Phys Med Biol, vol. 65, pp. 1–17, 2020.

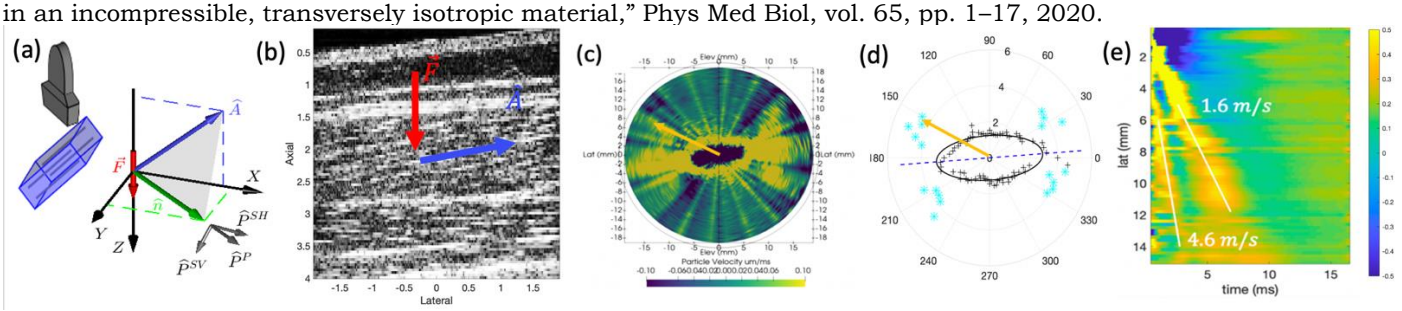

019 **3D MULTIFREQUENCY LIVER SHEAR WAVE ABSOLUTE VIBRO-ELASTOGRAPHY WITH AN XMATRIX ARRAY – PRELIMINARY IN-VIVO VALIDATION.**

Qi Zeng[1], Mohammad Honarvar[1], Julio Lobo[1], Caitlin Schneider[1], Gerard Harrison[2], Changhong Hu[2], James Jago[2], Robert Rohling[1], Septimiu E. Salcudean[1].*

[1]Electrical and Computer Engineering, The University of British Columbia, Vancouver, BC Canada V6T 1Z4; [2]Philips Healthcare, Bothell, WA 98021 USA.

Background: Liver fibrosis is the wound-healing response to chronic liver injury regardless of etiology and can progress to cirrhosis and its complications. Magnetic resonance elastography (MRE), which quantitatively estimates the shear modulus over a liver tissue volume, is commonly regarded as the non-invasive imaging-based gold-standard for fibrosis staging [1]. The ultrasound 3D shear wave absolute vibro-elastography solution (S-WAVE) previously developed by our group was able to generate volumetric hepatic stiffness measurements which are comparable to MRE, but its performance and efficiency is still limited by the conventional mechanical 3D ultrasound transducer [2].

Aims: In this work, we introduce a new 3D multifrequency S-WAVE implementation based on a state-of-the-art matrix array transducer. The resulting S-WAVE solution is able to utilize the large field of view and high-volume rate 3D scans to provide volumetric hepatic stiffness measurements that are strongly correlated with MRE, but are acquired with much shorter exam and imaging session time.

Methods: Our S-WAVE solution is based on an EPIQ 7G ultrasound machine with an X6-1 xMATRIX transducer (Philips Healthcare, Bothell, WA). A shaker board coupled to the patient's back is used to deliver the excitation to the liver. A 3D Color Power Angiography sequence was modified to achieve imaging of shear waves at three excitation frequencies simultaneously. A 3D scan with the field of view of 16 cm (depth) x 90° (lateral) x 40° (elevation) could be completed within 12 secs. The reconstruction is obtained using local spatial frequency estimation. A phantom study was completed using MRE as the ground truth. Six healthy volunteers and eight patients were imaged with MRE, S-WAVE and FibroScan®.

Results: The results of three tissue phantoms (CIRS, Norfolk, VA) reports variations within ± 0.2 kPa compared to MRE. The results of the 14 in-vivo cases showed that S-WAVE achieved a significant better agreement to the MRE measurements, with a cross-correlation of 96.33% and a R-squared value of 0.92 as shown in Figure 1, compared to the transient elastography (TE) baseline results shown in Figure 2.

Conclusions: Our in-vivo validation results shows that S-WAVE with a matrix array has the potential to deliver a similar assessment of liver fibrosis as MRI in a more accessible, inexpensive way, to a broader set of patients. Further evaluation with more patients is warranted.

Acknowledgements: This work is supported by a NSERC Collaborative Research and Development Grant - CRDPJ 486172-15, in collaboration with Philips Healthcare. Support from the Charles A. Laszlo Chair in Biomedical Engineering held by Professor Salcudean is gratefully acknowledged.

References:

1. S. Singh *et al*, "Diagnostic Performance of Magnetic Resonance Elastography in Staging Liver Fibrosis: A Systematic Review and Meta-analysis of Individual Participant Data," *Clin. Gastroenterol. Hepatol.*, vol. 13, no. 3, 2015

2. J. M. Abeysekera, R. Rohling, and S. Salcudean, "Vibro-elastography: absolute elasticity from motorized 3D ultrasound measurements of harmonic motion vectors," *in Proceedings – 2015 IEEE International Ultrasonics Symposium*, 2015, pp. 1–4.

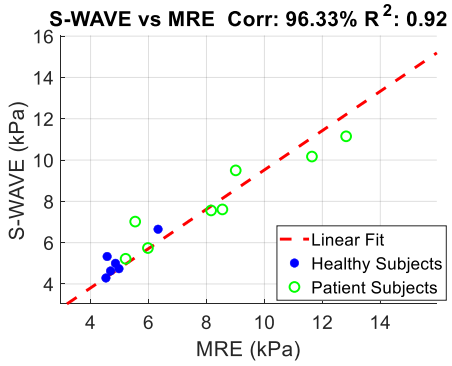

Figure 2. S-WAVE vs MRE in-vivo comparison

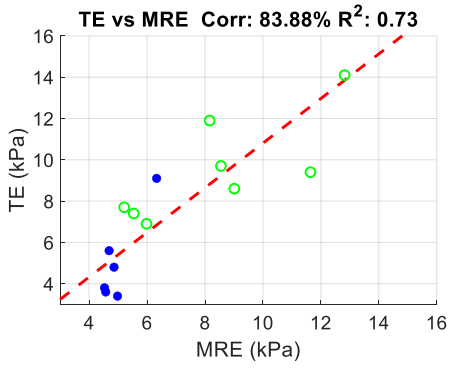

Figure 2. TE vs MRE in-vivo comparison

* *indicates Presenter*

024 **DETECTION OF CEREBRAL STIFFNESS BEFORE AND AFTER LUMBAR PUNCTURE BY NONINVASIVE TIME-HARMONIC ULTRASOUND ELASTOGRAPHY.**

Bernhard Kreft[1], Mehrgan Shahryari[1], Jürgen Braun[1], Ingolf Sack[1], Kaspar-Josche Streitberger[1], Heiko Tzschätzsch[1].*

[1] Charité – Universitätsmedizin, Berlin, Berlin, GERMANY.

Background: Ultrasound Elastography has become an important diagnostic tool for a variety of diseases [1]. However, application to in-vivo brain is limited due to refraction and shielding of ultrasound signals by the skull. In previous work, we proposed time-harmonic ultrasound elastography (THE) in the brain and detected brain stiffening due to the Valsalva maneuver [2] and hypercapnia [3]. Here, we investigate whether cerebral THE can detect brain stiffness changes due to lumbar puncture in patients with idiopathic intracranial hypertension (IIH).

Aims: Application of cerebral THE in patients receiving lumbar puncture for intracranial hypertension before and after treatment.

Methods: Shear waves introduced into the brain by an external shaker and measured by ultrasound were used to noninvasively quantify shear wave speed (SWS) as a surrogate marker of cerebral stiffness [4]. We consecutively investigated 22 patients with IIH (17 females, mean age: 34.4±10.5 years) and a group of age-matched healthy controls (9 females, mean age: 34.1±9.7 years). THE was performed before and after lumbar puncture including invasive pressure measurement. Figure 1 shows the B-mode image and the corresponding elastograms measured by cerebral THE.

Results: Figure 2a) shows mean SWS of healthy controls and patients pre and post lumbar puncture. Mean SWS in healthy subjects was significantly lower than in patients pre lumbar puncture (1.57±0.07 m/s versus 1.77±0.1 m/s, p<0.001). After treatment, mean SWS decreased to 1.57±0.06 m/s. Opening pressure correlated with the degree of reduction of CS (r=0.52, p=0.01), as shown in figure 2b).

Conclusions: The observed separation of patients, pre-treatment from healthy volunteers and the immediate drop of SWS to normal values after lumbar puncture suggest a tight link between cerebral stiffness changes and intracranial pressure. This interpretation is further supported by the correlation of opening pressure with difference-SWS between pre and post lumbar puncture. THE could be of clinical value as a noninvasive measurement method for intracranial pressure.

Acknowledgements: We acknowledge funding from the German Research Foundation (DFG, SFB1340 Matrix in Vision, GRK2260 BIOQIC)

References: [1] Bamber J *et al.*: Ultraschall Med. 2013. 34(2):169-84. doi: 10.1055/s-0033-1335205.
[2] Tzschätzsch H *et al.*: Sci Rep. 2018. 8(1):17888. doi: 10.1038/s41598-018-36191-9.
[3] Kreft B *et al.*: Ultrasound Med Biol. 2020. 46(4):936-943. doi: 10.1016/j.ultrasmedbio.2019.12.019.
[4] Tzschätzsch H *et al.*: Med Image Anal. 2016. 30:1-10. doi: 10.1016/j.media.2016.01.001.

Figure 1.

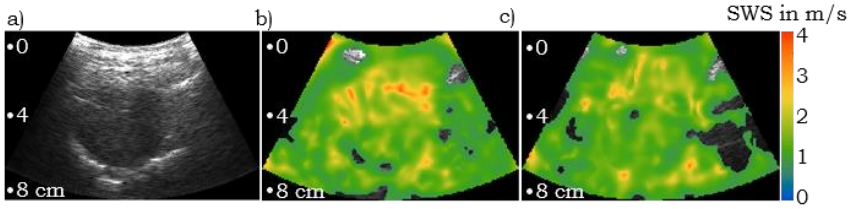

Figure 1.
a) Transcranial B-mode image.
Elastograms:
b) pre lumbar puncture
c) post lumbar puncture

Figure 2.
a)Correlation of SWS Difference and opening pressure.
b) Mean SWS of healthy control and patients pre/post treatment.

Figure 2.

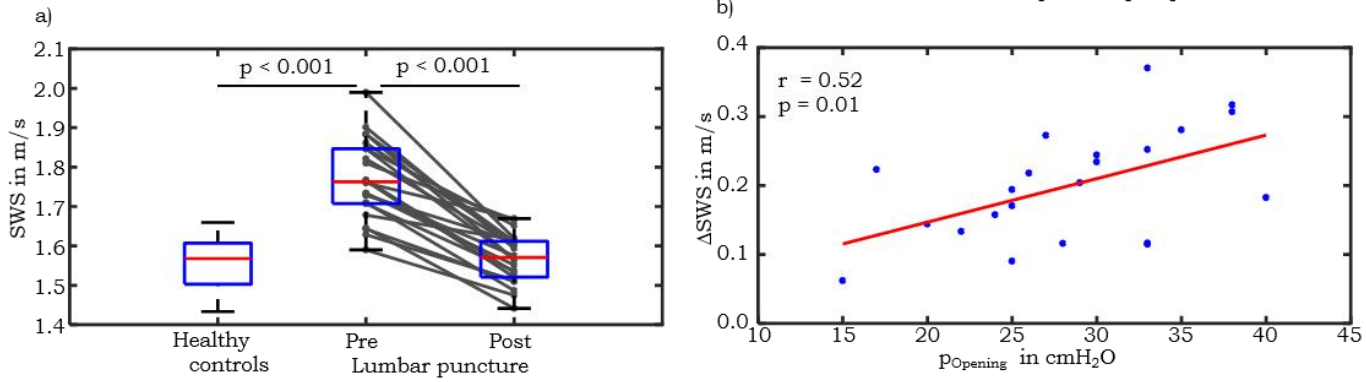

025 **DESIGN OF A "SMART" GRASPER ROBOT FOR TISSUE CLASSIFICATION.**

Y. Sosnovskaya[1], J. M. Jaime[1], W. Premvuti[1], B. Hannaford[1].*
[1]University of Washington, 185 E Stevens Way NE, Seattle, WA, 98195, USA.

Background: The low cost and small size of today's sensors lets one envision smart surgical instruments, detecting in real time the physiological and biomedical properties of tissues they manipulate. In complex surgeries, such instruments would support safer and more effective manipulation of easily damaged delicate tissues, and reduce the probability of tissue misidentification, particularly for tissues that are hard to identify visually. Prior to the present project, an early prototype of a multimodal "smart" surgical robot has been developed, based on a motorized surgical grasper. This prototype used pulse oximetry, thermal, bioimpedance and jaw force measurements to detect tissue ischemia. [1]

Aims: The end goal of the present project is to develop a new version of a "smart" grasper robot, capable of solving more advanced tissue classification tasks, and of providing higher fidelity data. The first intermediate goal was to design and build a new iteration of the original obsolete prototype grasper, replacing rigid sensor-mounting PCBs with newly designed flex PCBs, and redesigning and replacing all of the signal processing hardware and the sensors themselves. The second intermediate goal was to add sensors of new types to the robot, thus broadening the range of tissues it could classify. These two goals have been met. The next intermediate goal is to gather preliminary tissue data, to test the system and to train classification algorithms.

Methods: Upgrading the original sensors, the new "smart" grasper iteration was outfitted with new strain gauges, and a new thermistor, four electrodes, LEDs and photodiodes. These sensors measure grasping force, tissue temperature, bioimpedance and optical properties. We also added a 1 MHz ultrasonic transducer (not present on the original grasper), to measure the tissue's acoustic properties. Signal processing circuitry and flex PCBs to mount the sensors (on 7x7 mm jaws) were designed and built; besides initial filtering and digitalization, the signals are processed in software. To address dense sensor topology on the jaws, they were soldered using the LPKF pick-and-place system and reflow oven. Prior to testing the full system, calibration data were obtained for each individual sensor group; it is now being incorporated into the signal processing components. Preliminary tissue classification data were collected for the coupled ultrasonic transducer and thermistor, and used to train a MATLAB SVM Classifier model.

Results: The new iteration of a "smart" prototype grasper has been successfully designed and built, shown on the figure below. Relative to the original prototype, besides the complete overhaul of the entire system's components and topology, a 1 MHz ultrasonic transducer was added to it. Preliminary testing results of the ultrasonic transducer (classification between 1st dorsal interosseous muscle and distal phalanx) and thermistor pair are encouraging: it demonstrated at most 10% classification loss with the worst dataset, and 0% classification loss with better datasets. This also suggests that the SVM Classifier is a good model for this application.

Conclusions: So far in this project, we have built a new iteration of a "smart" prototype grasper robot for tissue classification, adding a new sensor: an ultrasonic transducer. Preliminary results for just two of the coupled sensors demonstrated 0 to 10% classification loss, which is encouraging. Currently the robot's subsystems are undergoing individual calibration; after finishing this phase, the full system will be used to collect datasets from animal organs, in-vitro and in-vivo. Animal experiments will be conducted in the UW Center for Video Endoscopic Surgery.

References:

[1] Roan, P., "An instrumented surgical tool for local ischemia detection," Ph.D. Thesis, Department of Electrical Engineering, University of Washington, Seattle, WA, USA, 2011.

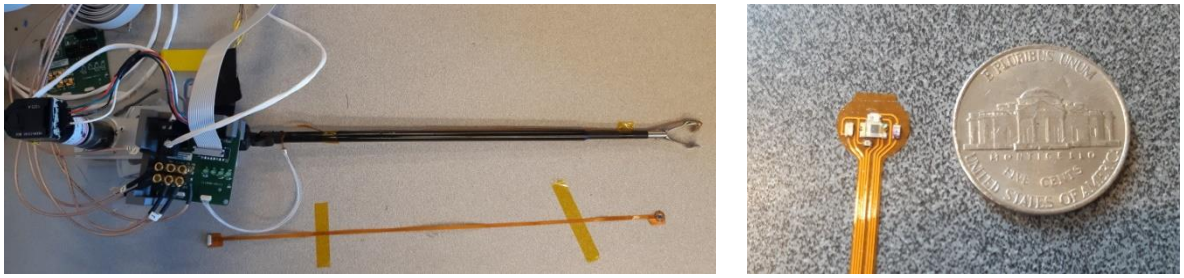

Left: New "smart" grasper prototype, with one of its flex PCBs separated (below); Right: One of the jaws, with the pulse oximetry LEDs and photodiodes, and the thermistor, next to a US 5 cent coin for scale

* *indicates Presenter*

030 **THREE-DIMENSIONAL IMAGING OF CELL AND EXTRACELLAR MATRIX ELASTICITY USING QUANTITATIVE MICRO-ELASTOGRAPHY.**

Matt S. Hepburn, [1,2] Jiayue Li,[1,2,4] Alireza Mowla,[1,2] Yu Suk Choi[3] and Brendan F. Kennedy[1,2,4]*
[1]BRITElab, Harry Perkins Institute of Medical Research, QEII Medical Centre, Nedlands, Western Australia, 6009, Australia and Centre for Medical Research, The University of Western Australia, Crawley, Western Australia, 6009, Australia. [2]Department of Electrical, Electronic & Computer Engineering, School of Engineering, The University of Western Australia, 35, Stirling Highway, Perth, Western Australia, 6009, Australia. [3]School of Human Sciences, The University of Western Australia, 35 Stirling Highway, Crawley, Western Australia, 6009, Australia. [4]Australian Research Council Centre for Personalised Therapeutics Technologies, Australia.

Background: Recent studies in mechanobiology have revealed the importance of cellular and extracellular mechanical properties in regulating cellular function in normal and disease states [1]. Although it is established that cells should be investigated in a three-dimensional (3-D) environment, most techniques available to study mechanical properties on the microscopic scale are unable to do so. Here, we describe our work in developing optical coherence elastography [2] to acquire volumetric images of cellular and extracellular elasticity in 3-D biomaterials.

Aims: Our aim is to improve the resolution and accuracy of OCE toward volumetric imaging of cellular and extracellular elasticity in 3-D biomaterials. Ultimately, we aim to provide biologists with a tool to characterize the link between mechanical properties and cell physiology in environments that better that better replicate the conditions found *in vivo* than conventional two dimensional substrates.

Methods: We have developed a compression OCE system, based on a Thorlabs OCT system. Our system generates quantitative elasticity volumes of live human cells embedded in soft hydrogels. This approach is based on quantitative micro-elastography (QME) [3]. We describe our sample preparation protocol for embedding cells in hydrogels to create samples suitable for imaging with QME. We demonstrate that our QME system can achieve an elasticity resolution of 39 μm. This capability is enabled by a novel 3-D weighted least-squares estimate of local axial strain. We demonstrate cell imaging over 3.8×3.8×0.45 mm (*xyz*) fields of view using a common-path OCT system with axial resolution of 4.8 μm and lateral resolution of 7.2 μm. In addition, we increase the lateral resolution of the OCT system to 4.4 μm and utilize a dual-arm configuration to improve the visualization of cells in OCT images, enabling co-registration of local regions of elevated elasticity with individual cells identified in OCT images. We image two cell types: cells with and without a modified mechanosensitive transcription factor.

Results: We present results that demonstrate that QME can reveal elevated elasticity in local regions surrounding cells, and can distinguish between cell types when a mechanosensitive transcription factor is modified, validated against confocal microscopy. Our results also demonstrate the complementary nature of QME with structural images of cells in the underlying OCT images.

Conclusions: We present the first images of cellular and extracellular elasticity of cells in 3-D biomaterials using QME. We describe the necessary sample preparation protocol, experimental setup and signal processing we have developed. We use this approach to present images of cells with different mechanical properties, validated against confocal microscopy.

Acknowledgements: We acknowledge funding received from the Australian Research Council, the Cancer Council Western Australia, an Industrial Transformation Training Centre scholarship, and a scholarship from the William and Marlene Schrader Trust of the University of Western Australia.

References:

[1] Ladoux BM and Mège RM, "Mechanobiology of collective cell behaviours," Nature Reviews Molecular Cell Biology, v.18, pp.743-757, 2017
[2] Kennedy BF et al, "The emergence of optical elastography in biomedicine", Nature Photonics, v.11, pp.215-221, 2017
[3] Kennedy KM et al, "Quantitative micro-elastography: imaging tissue elasticity using compression optical coherence elastography", Scientific Reports, v.5, pp.15538, 2015.

031 **CAMERA-BASED OPTICAL PALPATION TOWARDS *IN-VIVO* BREAST CANCER ASSESSMENT.**

Rowan W. Sanderson[1,2], Qi Fang[1,2], Andrea Curatolo[1,2,3], Wayne Adams[1,2], Devina D. Lakhiani[1,2], Hina M. Ismail[1,2], Ken Y. Foo[1,2], Benjamin F. Dessauvagie[4,5], Bruce Latham[4,6], Chris Yeomans[4], Christobel M. Saunders[7,8,9] and Brendan F. Kennedy[1,2,10]*

[1]BRITElab, Harry Perkins Institute of Medical Research, QEII Medical Centre, Nedlands and Centre for Medical Research, The University of Western Australia, Perth, Western Australia, 6009, AUSTRALIA; [2]Department of Electrical, Electronic & Computer Engineering, School of Engineering, The University of Western Australia, Crawley, Western Australia, 6009, AUSTRALIA; [3]Currently with Visual Optics and Biophotonics Group, Instituto de Óptica "Daza de Valdés", Consejo Superior de Investigaciones Cientificas (IO, CSIC), C/Serrano, 121, Madrid, SPAIN; [4]PathWest, Fiona Stanley Hospital, 11 Robin Warren Drive, Murdoch, Western Australia, 6150, AUSTRALIA; [5]Division of Pathology and Laboratory medicine, Medical School, The University of Western Australia, Crawley, Western Australia, 6009, AUSTRALIA; [6]The University of Notre Dame, Fremantle, Western Australia, 6160, AUSTRALIA; [7]Division of Surgery, Medical School, The University of Western Australia, Crawley, Western Australia, 6009, AUSTRALIA; [8]Breast Centre, Fiona Stanley Hospital, 11 Robin Warren Drive, Murdoch, Western Australia, 6150, AUSTRALIA; [9]Breast Clinic, Royal Perth Hospital, 197 Wellington Street, Perth, Western Australia, 6000, AUSTRALIA; [10]Australian Research Council Centre for Personalised Therapeutics Technologies, AUSTRALIA.

Background: Optical elastography represents an array of techniques, capable of imaging the mechanical contrast between healthy and diseased tissues with micrometer-scale spatial resolutions [1]. Despite this promise, many of these techniques incur high costs and suffer from a lack of mobility, limiting their potential applications particularly in low resource settings. Here we describe a simple and cost-effective optical elastography technique, termed camera-based optical palpation (CBOP), for imaging mechanical properties of biomedical tissues.

Aims: Our aim is to develop a simple, compact and cost-effective optical elastography technique capable of aiding surgeons in the detection, and ultimately excision, of cancerous breast tissue. In focusing on a simple and affordable imaging technique, we aim to provide an improved standard of healthcare to low resource settings and expand optical elastography to a broader range of applications.

Methods: CBOP is closely related to optical coherence tomography (OCT)-based optical palpation [2], however it replaces the need for an OCT system by capturing the transmission of light through a porous, compliant layer with a simple digital camera. We describe the porous layer fabrication and characterization procedure and also present a model which details optical transmission through a porous medium. We also describe the methodology used to convert the digital photographs acquired during CBOP to *en face* maps of the stress at the surface of a sample.

Results: We present a characterization of CBOP using silicone inclusion phantoms with inclusions ranging from 0.5-5 mm^3 and demonstrate an imaging resolution up to 280 μm, comparable to that of OCT-based optical palpation. In addition, we use CBOP to image freshly excised human breast tissue and differentiate between adipose, fibrous and malignant tissue based on mechanical contrast. These results are validated by gold-standard post-operative histology.

Conclusions: We have presented CBOP, an optical elastography technique which utilizes a simple digital camera and porous silicone layer to provide a cost-effective means to image mechanical contrast in breast tissue. This technique is demonstrated on silicone phantoms and freshly excised breast tissue where its results are validated by OCT-based optical palpation and post-operative histology, respectively.

Acknowledgements: This work was supported by research grants from the Australian Research Council, the Department of Health, Western Australia and the Cancer Council, Western Australia; a research contract with OncoRes Medical; and the War Widows Guild of Western Australia Top-up Scholarship for Research into Breast Cancer.

References:

[1] Kennedy BF et al, "The emergence of optical elastography in biomedicine", Nature Photonics, v.11, pp.215-221, 2017.

[2] Kennedy KM et al, "Optical palpation: optical coherence tomography-based tactile imaging using a compliant sensor", Optics Letters, v.39, pp.3014-3017, 2014.

* *indicates Presenter*

032 **Hb-OCE: CORNEAL BIOMECHANICAL RESPONSE TO HEARTBEAT PULSATION.**

Achuth Nair[1], Manmohan Singh[1], Salavat Aglyamov[2], and Kirill V. Larin[1].*

[1]University of Houston, Department of Biomedical Engineering, [2]Department of Mechanical Engineering, Houston, TX, USA.

Background:

Corneal pathologies such as keratoconus and post-surgical ectasia can lead to tissue damage and alter corneal biomechanical properties [1]. An established method to directly assess the mechanical properties of tissue is elastography. Typically, elastography uses external excitation to induce deformation in the tissue. However, passive methods of elastography are currently being investigated, where which deformation induced by physiological sources are analyzed to assess biomechanical properties [2].

Aims:

In this study, we describe heartbeat optical coherence elastography (Hb-OCE), an elastography technique used to assess the mechanical properties of the *in vivo* rabbit cornea due to deformation caused by the heartbeat induced ocular pulse. Qualitative measure of stiffness is obtained, and corneal stiffness is distinguished between untreated control cornea and a collagen crosslinked cornea.

Methods:

An SD-OCE system in the common-path configuration is used to acquire images of the apex of the cornea of an anesthetized rabbit. The rabbit heartbeat is acquired using a pressure transducer applied externally to the rabbit's chest. A rabbit with an untreated cornea was initially measured, followed by a rabbit that had its cornea crosslinked. For both measurements, a rebound tonometer detected an intraocular pressure (IOP) of 10 mmHg. OCT images are synchronized to heartbeat measurements in a post processing step. Motion in the cornea as a result of the ocular pulse is detected, and the displacement in the cornea is measured. This displacement is then translated to strain, and the strain is compared between the untreated and crosslinked corneas.

Results: Displacement and strain in the untreated sample is significantly greater over the entire measurement period. Average strain measured over heart cycles was compared, and the results showed a significant difference in strain between tissue types. Results are shown in Figure 1.

Conclusions: The results suggest that Hb-OCE is feasible for assessing the biomechanical properties of the cornea and can distinguish a crosslinked cornea from an untreated one. Currently, measurement is performed by direct contact, but non-contact measurements are an area of investigation. Furthermore, our technique is currently limited to qualitative assessment of strain, but quantitative assessment is an important area of development.

Acknowledgements:

This work was funded in part by the NIH under grants R01EY022362 and P30EY007551. Manmohan Singh was partially supported by a fellowship from the Gulf Coast Consortia, on the NLM Training Program in Biomedical Informatics and Data Science T15LM007093.

References:

[1] Garcia-Porta, N. et al; *ISRN ophthalmology (*2014).

[2] Larin, K. V., Sampson, D. D.; *Biomedical optics express*, (2017).

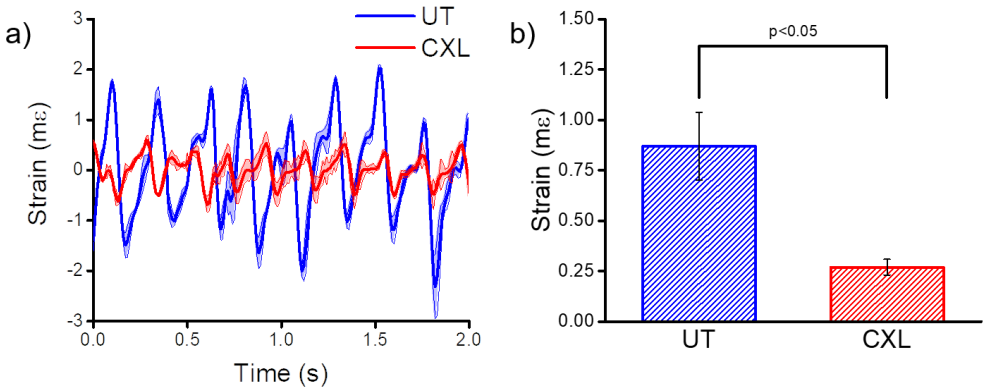

Figure(1): (a) Strain measured over time in the UT and CXL cornea. (b) Average corneal strain over pulse period is statistically significant.

007 **TUTORIAL - WHAT TO EXPECT FROM PASSIVE ELASTOGRAPHY?**

*Stefan Catheline**
University of Lyon, INSERM LabTAU U1032, Lyon, FRANCE.

Elastography, sometimes referred as seismology of the human body, is an imaging modality recently implemented on medical ultrasound systems. It allows to measure shear waves within soft tissues and gives a tomography reconstruction of the shear elasticity. The idea inspired by seismology, is to take advantage of shear waves naturally present in the human body due to muscles activities to construct shear elasticity map of soft tissues. It is thus a passive elastography approach since no shear wave sources are used. A general overview of this field starting from the very beginning with the early work of Dickinson [1] in ultrasound, and Campillo [2] in seismology is given in the first part of the presentation. The last part, is devoted to the potential applications of passive elastography in seismology, MRI, optics and ultrasounds to detect shear waves and reconstruct a speed tomography in San Andrea fault (CA), a human liver, thyroid, brain, in a rat eye and a single cell. Perspective of fast biomechanics imaging at a cellular level for monitoring is finally discussed.

[1] R.J.Dickinson, C.R.Hill, “measurement of soft tissues motion using correlation between A-Scans”, Ultr.MedBio. 8(3), pp.263 (1981).
[2] A.Paul, M.Campillo “Long range correlations in the diffuse seismic coda”, Science 299 (5606), pp.547 (2003).

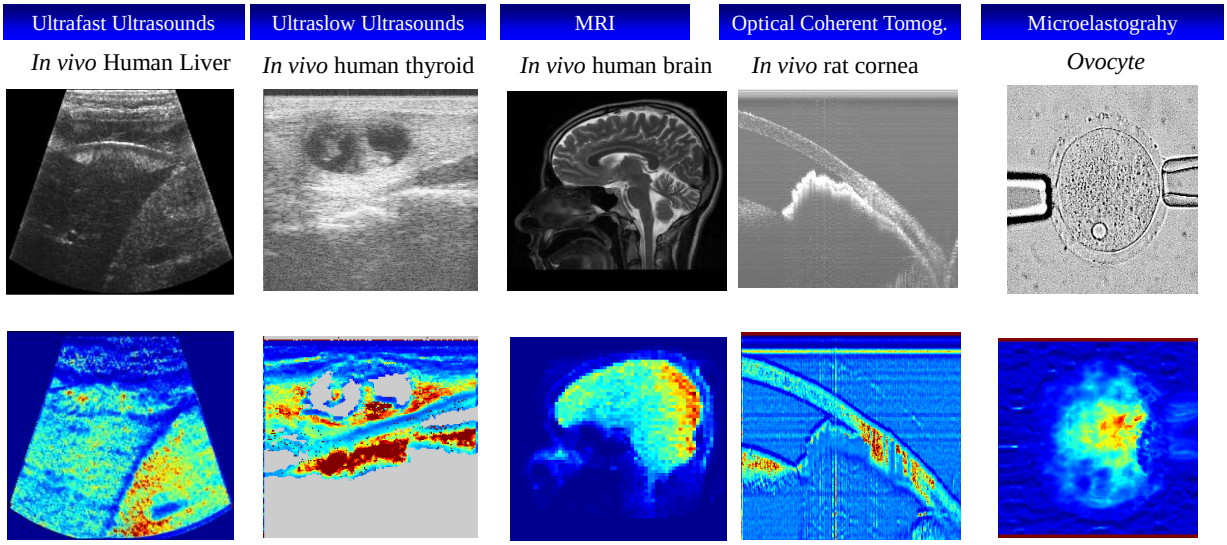

Examples of standard imaging (top raw) and passive elastography reconstruction (bottom raw)

* *indicates Presenter*

033 **HIFU LESION DETECTION IN PROSTATE CANCER USING PASSIVE ELASTOGRAPHY BASED ON CONVENTIONAL B-MODE IMAGES.**

Thomas Payen[1], Sébastien Crouzet[1], Nicolas Guillen[2], Jean-Yves Chapelon[1], Cyril Lafon[1], Stefan Catheline[1].*

[1]LabTau, U1032 INSERM, Lyon, France ; [2]EDAP-TMS, Vaulx-en-Velin, FRANCE.

Background: High intensity focused ultrasound (HIFU) is clinically used in the context of non-metastatic prostate cancer, where it provides an efficient, local, non-ionizing and minimally invasive treatment option. In order to preserve the surrounding tissues and limit the side effects for the patient, it is however crucial to monitor the sudden rise in temperature in the treated area. A significant increase in tissue stiffness is a well-known marker of HIFU lesions. However, the deep-seeded prostate remains a challenge for conventional elastography techniques. In contrast, passive elastography uses the wave field naturally present in the human body to estimate elasticity in the whole organ.

Aims: This work investigates passive elastography for HIFU lesion detection in prostate cancer using slow-rate B-mode images acquired on a clinical ultrasound system.

Methods: Passive elasticity maps were first obtained in a vibrated calibrated phantom with stiff inclusions. Raw IQ data was acquired and B-mode images were reconstructed from the same data set. Frame-to-frame displacement was estimated by phase tracking and the GLobal Ultrasound Elastography (GLUE) technique [1,2], respectively. Elasticity was then estimated using an autocorrelation-based algorithm. Five prostate cancer HIFU patients with various Gleason scores were imaged for 10 seconds before and after HIFU treatment using the Focal One® system. The GLUE method was again used to estimate the displacement in this slow-rate acquisition (22 Hz). The resulting pre and post passive elastography maps were compared to estimate the treatment effect on the prostatic tissue. Per-operative contrast-enhanced ultrasound and post-operative multiparametric MRI were used as comparators to assess the treatment success.

Results: In the phantom, the shear wave velocity was estimated in the background and in the inclusion at 2.93 ± 0.71 and 5.53 ± 0.89 m/s, respectively, using IQ data, and 3.13 ± 0.81 and 5.17 ± 0.95 m/s using the reconstructed B-mode images, in good agreement to the manufacturer's values of 2.89 and 5.16 m/s. In addition, the maps demonstrated sharp boundaries for inclusion delineation. In patients, the shear wavelength was in average 37% higher in the tumor than in adjacent prostate tissue prior to treatment indicating stiffer tissue. In addition, the elasticity values increased by 26% after treatment in the ablated region while they remained similar in untreated areas.

Conclusions: Passive elastography can be performed using B-mode images acquired with low frame rate conventional US scanners with results comparable to the ones obtained based on ultrafast IQ data. This technique compatible with clinical systems has the potential to see a quick transfer to the clinic for prostate cancer diagnostic and HIFU monitoring.

Acknowledgements: This work was supported by the RHU PERFUSE (ANR-17-RHUS-0006) of Université Claude Bernard Lyon 1 (UCBL), within the program "Investissements d'Avenir" operated by the French National Research Agency (ANR).

References: [1] Hashemi H, Rivaz H. Global time-delay estimation in ultrasound elastography. IEEE Trans UFFC. 2017:1625–1636. [2] Rabin, C, Benech, N. Quantitative breast elastography from B-mode images. Medical physics. 2019;46(7), 3001-3012.

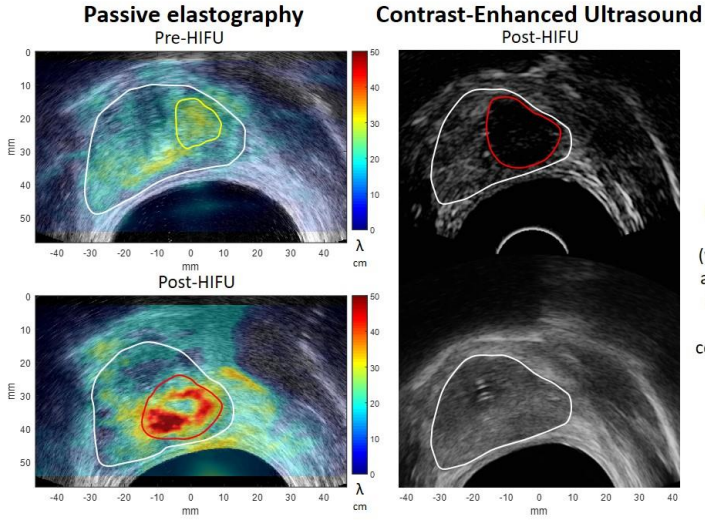

Figure: Passive elastography (left) was performed before (top) and after (bottom) HIFU treatment in a cancerous prostate (white), detecting the mass (yellow) and the ablated region (red). The vascular depletion in the treated volume was confirmed with contrast agents (top right) with the corresponding B-mode image (bottom right).

* *indicates Presenter*

004 **COMPARISON OF PLANE WAVE IMAGING AND FOCUSED SINGLE LINE TRANSMIT ECHOGRAPHY FOR DETERMINATION OF THE PULSE WAVE VELOCITY IN VIVO.**

Melissa GM van de Steeg[1,2], Stein Fekkes[1], Anne ECM Saris[1], Hendrik HG Hansen[1], Chris L de Korte[1].*

[1]Radboud university medical center, Nijmegen, THE NETHERLANDS; [2]Catharina Hospital, Eindhoven, THE NETHERLANDS.

Background: Arterial stiffness has shown to be of prognostic relevance for cardiovascular risk. It can be obtained directly and noninvasively by measuring the pulse wave velocity (PWV) using ultrasound. The gold standard is to obtain the PWV between the common carotid and the femoral artery (cfPWV), where cfPWV values larger than 10 m/s indicate vascular damage [1]. Since cfPWV is affected by variations of mechanical properties of the artery (diameter, branching), assessment of the local PWV might be of great value. Ultrasound-based methods to estimate local PWV have been proposed based on conventional focused Single Line Transmit (SLT) imaging and on Plane Wave Imaging (PWI). Usually, PWI has the advantage of a higher frame rate compared to SLT, at the cost of lateral resolution.

Aims: The goal of this study is to compare the accuracy of the estimated *in vivo* pulse wave velocity using SLT and PWI ultrasound methods and investigate which method should be preferred in clinical practice.

Methods: Radiofrequency ultrasound data of the carotid artery were acquired in ten healthy volunteers (mean: 33.6 years, range: 25-57 years) using a Verasonics Vantage256 ultrasound research imaging system (Verasonics Inc., Kirkland, WA, USA) with a linear array transducer (ATL L12-5 50 mm, Bothell, WA, USA). Acquisition was performed covering a 25 mm wide and 24 mm depth field-of-view using both SLT and PWI. These methods were executed consecutively in a single measurement session (3.5 seconds each), with three measurement sessions per volunteer. SLT was performed with 12 lines, with a pulse repetition frequency (PRF) of 7200 Hz (resulting in 600 fps). The focal depth was 15 mm. PWI was performed with a PRF of 2000 Hz. The PWV was determined at two time-reference points, namely dicrotic notch (DN) and systolic foot (SF), for each imaged pressure cycle. In the analysis, a Butterworth low pass filter with different cut-off frequencies (10-200 Hz) was additionally applied on the acceleration curve of the vessel wall to assess the influence on the PWV. The obtained measurements were filtered by removing all measurements with $R^2<0.6$ (where R^2 is the coefficient of determination of the linear fit of the vessel wall) or a PWV smaller than 1 m/s or larger than 16 m/s [3].

Results: Table 1 summarizes the estimated PWV for different volunteers using both SLT and PWI, with a cut-off frequency of 100 Hz (a stable PWV from this frequency is observed). No significant bias between the two approaches in estimating the PWV was found (two-sided Wilcoxon signed rank test $p>0.70$). The PWV and R^2 at DN is on average higher compared to SF. In terms of accuracy, both approaches have comparable R^2 over the range of cut-off frequencies. Only when no low-pass filter is applied, the PWV is estimated with a higher R^2 for SLT compared to PWI (R^2 at SF 0.88 vs 0.72; at DN 0.89 vs 0.77).

Conclusions: Based on these results, there is no clear difference in estimated PWV's and the accuracy of the estimates using SLT or PWI. In general, the accuracy of the PWV at DN is higher compared to SF. In clinical practice, the preferred method can therefore be selected based on experiences of the clinician.

Acknowledgements: Ethical clearance for this study has been obtained from the Central Committee on Research involving Human Subjects (CMO, region Arnhem-Nijmegen) under number CMO2016-2274 project 19040.

References: [1] B. Williams et al. (2018). 2018 ESC/ESH Guidelines for the management of arterial hypertension: the task force for the management of arterial hypertension of the European Society of Cardiology (ESC) and the European Society of Hypertension (ESH). *European Heart Journal* **39**(33):3021-3104. [2] I. Simova et al. (2016). Comparison between regional and local pulse-wave velocity data. *Echocardiography* **33**:77-81. [3] C. Huang et al. (2016). Comparison of different pulse waveforms for local pulse wave velocity measurement in healthy and hypertensive common carotid arteries in vivo. *Ultrasound in Medicine & Biology* **42**(5):1111-1123.

Table 1: PWV of ten volunteers at SF and DN using either SLT or PWI, at cut-off frequency 100 Hz. Reported results are averaged values of the PWV and coefficients of determination (R^2) of the linear fit of the blood vessel wall.

			Vol. 1	Vol. 2	Vol. 3	Vol. 4	Vol. 5	Vol. 6	Vol. 7	Vol. 8	Vol. 9	Vol. 10
SLT	**SF**	**PWV**	2.58	5.86	4.77	5.02	5.98	6.57	5.38	7.91	9.70	4.96
		R^2	0.95	0.89	0.95	0.98	0.92	0.92	0.93	0.93	0.74	0.91
	DN	**PWV**	8.84	6.63	4.30	6.25	6.29	8.83	5.73	6.54	6.03	4.78
		R^2	0.92	0.74	0.95	0.89	0.94	0.96	0.92	0.97	0.97	0.94
PWI	**SF**	**PWV**	2.68	7.08	4.74	4.85	6.23	5.99	4.86	6.28	12.89	3.98
		R^2	0.96	0.76	0.91	0.98	0.88	0.88	0.88	0.85	0.79	0.84
	DN	**PWV**	8.01	9.40	4.65	6.82	6.28	10.35	5.13	5.60	5.26	5.74
		R^2	0.98	0.83	0.97	0.92	0.99	0.98	0.98	0.99	0.99	0.99

* *indicates Presenter*

039 **ULTRASOUND VIBRATIONAL SHEAR WAVE ELASTOGRAPHY IN PRECLINICAL HUMAN XENOGRAFT TUMOR MODELS.**

J Civale[1], JC Bamber[1], EJ Harris[1].*
[1]The Institute of Cancer Research, London, UNITED KINGDOM.

Background: Radiotherapy is one of the principal treatment modalities offered to cancer patients. A wide range of side effects and complications may arise during or following radiotherapy treatment. There is a clinical need to identify at an early stage during treatment those patients who may be at increased risk of developing complications, thus providing the opportunity to alter or seek alternative treatments for improved clinical outcomes. A key biomarker is tissue stiffness which may be estimated in relative or absolute terms by a variety of elastography techniques that have been reported in the literature. Our group is currently investigating ultrasound imaging techniques at the preclinical stage in human xenograft tumor models in mice. These models offer characterization of the tumor tissue which can be correlated to underlying tissue pathology.

Aims: To develop and optimize an ultrasound imaging system capable of characterizing shear wave fields in small (<1cm) preclinical tumor models in order to then quantify shear wave speed.

Methods: A Verasonics (Kirkland, WA, USA) Vantage system was used in conjunction with a L22-14vX high frequency probe (18 MHz centre frequency) to characterize the shear wave field generated in a preclinical tumor model. Shear waves were generated by means of a mechanical shaker (model 4810, Bruel and Kjaer, Denmark) driven continuously at a single frequency (ranging from 200 to 1000 Hz) in contact with the tumor. Initial tests were performed using an unfocused planar wave imaging sequence similar to the one reported by of Ormachea et al[1]. Ultrasound signal to noise ratio with the L22-14vX probe in planar imaging mode was however unsatisfactory. A focused, line-by-line scanning imaging sequence synchronized with the source vibration signal was developed to improve the quality of the detected shear wave field data. The sequence was first tested in a breast phantom (model 059, CIRS, VA, USA), and subsequently used to characterize the shear wave fields generated in the preclinical tumor model.

Results: Breast phantom measurements with the L22-14vX probe showed an increase (>10dB) in ultrasound signal to noise ratio using the focused, line-by-line imaging sequence when compared to the unfocused planar wave imaging sequence. Similar improvements in signal to noise ratio, and significant reduction of image artefacts were observed in the tumor model (Figure 1a, 1b). These improvements in image quality corresponded directly with improved shear wave field characterization (Figure 1c, 1d) using the line-by-line scanning technique.

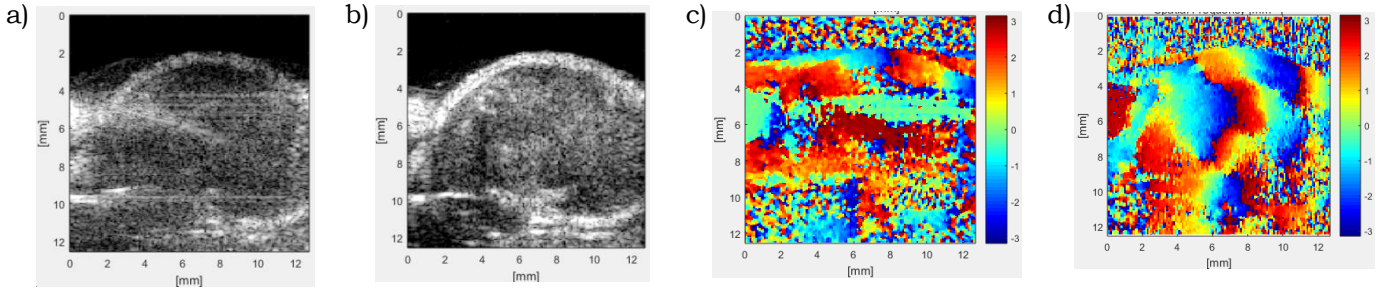

Figure 1. Preclinical tumor B-mode (a, b) and shear wave phase images (c, d) obtained with a vibration source frequency of 800 Hz, using unfocused planar wave imaging (a, c), and focused line-by-line imaging (b, d) methods respectively.

Conclusions: A line-by-line ultrasound imaging method to detect shear wave propagation in a preclinical mouse tumor model using a high frequency imaging probe has been demonstrated. The line-by-line scanning technique places greater demands on the imaging system's memory and increases data acquisition times. These constraints however do not impede near real-time visualization of the shear wave field. Further work is now required the optimize the transmission of the mechanical energy into the tumor, and novel methods are required to quantify shear wave speed from the detected shear wave field.

References: [1] Ormachea *et al.* Shearwave speed estimation using reverberant shearwave field: implementation and feasibility studies, UMB, 44, 963-977, 2018
[2] Parker *et al.* Reverberant shear wave fields and estimation of tissue properties, PMB, 62, 1046-1061, 2017

* *indicates Presenter*

040 **SHEAR WAVE SPEED ESTIMATION WITH A DIRECTIONAL DETECTOR IN PRECLINICAL HUMAN XENOGRAFT TUMOR MODEL.**

J Civale[1], JC Bamber[1], EJ Harris[1].*
[1]The Institute of Cancer Research, London, UNITED KINGDOM.

Background: A key biomarker in tumor characterization is tissue stiffness which may be characterized in terms of shear wave speed using ultrasound imaging methods. Our group is currently developing techniques capable of mapping shear wave fields induced in preclinical human xenograft tumors in athymic nude mice. A reverberant shear wave elastography approach[1] to estimate shear wave speed in the tumors is challenging for a number of reasons: the small size of the tumor, the relatively large tissue stiffness, and the difficulty in placing a large number of vibration sources in contact with the tumor. A low vibration frequency (<500 Hz) is required to generate reverberant conditions if using a single vibration source. A consequence is poor spatial resolution that is insufficient to distinguish internal features of the tumor. To overcome this limitation higher frequencies may be used which however are more highly attenuated and produce shear wave fields that would be better described as a progressive wave. In this work we present a directional detector that may be used to estimate shear wave speed in these non-reverberant field conditions.

Aims: To develop a shear wave directional detector capable of quantifying the direction and wavelength, and by extension the shear wave speed, associated with a non-reverberant shear wave field.

Methods: An autocorrelation function can be determined from an experimentally measured shear wave field, and may be used to estimate the local shear wave speed[1]. In the case of a non-reverberant shear wave field featuring a progressive wave, the 2D autocorrelation function (Figure 1a) may be used to determine the direction associated with the progressive shear wave. An estimate of the wavelength wave can then be obtained from a linear resampling of the autocorrelation function along the direction of propagation. Our proposed directional detector was initially tested in a breast elastography phantom (model 059, CIRS, VA, USA) using a Verasonics (Kirkland, WA, USA) Vantage system with a Philips L7-4 probe (5 MHz center frequency). Shear waves were generated with a mechanical shaker (model 4810, Bruel and Kjaer, Denmark) placed in contact with the surface of the phantom. The directional detector was tested in our tumor model using a high frequency (18 MHz) L22-14vX imaging probe with vibration frequencies up to 1200 Hz.

Results: Measurements in the breast phantom showed the potential of the directional detector by allowing estimation of the shear wave speed in non-reverberant fields with frequencies up to 800 Hz. Shear wave speed images showed good correlation with the location of the stiff inclusion visible under B-mode imaging (Figure 1b, 1c). Progressive shear waves were detected in the tumor models.

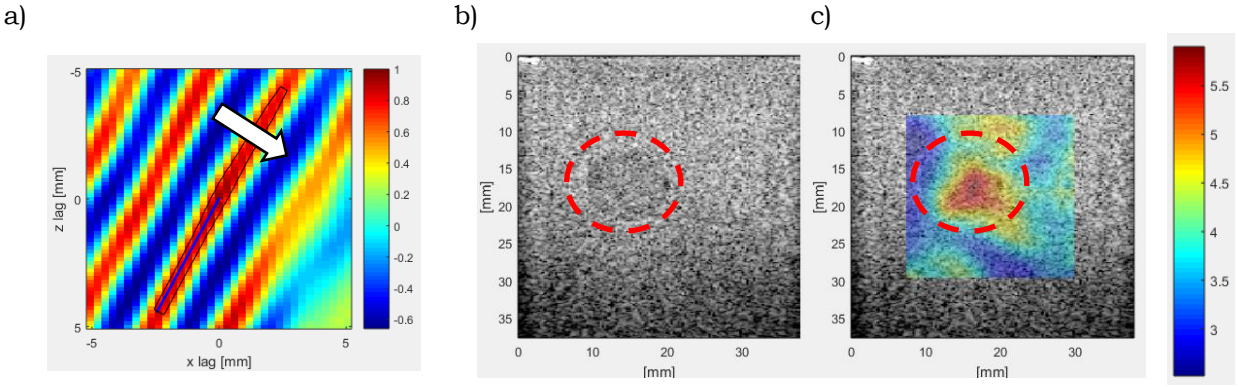

Figure 1. 2D autocorrelation function for a progressive wave, with propagation direction indicated by the arrow (a); B-mode image showing the location of the stiff inclusion in the CIRS breast elastography phantom (b); and shear wave speed (m/s) image superimposed on the original B-mode image (c).

Conclusions: The potential use of a directional shear wave detector based on computation of the autocorrelation function has been demonstrated in a phantom and in a preclinical tumor model. The directional detector provides the ability to estimate shear wave speeds in situations where a fully reverberant shear wave field may not be achievable in practice.

References: [1] Parker *et al.* Reverberant shear wave fields and estimation of tissue properties, PMB, 62, 1046-1061, 2017

034 **INCORPORATING SECOND ORDER REGULARIZATION IN ULTRASOUND ELASTOGRAPHY.**

Md Ashikuzzaman[1], Ali Sadeghi-Naini[2], Abbas Samani[3], Hassan Rivaz[1]*

[1]Concordia University, 1455 Boulevard de Maisonneuve O, Montreal, QC, H3H 2A3, CANADA; [2]York University, 4700 Keele St, Toronto, ON, M3J 1P3, CANADA; [3]The University of Western Ontario, 1151 Richmond St, London, ON, N6A 3K7, CANADA.

Background: Ultrasound elastography, which is a non-invasive medical imaging modality, is increasingly being used to differentiate between healthy and pathological tissues. Estimating tissue displacement field (e.g. using TDE: time-delay estimation) between pre- and post-deformed radio-frequency (RF) frames is a crucial step of quasi-static ultrasound elastography. This is an ill-posed problem which has multiple solutions. As such, cost functions used in energy-based TDE techniques combine a regularization term with the data amplitude similarity term. However, such solutions [1] penalize the first order derivative of the displacement field to regularize the resulting displacement field. This first order regularization does not sufficiently highlight the inclusion-background boundary and therefore, often leads to a low quality strain map.

Aims: In this paper, we formulate a novel cost function for energy-based ultrasound elastography where the second order derivative of the displacement field has been considered as the regularization function, instead of the first-order derivative. In other words, we impose this continuity constraint on strain rather than displacement. By introducing the aforementioned second-order regularization scheme, we aim to increase the smoothness in the background and sharpen the boundary between different elastic regions.

Methods: Let $I_1(i,j)$ and $I_2(i,j)$ be two ultrasound RF frames collected before and after tissue deformation where $1 \le i \le m$ and $1 \le j \le n$ indicate the depth and width of corresponding images, respectively. Our first step is to calculate $a(i,j)$ and $l(i,j)$, the initial axial and lateral displacement fields between I_1 and I_2 using Dynamic Programming (DP) [2]. We devise a non-linear penalty function to refine this initial TDE: $C = D + R$. Here, D is the data amplitude similarity term which is defined as: $D = \sum_{j=1}^{n}\sum_{i=1}^{m}\{I_1(i,j) - I_2(i + a_{i,j} + \Delta a_{i,j}, j + l_{i,j} + \Delta l_{i,j})\}^2$, where Δa and Δl are the refinement fields to be estimated. The principal novelty of this work is incorporating the second order spatial regularization term R in the cost function which is defined as:

$$R = \sum_{j=1}^{n}\gamma(a_{1,j} + \Delta a_{1,j})^2 + \sum_{j=1}^{n}\sum_{i=1}^{m}\{\alpha_1(a_{i-1,j} + \Delta a_{i-1,j} + a_{i+1,j} + \Delta a_{i+1,j} - 2a_{i,j} - 2\Delta a_{i,j})^2 + \alpha_2(a_{i,j-1} + \Delta a_{i,j-1} + a_{i,j+1} + \Delta a_{i,j+1} - 2a_{i,j} - 2\Delta a_{i,j})^2 +$$

$$\beta_1(l_{i-1,j} + \Delta l_{i-1,j} + l_{i+1,j} + \Delta l_{i+1,j} - 2l_{i,j} - 2\Delta l_{i,j})^2 + \beta_2(l_{i,j-1} + \Delta l_{i,j-1} + l_{i,j+1} + \Delta l_{i,j+1} - 2l_{i,j} - 2\Delta l_{i,j})^2\},$$

where $\alpha_1, \alpha_2, \beta_1, \beta_2$ and γ denote the regularization parameters. We analytically optimize C to fine-tune the DP initial estimate. The final displacement tensor is spatially differentiated to obtain the axial strain image. The above forms the basis of the proposed technique which will be henceforth called SoftGLUE (Second-Order FuncTion regularization GLUE) since a second order regularization term was incorporated in its development.

Results: We validate SoftGLUE with soft and hard inclusion simulation datasets. Figs 1 and 2 show that SoftGLUE substantially outperforms GLUE [3] in terms of boundary sharpness and background smoothness.

Conclusions: The novel regularization term proposed in this work substantially improves TDE, and the presented simulation results show that SoftGLUE resolves the boundary-blurring issue in GLUE.

References:

[1] Ashikuzzaman, M. et al., IEEE Trans UFFC, vol. 66, no. 5, pp. 876–887, 2019.
[2] Rivaz, H. et al., IEEE Trans Medical Imaging, vol. 27, no. 10, pp. 1373–1377, 2008.
[3] Hashemi, H S. and Rivaz, H, IEEE Trans UFFC, vol. 64, no. 10, pp. 1625–1636, 2017.

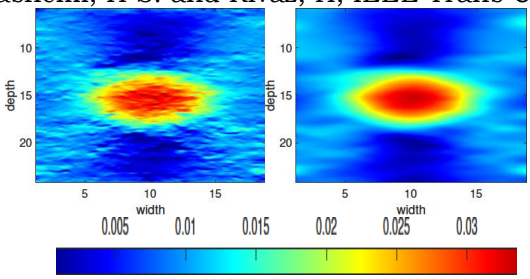

Fig. 1 Soft inclusion: GLUE & SoftGLUE strains

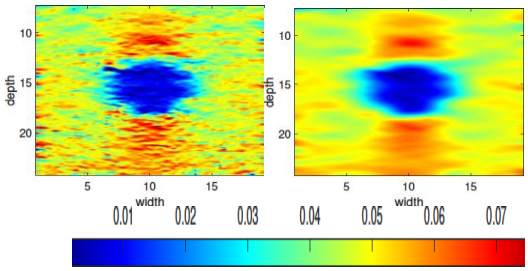

Fig. 2 Hard inclusion: GLUE & SoftGLUE strains

* *indicates Presenter*

035 **BIOMECHANICAL AND STRUCTURAL CHARACTERIZATION OF PERIPHERAL NERVE TISSUE DURING DEVELOPMENT.**

Gonzalo Rosso[1,2], Jochen Guck[1].*
[1]Max Planck Institute for the Science of Light & Max-Planck-Zentrum für Physik und Medizin Staudtstr. 2 91058 Erlangen, GERMANY; [2]Institute of Physiology II, University of Münster. Robert-Koch Str. 27b, 48149 Münster, GERMANY.

Background: Neurons and myelinating Schwann cells in peripheral nerves must withstand mechanical stresses associated with body growth and limb movements. Although some biomechanical aspects of peripheral nerves are known, the link between nerve biomechanics and tissue microstructure during development and maturation is poorly understood.

Method: Atomic force microscope (AFM) from JPK Instruments (Berlin, Germany). Confocal microscope SP5 (Leica Microsystems, Germany).

Aim: We used an AFM to investigate the mechanical properties of living mouse peripheral nerve tissue ex vivo at distinct stages of development, and correlated the elastic moduli with various cellular and extracellular aspects of the underlying tissue microstructure with confocal microscopy [1].

Results: Our data show that local nerve tissue stiffness is spatially heterogeneous and evolves biphasically during maturation. In addition, we found the intracellular microtubule network and the extracellular matrix collagen type I as major contributors to the nerves' biomechanical properties, but surprisingly not cellular density and myelin content as previously shown for the central nervous system.

Conclusions: Overall, these findings characterize the mechanical microenvironment that surrounds Schwann cells and neurons and will further our understanding of their mechanosensing mechanisms during nerve development. These data also provide the design of artificial nerve scaffolds to promote biomedical nerve regeneration therapies by considering mechanical properties that better reflect the nerve microenvironment.

Acknowledgements: This work was financially supported by the Innovative Medical Research Fund of the University of Münster Medical School (Project No. RO 51 17 01 to G.R.) and the Alexander-von-Humboldt Stiftung (Humboldt-Professorship to J.G.).

036 **TOWARDS UNDERSTANDING THE MECHANICAL FINGERPRINT OF REGENERATING SPINAL CORD TISSUE.**

S Möllmert[1], M Kharlamova[2], R Schlüßler[3], J Guck [1].*
[1]Max Planck Institute for the Science of Light and Max-Planck-Zentrum für Physik und Medizin, Erlangen, GERMANY; [2]Universität Tübingen, Tübingen, GERMANY; [3]Technische Universität Dresden, Dresden, GERMANY.

Background: Overcoming the irreversible loss of motor and sensory function after spinal cord injury (SCI) in mammals, including humans, appears to be one of the most staggering tasks in neuroscience and medical research. The vast amount of previous studies attempting to understand the mechanisms behind (un)successful regeneration of spinal cord tissue have focused on biochemical interactions between individual tissue components. Only recently, mechanical tissue properties and mechanical signaling have been given special emphasis in the context of nervous system development and pathology, and were proposed to have a determining influence on potential repair mechanisms. Zebrafish, in contrast to mammals, display functional recovery and tissue repair even after complete spinal cord transection.

Aims: To understand the role of mechanical tissue properties and mechanical signals after SCI, we quantified the mechanical properties of successfully regenerating zebrafish spinal cord tissue.

Methods and Results: Using atomic force microscopy (AFM)-enabled nanoindentation, we systematically assessed the pro-regenerative mechanical fingerprint of the lesioned spinal parenchyma during repair, and found a transient stiffening in adult specimens at a time point when re-growing axons actively traverse the injury site and form new synaptic connections [1]. Using Brillouin microscopy, we furthermore investigated the mechanical response to spinal cord injury in larval zebrafish *in vivo* and found a significant change of mechanical tissue properties immediately after the injury, which was followed by a gradual restoration of the Brillouin shift to pre-lesion levels [2].

Conclusions: Our results show that the regenerating spinal parenchyma provides distinct mechanical signals, at different developmental stages as well as at different time- and length scales, to cellular repair mechanisms occurring after SCI in zebrafish. Our work lays the foundation to not only understand the role of mechanical tissue properties and signaling during successful spinal cord repair, but potentially exploit the mechanical susceptibility of neural cells to advance therapeutic strategies after SCI in humans.

Acknowledgements: Financial support from the Alexander-von-Humboldt Stiftung (Humboldt-Professorship to J.G.), the Sächsisches Ministerium für Wissenschaft und Kunst (European Fund for Regional Development — EFRE to the light microscopy and electron microscopy facilities at CMCB, TU Dresden) and the European Commission through a European Research Council Starting Grant ("Light Touch", grant agreement number 282060 to J.G.) is gratefully acknowledged.

References: [1] Möllmert S, et al., Zebrafish spinal cord repair is accompanied by transient tissue stiffening, *Biophysical Journal*, 118:448-463, 2020. [2] Schlüßler R, Möllmert S, et al., Mechanical mapping of spinal cord growth and repair in living zebrafish larvae by Brillouin imaging, *Biophysical Journal*, 115:911-923, 2018.

008 **SUPER-RESOLUTION MAGNETIC RESONANCE ELASTOGRAPHY OF THE HUMAN BRAIN USING MULTIPLE FREQUENCIES.**

Aaron T. Anderson[1,2], Alexander M. Cerjanic[1], Bradley P. Sutton[1], Elijah E.W. Van Houten[3].*
[1]University of Illinois at Urbana-Champaign, 405 N Mathews Ave, Urbana, IL, 61801, USA; [2]Carle Foundation Hospital, 611 W Park St, Urbana, IL, 61801, USA; [3]Université de Sherbrooke, 2500 Boulevard de l'Université, Sherbrooke, QC J1K 2R1, CANADA.

Background: Improving the resolution is a goal of every imaging technique. For magnetic resonance elastography (MRE), improving resolution is achieved either during MR imaging acquisition of the displacement field or when estimating the material properties (or both). MRI resolution increases are achieved through custom imaging sequences and image reconstruction methods. Increasing resolution through material estimation relies on having additional data, material modeling, or both. The super-resolution method presented here uses multiple imaging acquisitions at three frequencies and the power-law relationship of viscoelastic materials to achieve resolution higher than acquired (i.e. super-resolution).

Aims: Use multiple frequencies of actuation during an MR imaging of the human brain with a power-law based nonlinear inversion algorithm to estimate super-resolution MRE material properties.

Methods: All data was acquired using a Siemens 3T Prisma whole-body MRI with a 64-channel head coil (Siemens Healthineers, Erlangen, GERMANY). External vibrations were applied posterior to the head using a commercial pneumatic actuator (Resoundant™, Rochester, MN, USA). The MRE acquisition was via a custom 3D multiband, multishot spiral sequence [1]. Multiple frequencies of actuation, 40, 50, and 60 [Hz], were acquired at 2 [mm] (iso) resolution and a single frequency, 50 [Hz], at 1.6 [mm] (iso) resolution. The material reconstruction uses a viscoelastic iterative nonlinear inversion (NLI) employing a conjugate gradient scheme and randomized domain decomposition [2]. Super-resolution is achieved by incorporating a power-law relationship for the frequency dependence of the viscoelastic material and leveraging the additional information to improve the resolution [3,4]. Previous studies have only had a single resolution of acquisition and this study includes higher-resolution acquisition for comparing with the super-resolution results.

Results: An NLI material reconstruction was performed on each mono-frequency: 40, 50, and 60 [Hz] at 2 [mm] and 50 [Hz] at 1.6 [mm]. The three frequencies were combined within the NLI framework to estimate material properties at the acquired resolution of 2 [mm] and a super-resolution of 1.6 [mm].

Conclusions: Mono-frequency estimation tends to smooth variations throughout the brain while adding additional frequencies improves the contrast when reconstructing at the acquired resolution and improves resolution and contrast for super-resolution. Additional frequencies at multiple resolutions will be acquired to further investigate the relationships between acquired resolution and resolution achievable with super-resolution NLI within specific regions of the brain.

Acknowledgements: Anderson is funded by the Carle Foundation Hospital and Beckman Institute Postdoctoral Fellowship. The Biomedical Imaging Center at the Beckman Institute provided MRI scanning time and Compute Canada (www.computecanada.ca) provided the computational resources.

References: [1] Johnson, C. *et al.*, Brain MR Elastography with Multiband Excitation and Nonlinear Motion-Induced Phase Error Correction, *24th Annual Meeting of the International Society for Magnetic Resonance in Medicine*, 2016.
[2] McGarry, M. *et al.* Multiresolution MR Elastography Using Nonlinear Inversion, *Medical Physics*, 2012; 39(10):6388-6396. [2] Testu, J. *et al.* Viscoelastic power law parameters of in vivo human brain estimated by MR elastography. *J Mech Behav Biomed*, 2017; **74,** 333 341. [3] Van Houten, E. *et al.* Power-Law Multi-Frequency MR Elastography of the Human Brain with Super-resolution Imaging via Non-Linear Inversion. *26th Annual Meeting of the International Society for Magnetic Resonance in Medicine*, 2018.

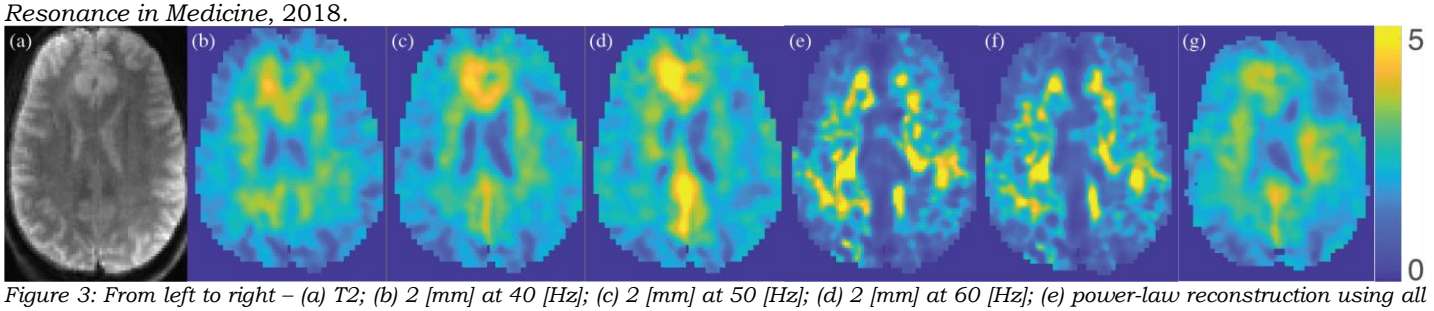

Figure 3: From left to right – (a) T2; (b) 2 [mm] at 40 [Hz]; (c) 2 [mm] at 50 [Hz]; (d) 2 [mm] at 60 [Hz]; (e) power-law reconstruction using all three frequencies at 2 [mm] at 50 [Hz]; (f) power-law reconstruction using all three frequencies at 1.6 [mm] at 50 [Hz]; (g) 1.6 [mm] at 50 [Hz].

013 **A SHEAR-ONLY SELECTIVE WAVE FIELD FILTER FOR IMPROVED SHEAR MODULUS ESTIMATION IN ELASTOGRAPHY.**

T Deruelle[1], O. Rouvière[2], S. Catheline[1], R Souchon[1].*
[1]INSERM, Université Lyon 1, Lyon, FRANCE ; [2]Hospices Civils de Lyon, Lyon, FRANCE.

Background: Magnetic resonance elastography is a technique to assess tissue mechanical properties by analyzing the behavior of propagating shear waves. Generally, waves are generated by a drum-like driver positioned in contact with the patient. As they are mainly acting in compression, the wavelengths close to the source appear longer than expected [1]. This would lead to overestimated shear modulus. To remove the longitudinal motion contribution, it is common to use the mathematical curl operator or high-pass filtering. However, these techniques induce either noise or a bias in the estimation.

Aims: The aim of this study is to present a new preprocessing to retrieve only the shear wave field from the measured displacement field, without loss of SNR, precision, accuracy nor resolution.

Methods: 2D visco-elastic simulations were performed with the Matlab Toolbox k-Wave. The simulated medium was a bilayer (c_s=2 [TOP] and 4m/s [BOTTOM], c_p=1500m/s, v=0.2Pa.s), and the source a vibrating membrane (simulating common pneumatic drivers) at 100Hz, positioned on top of the image. Helmholtz decomposition [2] is used to retrieve the shear-only wave field from the displacement.

The simulated displacement field was first degraded with three different levels of noise. Each one of these datasets underwent three different preprocessings (none, curl operator, proposed method). Finally, reconstruction from preprocessed fields to shear velocity was performed with Local Frequency Estimation.

Results: Without any preprocessing, the recovered values are overestimated (2.6 {2} and 5 {4} m/s as shown in Fig. 1,3). The use of the curl operator corrects for this bias but is quickly impaired by the noise (Fig. 1,3). With the exposed method, the recovered values are closer to expectation, and are more noise-resistant than when using no preprocessing (Fig. 1,3). All three methods present a similar resolution (~1cm) (Fig. 2).

Conclusions: If no preprocessing is performed, the recovered velocity is overestimated. In images with very high SNR, the use of the curl is preferred as it corrects for the overestimation, and is very quick. However, with noisy data, the proposed method is the best tradeoff as it is possible to recover the geometry of the tissues even at low SNR and limit the overestimation.

Acknowledgements: This work was supported by the RHU PERFUSE (ANR-17-RHUS-0006).

References: [1] M. Yin et al, "Diffraction-biased shear wave fields generated with longitudinal magnetic resonance elastography drivers," Magn. Reson. Imaging, 2008; 26(6): 770–780.
[2] Y. F. Gui et al, "A rigorous and completed statement on Helmholtz theorem," Prog. Electromagn. Res., vol. 69, pp. 287–304, 2007.

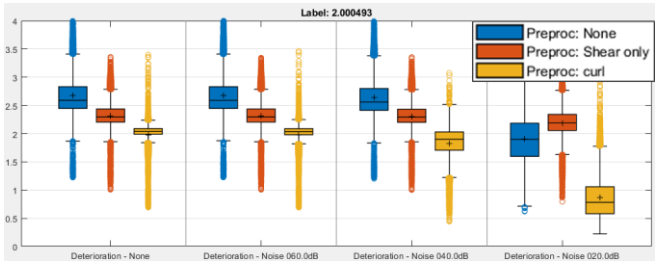

Figure 1: LFE reconstruction for the 2m/s medium at different levels of noise (∞, 60, 40, 20).

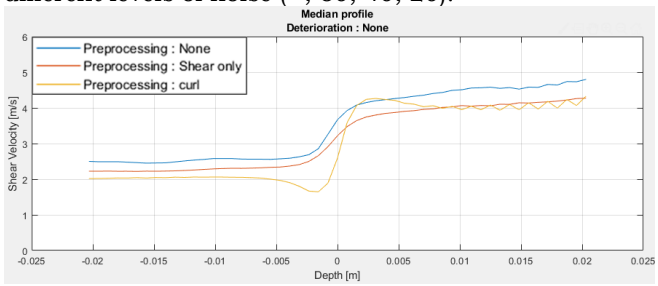

Figure 2: Median profile of the reconstructed velocities. **BLUE**: No preprocessing, **ORANGE**: with Shear only method, **YELLOW**: with curl operator

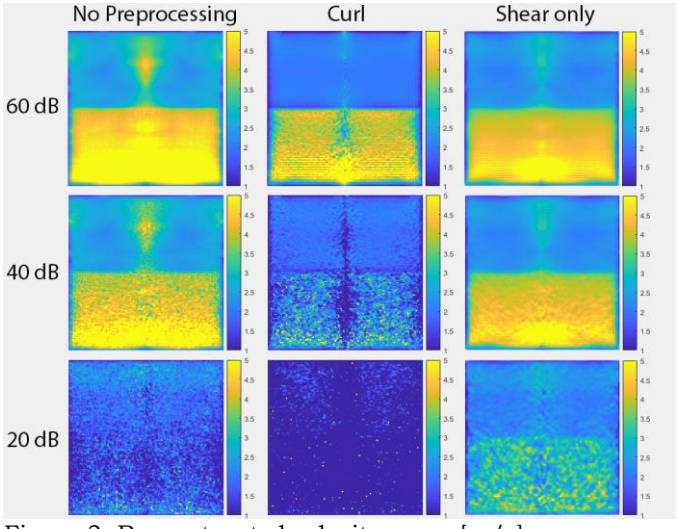

Figure 3: Reconstructed velocity maps [m/s]

* *indicates Presenter*

020 **ANATOMY GUIDED TOTAL VARIATION FOR ELASTICITY RECONSTRUCTION WITH BI-CONVEX ALTERNATING DIRECTION METHOD OF MULTIPLIERS.**

Shahed K Mohammed[1], Mohammad Honarvar[1], Piotr Kozlowski[1], Septimiu E Salcudean[1].*
[1]Electrical and Computer Engineering, The University of British Columbia, 2332 Main Mall, Vancouver, BC, V6T 1Z4, CANADA; [2] UBC MRI Research Centre, The University of British Columbia, 2350 Health Sciences Mall., Vancouver, BC, V6T 1Z3, CANADA.

Background: Magnetic resonance elastography (MRE) captures the tissue displacement in the phase of magnetic resonance imaging (MRI). The reconstructed elasticity map from the displacement suffers from a lack of anatomical information due to the ill-posedness of the elasticity reconstruction problem. In such cases, MRI magnitude image provides additional anatomic details for diagnostics. As the MRI magnitude image is registered with the displacement data, the MRI magnitude can be used as an anatomical prior (AP) in reconstruction algorithm such as ERBA [2], which would increase the contrast to noise ratio (CNR). MR magnitude has been used as a soft prior in the nonlinear inversion of elasticity maps [1], but was not aimed to promote sparsity such as, for example, a total variation method (TV). [2,3].

Aims: To evaluate the feasibility of AP guided TV for ERBA [3], obtaining the AP from MRI magnitude image.

Methods: The elasticity map is reconstructed by solving the optimization problem given below [3], where μ is shear modulus, v is the measured displacement, and u is the calculated displacement from a bi-convex finite element model A(u, μ) representing the 3D wave constraint model [2]:

$$(\mu, u) = \underset{\mu, u}{argmin} \left\{ \frac{1}{2} ||u - v||_2^2 + \gamma ||w|\nabla\mu|||_1 \right\} \quad \text{, such that } A(u, \mu) = 0 \text{ and } w = \frac{\varepsilon}{(\varepsilon^2 + |\nabla m|^2)^{\frac{1}{2}}}$$

Here, the second term represents the anatomy guided total variation, where the weights w are related to the gradient of the magnitude image m. ε is a regularization parameter that controls the effect of magnitude image [4]. The algorithm is solved using alternating direction method of multipliers, where the anatomical guided total variation is implemented with fast gradient projection method.

The reconstruction performance was evaluated on a numerical liver shaped phantom with two inclusions. Corresponding displacement pattern was simulated in COMSOL Multiphysics 5.4a. The magnitude image had similar structure as the ground truth elasticity map but with different scale. We also tested the reconstruction performance on an agar phantom with irregular shaped inclusion. Different concentrations were used for the background and inclusion. Also, a T2 contrast agent was used in the inclusion solution to provide contrast in the magnitude image. The phantom was imaged with a Philips Achieva 3.0T MR system, with a harmonic excitation at 300 Hz induced by a Lorentz coil. The reconstruction performance is compared between local frequency estimation (LFE), 3D ERBA [2], and proposed method (3D ERBA+AP).

Results: Using AP gives lower root mean square error (RMSE). Also, compared to 3D ERBA, 3D ERBA+AP increased contrast to noise ratio (CNR) by 4dB for the hard inclusion and 11 dB for the soft inclusion. The use of AP reduced the intra-class variation and provided better delineation of the inclusion. In the agar phantom, similar reduction in intra-class variation is seen. Moreover, the area under the curve (AUC) for detecting the inclusion in the agar phantom is also increased to 0.97 from 0.96 by using the 3D ERBA+AP.

Conclusions: These preliminary results suggest that incorporating anatomical information from the magnitude image with anatomy guided total variation can improve elasticity reconstruction performance.

Acknowledgements: This work was funded by NSERC, CIHR and the Charles Laszlo Chair in Biomedical Engineering held by Professor Salcudean.

References: [1] M. McGarry et al. IEEE Trans. on Medical Imaging, vol. 32, no. 10, page: 1901-1909; [2] S. Mohammed, et al. In 2019 IEEE 16th International Symposium on Biomedical Imaging (ISBI 2019) (pp. 1683-1687); [3] S. Mohammed et al. ISMRM 2020 - 28th Annual Meeting & Exhibition, Apr 2020, Sydney, Australia; [4]M. Ehrhardt et al. (2016), SIAM Journal on Imaging Sciences, vol 9, no. 3, pp.1084-1106

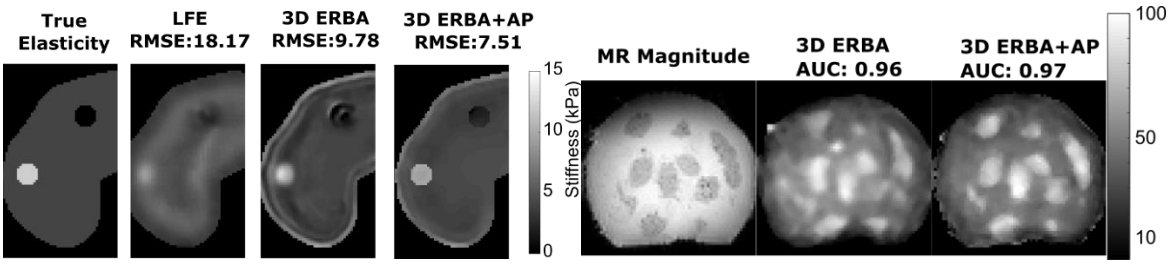

(a) (b)

Fig1: Comparison of elasticity reconstruction in (a) Numerical phantom and (b) Agar Phantom. Both result show that incorporating AP improves the reconstruction quality by reducing intra-class

026 **AXIAL AND TORSIONAL ACTUATION FOR MAGNETIC RESONANCE ELASTOGRAPHY OF ANISOTROPIC SAMPLES.**

*Martina Guidetti[1], Chiara Gambacorta[1], Dieter Klatt[1], Thomas J. Royston[1, *].*
[1]University of Illinois at Chicago, Chicago, Illinois, USA.

Background: Elastography is a non-invasive imaging technique first implemented using Magnetic Resonance Imaging in 1995 by Muthupillai et al. for evaluating shear viscoelastic properties of soft tissues [1]. After successive developments, elastography became a reliable improvement upon the traditional methods for soft tissue stiffness evaluation, such as qualitative manual palpation -- when the tissue is within reach -- or invasive biopsy. In particular, Magnetic Resonance Elastography (MRE), has shown promising results for the detection and monitoring of many diseases affecting isotropic soft tissues, thanks to its ability to offer deep tissue penetration approaching sub-millimeter resolution [2]. Research is still early stage for anisotropic tissues where material properties are direction-dependent, such as in striated (skeletal and cardiac) muscle. In these cases, MRE evaluations become more complex and there is the need/potential of extraction of more information.

Aims: The aim of our current research is the implementation in a table-top MRI system with an interchangeable MRE setup for both axial and torsional actuation of samples. Its application to anisotropic samples, such as skeletal muscle, would enable measurement of direction-dependent properties.

Methods: Multifrequency MRE experiments in the range from 500 to 2000 Hz are run on mouse calf and thigh muscles and on a muscle-mimicking phantom made of PDMS fibers (diameter of 100 um) in a soft plastic matrix obtained through an Embedded Direct Ink Writing technique [3] implemented with an automated dispensing system (E3V, Nordson EFD). The fibers are lying in the cross-sectional plane of the test tube so that it is possible to excite both slow and fast shear waves interchanging between the axial and torsional actuation. The sample is subjected to radially converging axial and torsional transverse wave motion, respectively. The axial excitation is obtained via the use of a piezoelectric actuator, while torsional excitation is implemented via a stepper motor. Mechanical vibrations are synchronized with the Motion Encoding Gradient (MEG) used to encode the motion into the MRI phase images. The wave images obtained from the MRE experiments are spatially distorted by the anisotropic ratio calculated with the Transformation Elastography (TE) technique [4,5]. The result of this operation consists in isotropic wave images on which conventional reconstruction techniques can be applied to generate the elastograms.

Results: The reconstruction algorithm based on the TE approach led to a more accurate estimation of the anisotropic shear storage and loss moduli than the estimations based on isotropic assumptions. Experimental results demonstrate the capability of the novel set-ups for axial and torsional excitations when compared to the pattern obtained from numerical studies on similar anisotropic geometries.

Conclusions: Axial and torsional actuations of anisotropic samples offer the possibility to get more accurate estimations of the direction-dependent mechanical properties of anisotropic samples, information that may have clinical value for the early detection and monitoring of diseases affecting skeletal muscle tissue.

Acknowledgements: The authors acknowledge funding from NSF Grant No. 1852691 and NIH Grant No. AR071162.
References: 1. Muthupillai R.,Science,1195,269,5232. 2. Hiscox L.V.,NeuroBiol. Aging,2018,65:158-167. 3. Truby R.L.,Advanced Materials,2018,30, 15, 1706383. 4. Guidetti M.,J. Acous. Soc. Am.,2019,146:EL451-457. 5. Guidetti M.,J Acous. Soc. Am.,2018,144,2312-23.

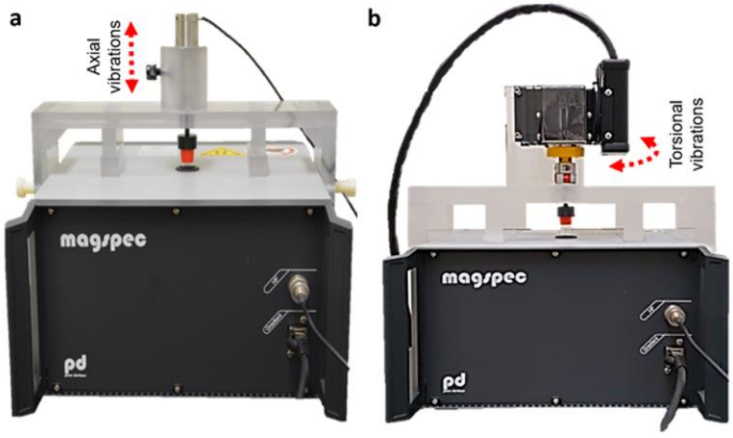

Figure. MRE setups mounted on tabletop MRI system by Pure Devices GmbH, Würzburg, Germany hosting piezoelectric actuator for axial MRE experiments (a) and stepper motor for torsional MRE experiments (b).

028 **MULTIFREQUENCY MR ELASTOGRAPHY REVEALS DIFFERENCES IN MURINE CORTICAL AND HIPPOCAMPAL MECHANICAL HETEROGENEITY.**

Shreyan Majumdar[1], Dieter Klatt[1].*
[1]Richard and Loan Hill Department of Bioengineering, University of Illinois at Chicago, 851 S Morgan St, Chicago, Illinois, 60607, USA.

Background: Magnetic resonance elastography (MRE) involves mechanical excitation of biological tissue through harmonic vibrations. The resulting wave propagation is analyzed to quantify mechanical properties such as the shear modulus. MRE is commonly applied to murine cerebral research where disease related mechanical changes are assessed, especially inside the cerebral cortex, comprising of the outer cortical plate and inner hippocampal regions. Multiple studies have shown that the hippocampal region in the brain is stiffer than the outer cortical region [1].

Aims: A cerebral MRE study was performed to estimate MRE parameters of murine brain sub-regions by using a multifrequency approach known as Multi Dual Elastovisco (MDEV) inversion [2]. MDEV inversion has demonstrated greater stability in generating reliable parameter values inside small regions of interest (ROI) by compensating for frequency dependent regions of noise, and shear wave interferences [3].

Methods: Cerebral MRE scans were performed on B6SLJ wild-type mice (n = 10) using a 9.4T Agilent preclinical MRI scanner at the University of Illinois at Chicago. Data was acquired at three actuation frequencies of 900, 1000 and 1100 Hz with a spin-echo based SLIM-MRE sequence [5]. The magnitude of the complex shear modulus, $|G^*|$ was determined by combining the multifrequency data as shown in equation 8 in Hirsch *et al.* Using a Wilcoxon matched-pairs signed rank test, $|G^*|$ and its spatial variation in the form of the spatial coefficient of variation (CV), was calculated inside the cortical and hippocampal sub-regions of the brain in each mouse (represented by ROIs CC and HC respectively in Figure 1).

Results: $|G^*|$ values inside HC were higher compared to the values calculated inside CC. On inspecting the CV values, they were significantly greater ($P < 0.01$) in the outer cortical region compared to the hippocampal region as shown in Figure 2.

Conclusions: Results demonstrated the hippocampal region HC was stiffer compared to the cortical region CC. On the other hand, the outer cortical region highlighted greater stiffness heterogeneity with significantly higher CV being reported. This can potentially be due to ROI CC being a part of the outer neocortex, which has more layers and neurons compared to the inner allocortex, which contains the hippocampal region HC [5]. The coefficient of variation of mechanical properties can potentially be a biomarker for conditions where the mechanical heterogeneity changes during disease progression.

Acknowledgements: This research is supported by a grant through the University of Illinois at Chicago Chancellor's Discovery Fund for Multidisciplinary Research.

References: [1] Bigot M, Chauveau F, Beuf O, Lambert SA: Magnetic Resonance Elastography of Rodent Brain. *Front Neurol* 2018; 9:1010. [2] Hirsch S, Guo J, Reiter R, et al.: MR Elastography of the Liver and the Spleen Using a Piezoelectric Driver, Single-Shot Wave-Field Acquisition, and Multifrequency Dual Parameter Reconstruction. *Magn Reson Med* 2014; 71:267–277. [3] Majumdar S, Klatt D: Comparison of MR Elastography data from the mouse brain using single-frequency algebraic inversion and MDEV inversion. In *IEEE EMBS Int Conf Biomed Heal Informatics*. Chicago, IL, USA, 19-22 May; 2019. [4] Kearney SP, Majumdar S, Royston TJ, Klatt D: Simultaneous 3D MR elastography of the in vivo mouse brain. *Phys Med Biol* 2017; 62:7682–7693. [5] Klingler E: Development and organization of the evolutionarily conserved three-layered olfactory cortex. *eNeuro* 2017; 4: ENEURO.0193-16.2016.

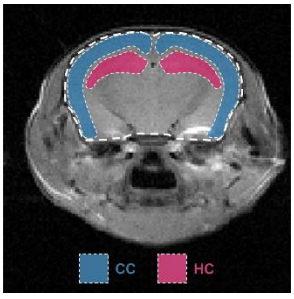

Figure 1. Regions of interest HC (in red) and CC (in blue) inside the mouse brain over which magnitude of the complex shear modulus |G*| and its spatial CV was calculated.

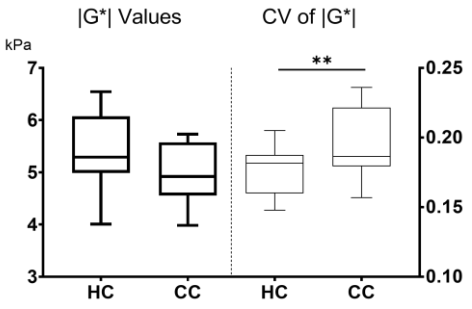

Figure 2. The magnitude of the complex shear modulus |G*| and its spatial coefficient of variation (CV) inside ROIs HC and CC.

* *indicates Presenter*

021 **A COMPREHENSIVE LIVER VISCOELASTIC CHARACTERIZATION; ASSESSMENT OF SHEAR WAVE (GROUP AND PHASE) VELOCITY, ATTENUATION, DISPERSION, AND THEIR RELATIONSHIP UNDER A POWER LAW MODEL.**

J Ormachea[1], KJ Parker[1].*

[1]University of Rochester, Rochester, NY, USA 724 Computer Studies Building, Box 270231, Rochester, NY 14627, USA.

Background: The parameters that can now be measured with shear wave elastography include shear wave speed (SWS), shear wave dispersion (SWD) and attenuation (SWA). Some tissues exhibit a rheological power law behavior. Thus, SWD is linked to SWA via the Kramers-Kronig relations and the power law coefficient [1]. In that context, dispersion of phase velocity in a liver should be linked to the lossy, attenuating nature of the tissue.

Aims: This study independently measured SWS, SWD, SWA, and the power law coefficient (PLC) which is directly related to SWD. Dispersion was also used to approximate the SWA as another method to calculate the SWA parameter.

Methods: Estimators of group-SWS and SWA are derived from the analytical transform solutions to the 2D wave equation [2], the phase-SWS was derived by analyzing the 2D Fourier transform (2D-FT) of the particle velocity and measuring the corresponding spatial frequency at the peak 2D-FT signal for each temporal frequency [3]. Then, SWD and PLC were obtained by fitting the phase-frequency curves with a linear and power law equation [1]. All these parameters were assessed in 20 *in vivo* livers using a Samsung RS85 ultrasound scanner. The liver biopsy samples were sent for analysis ordered by the referring physician.

Results: Across the population studied and as illustrated in Figure 1, SWS varied from 1.2 to 2.5 m/s, SWD from 2 to 20 m/s/kHz, PLC from 0.1 to 0.4, and SWA estimated at a shear wave frequency of 150 Hz varied from 3 to 25 dB/cm, with the lower values of SWD, PLC, and SWA associated with non-steatotic livers. Finally, median SWS and PLC values were used to approximate the corresponding SWA with reasonable agreement with the elastography measurements of SWA (black line in figure 1d).

Conclusions: A complete viscoelastic tissue characterization was obtained and correlated with different fibrotic and steatotic stages. This preliminary study indicates the possible utility of the measurements for non-invasive and quantitative assessment of steatosis using shear wave dispersion and attenuation, so long as these materials are reasonably approximated by power law model.

Acknowledgements: We are grateful for support from Samsung Medison and for the loan of equipment. We also thank Dr. D. Rubens and Dr. A. Sharma for clinical data acquisition and Z. Hah Ph.D. for his technical support and suggestions.

References: [1] Parker K J et al. 2018 Group versus phase velocity of shear waves in soft tissues Ultrason Imaging. [2] Parker K J, et al. 2018 Analysis of Transient Shear Wave in Lossy Media Ultrasound Med Biol. [3] Nenadic I et al. 2013 Model-free quantification of shear wave velocity and attenuation in tissues and its in vivo application J Acoust Soc Am.

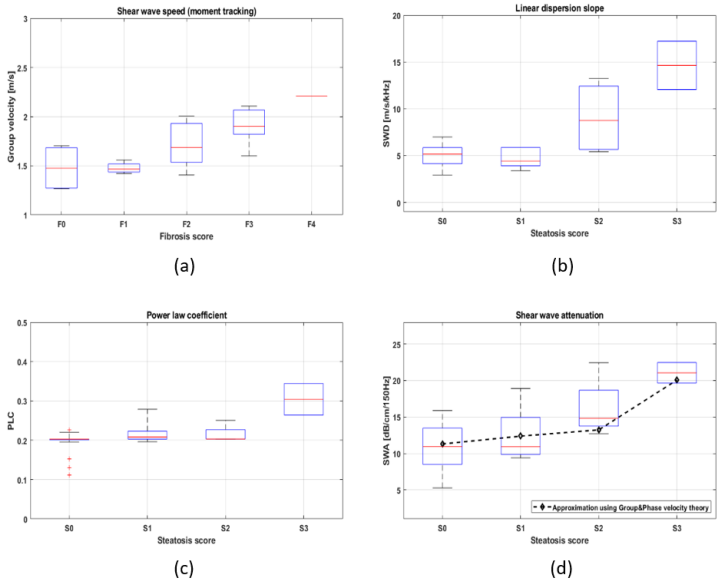

Figure 1. (a) Group-SWS as a function of fibrosis score. (b-d) SWD, PLC, SWA as a function of steatosis score, respectively. These indicate some trends: increasing speed with increasing fibrosis score and increasing SWD, PLC, SWD with steatosis score. (d) In addition, dashed line indicates the SWA results using median SWS and PLC and the power law approximation.

* *indicates Presenter*

038 **ULTRASOUND ECHO AND PHOTOACOUSTIC VECTORAL DOPPLER IMAGING FOR HUMAN IN VIVO SOFT TISSUE AND BLOOD.**

Chikayoshi Sumi[1], Ryo Nakagawa[1], Kanta Ueno[1]*
[1]Sophia University, 7-1, Kioi-cho, Chiyoda-ku, Tokyo, JAPAN.

Abstract Body With ultrasound (US) echo and/or photoacoustic (PA) signals, in addition to a high accuracy vectoral Doppler imaging, a high accuracy strain (rate) tensor imaging is performed both for a human *in vivo* wrist soft tissue motion and the arterial blood flow. An automatic detection method is reported in detail regarding the boundary between an arterial vessel and a lumen using high intensity PA signals generated at the blood flow positions adjacent to the vessel. The method allows imaging the dynamics of respective soft tissue and slow blood. Simultaneous imaging is also performed for the soft tissue and the blood.

Background: We have been developing high accuracy ultrasonic (US) Doppler methods for observing a human *in vivo* tissue displacement, velocity or acceleration vector, and a strain or strain rate tensor [IEICE 1995 ; IEEE UFFC 1999; 2008; JJAP 2018, etc.]. Recently we started to observe the mechanical quantities based on photoacoustic (PA) imaging, and we reported the observations of an axial strain [IEEE EMBS 2018] and a strain tensor (a displacement vector) [IEEE EMBS 2019 ; IUS2019] for human *in vivo* superficial wrist tissues. Only a few *in vivo* PA imaging had been performed for observing a soft tissue strain and a blood flow. We had previously proposed to clinically perform simultaneous Doppler observations for a soft tissue and a blood, and such observations were reported, e.g., at IEEE EMBS 2019; IUS2019.

Aims: At first, the simultaneous US or PA vectoral Doppler observation is reviewed. Next, a simple PA method for detecting a boundary between an arterial vessel and a lumen is reported in detail. The method allows US and PA Doppler imaging of each dynamics of a soft tissue and a slow blood.

Methods: A Commercial PAI system, AcousticX (CYBERDYNE, Inc., Japan), was used. The volunteer was 54-years-old male. Via a water bag (10 mm depth), plane waves of an LED light (850nm, totally 400 μJ) and an ultrasound (a linear-array type with a nominal freq., 7 MHz) were interchangeably transmitted to his superficial wrist tissues. Generated US-echo and PA frame rates were 15.4 Hz. By performing a reception dynamic focusing, the lateral modulations (LMs) with crossed beams (±20 or ±10 degrees) and the nonsteered beams were respectively generated over the ROI (40 mm depth). For a 2D displacement vector measurement, the 2D autocorrelation method [IEEE UFFC 2008] was used (a window size, 0.77×3.15 mm^2). For the differentiation between the arterial blood and the surrounding soft tissue, the blood flow positions adjacent to the blood vessel were estimated by detecting large PA intensity changes along the depth direction.

Results: Fig. 1 shows the snapshots of simultaneous vectoral Doppler imaging obtained from nonsteered, (a) rf-echo and (b) PA data, i.e., those of axial and lateral displacements and shear strains (non-median-filtered results of those of IEEE EMBS 2019). Others including accelerations are omitted. Various dynamic data were obtained, e.g., shear phenomena at the vessel (Fig. 1). The boundary detection was also successfully performed. Lateral measurements were substantially stabilized by increasing steering angles up to ±20 degrees (omitted). The effects in disregarding a lateral low frequency spectra [Rep in Med Imag:5, 57-101, 2012] will also be reported.

Conclusions: In the practical applications of rf-echo and PA vectoral Dopplers, such mechanical quantities can be respectively imaged in a real time; and the quantities measured from rf-echo and PA data can also be imaged interchangeably and/or in a slow motion mode since they have more information about the tissue dynamics than the past color Doppler or Elastography. Different colors may also be used for visualizing the dynamics of a soft tissue and a blood including fast one. Reconstructions about elasticity, visco-elasticity, viscosity and a pressure will also be reported for the tissues. In the near future, reported will be the results obtained for an arteriosclerosis, a thrombus, a stenosis, a cancerous lesion with a circulatory, and a fatty tissue, etc.

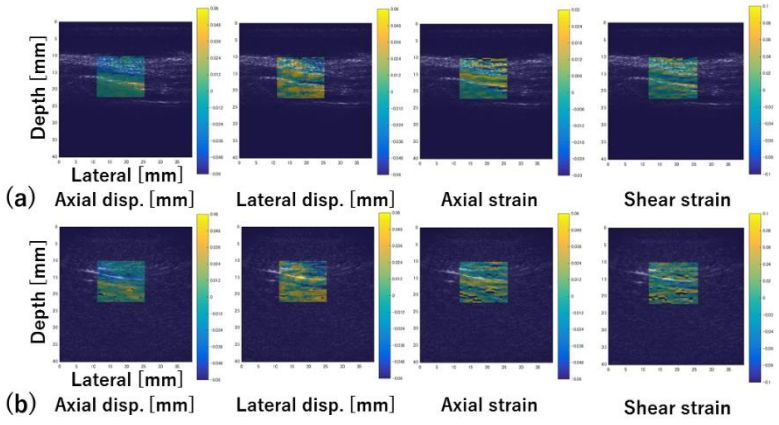

Fig. 1. Vectoral imaging. (a) US and (b) PA.

* *indicates Presenter*

023 **A DISPERSIVE ELASTOGRAPHY PHANTOM WITH VISCOELASTIC PROPERTIES SIMILAR TO HEALTHY LIVER.**

Anna Morr[1], Helge Herthum[1], Felix Schrank[1], Steffen Görner[1], Jürgen Braun[2], Ingolf Sack[1], Heiko Tzschätzsch[1].*

[1]Department of Radiology, Charité – Universitätsmedizin Berlin, Berlin, GERMANY; [2]Institut of Medical Informatics, Charité – Universitätsmedizin Berlin, Berlin, GERMANY.

Background: Viscoelastic phantoms are necessary for the technical development and comparison of elastography methods. However, current elastography phantoms are non-dispersive [1] and do not fit to the viscous and elastic properties of healthy *in vivo* liver (Figure 1) [2-8]. The comparison of elastography methods, which use transient stimulations, is especially limited due to the viscoelastic dispersion of biological tissue.

Aims: To develop a phantom with viscoelastic properties similar to *in vivo* healthy liver tissue which is suitable for ultrasound and MR elastography.

Methods: A phantom was produced from polyacrylamide, using microcrystalline cellulose as a scatter for ultrasound. The proposed phantom was investigated with shear oscillatory rheometry (5 – 60 Hz), time-harmonic ultrasound elastography (THE) (20 – 200 Hz), 3-Tesla MR-Elastography (20 – 200 Hz) and 0.5-Tesla tabletop MR elastography (225 – 3000 Hz). In addition, the reproducibility of phantom production was tested 2 times using 0.5-Tesla tabletop MR elastography. Shear wave speed (SWS) and shear wave damping (SWD) (SWD not shown in figure 1) were reconstructed for each frequency using plane wave fits or Bessel functions.

Results: The SWS of the proposed phantom well agrees with *in vivo* properties over a wide frequency range. The fractional springpot model (complex shear modulus $G^* = \mu^{1-a} \cdot (i\,\omega\,\eta)^a$; ρ = 1000 kg / m^3, η = 1 Pa s) fitted to SWS and SWD yielded a = 0.427 ± 0.004 and μ = (6.49 ± 0.09) kPa. The reproducibility of the phantom production gave a mean absolute deviation of 0.2 m/s (8 % respectively) for SWS.

Conclusions: The proposed polyacrylamide phantom provides a realistic SWS-dispersion which agrees to *in vivo* data published in the literature by different elastography techniques, is suitable for MR and ultrasound elastography and can be produced in a reproducible way. Collectively, the proposed phantom provides an important test material to make elastography more reproducible, consistent and diagnostically accurate.

References: [1] Schrank et al. 1st International MRE Workshop & 1st BIOQIC Day, "Heparin as MRE phantom material with viscoelastic powerlaw properties similar to soft biological tissues" 2017 Sep
[2] Chen et al. Radiology. 2013 Mar;266(3):964-70. doi: 10.1148/radiol.12120837. Epub 2012 Dec 6
[3] Muller et al. Clinical Trial Ultrasound Med Biol. 2009 Feb;35(2):219-29
[4] Nightingale et al. IEEE Trans Ultrason Ferroelectr Freq Control. 2015 Jan;62(1):165-75
[5] Tzschätzsch et al. Med Image Anal. 2016 May;30:1-10. doi: 10.1016/j.media.2016.01.001. Epub 2016 Jan 13
[6] Tzschätzsch et al. Ultrasound Med Biol. 2016 Nov;42(11):2562-2571. doi: 10.1016/j.ultrasmedbio.2016.07.004
[7] Hudert et al. Invest Radiol. 2019 Apr;54(4):198-203. doi: 10.1097/RLI.0000000000000529
[8] Dittmann et al. Magn Reson Med. 2016 Oct;76(4):1116-26. doi: 10.1002/mrm.26006. Epub 2015 Oct 20

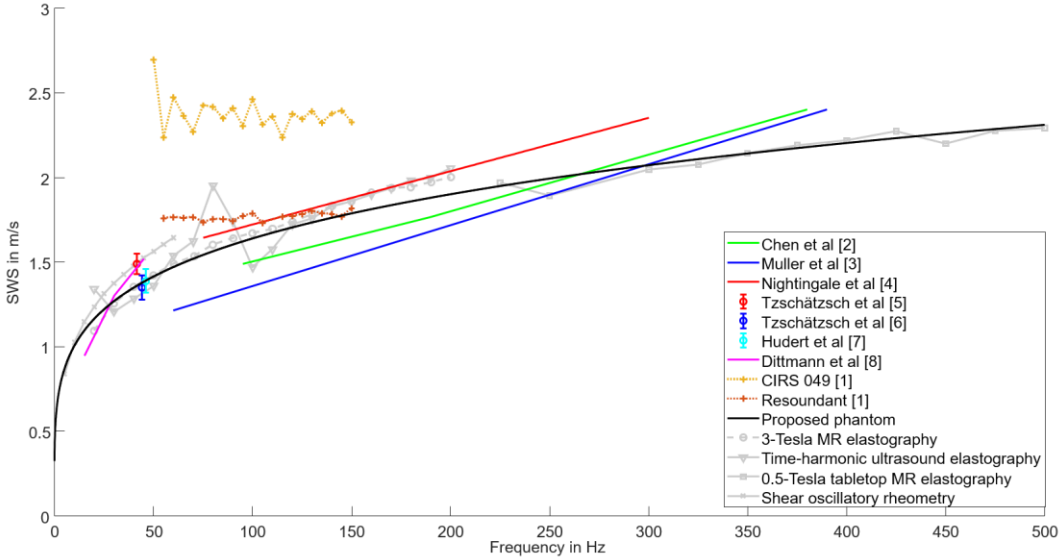

Figure 4 SWS over frequency for in vivo healthy liver, CIRS Model 049 and Resoundant Inc. (Rochester, Minnesota, USA) phantom and rheological fractional model of the proposed phantom.

* *indicates Presenter*

010 **OPTICAL COHERENCE ELASTOGRAPHY AND BRILLOUIN SPECTROSCOPY FOR BIOMECHANICAL MAPPIN OF TISSUES.**

*Kirill V. Larin.**
University of Houston, Houston, TX, USA.

Background: This presentation describes recent progress on combining optical coherence elastography (OCE) and Brillouin microscopy[2] (BM) for biomechanical mapping of (1) mammalian embryos and (2) crystalline lens of the eye. Embryonic development involves the interplay of driving forces that shape the tissue and the mechanical resistance that the tissue offers in response. While increasing evidence has suggested the crucial role of physical mechanisms underlying embryo development, tissue biomechanics is not well understood due to the lack of non-contact techniques that can quantify the stiffness of tissue *in-situ* with 3D high-resolution. Here we used two all-optical techniques, OCT and BM, to map the longitudinal modulus of the tissue from mouse embryos *in-situ*. Assessing the biomechanical properties of the crystalline lens can provide crucial information for diagnosing disease and guiding precision therapeutic interventions. Existing noninvasive methods have been limited to global measurements. Here, we demonstrate the quantitative assessment of the elasticity of the crystalline lens with multimodal optical elastography, combining dynamic wave based OCE and BM, overcoming the drawbacks of each modality.

Methods: A home-built Brillouin microscopy system was based on a single-mode 660 nm laser (Torus, Laser Quantum Inc., Fremont, CA) and a two stage VIPA (virtually imaged phased array) spectrometer. The incident power on the sample was ~24 mW. The Brillouin microscope utilized a 4X microscopic objective with a 0.12 numerical aperture to focus the laser beam into the sample. The lateral resolution was ~9 μm and axial resolution was ~70 μm, as defined by the Rayleigh range, and were measured using a beam viewer (LaserCam-HR II, Coherent Inc., CA, USA).

The OCE system was based on a phase-stabilized swept source OCT system with a focused micro air-pulse to induce elastic waves in the sample (figure 2). The swept source laser had a central wavelength of 1310 nm, scan range of ~150 nm, and scan rate of 30 kHz. The axial resolution was ~12 μm, and the transverse resolution was ~16 μm, both in air.

Results: In our embryonic studies using a mouse model, we initially observed tissue stiffening of the neural folds by comparing embryos with open (E 8.5) and closed (E 9.5) neural tubes (Figure 1). The representative morphologies of two embryos was imaged with OCT (Fig.1a-2b), where the open and closed neural tube can be clearly seen. As shown in the co-localized Brillouin images, the closed neural tube (Fig. 1d) is distinctly stiffer than the opened neural tube (Fig.1c). We quantified the averaged Brillouin shift of the whole neural tube region (Fig.1e), and the results suggest ~80% relative increase of Young's modulus ($\delta E'/E'$).
In our lens studies, we first experimentally determined the parameters of Brillouin modulus versus Yong's modulus from the lens surface. Once these parameters were known, the Young's modulus for the entire lens can be deduced based on the mapping of Brillouin modulus, as shown in Figure 2.

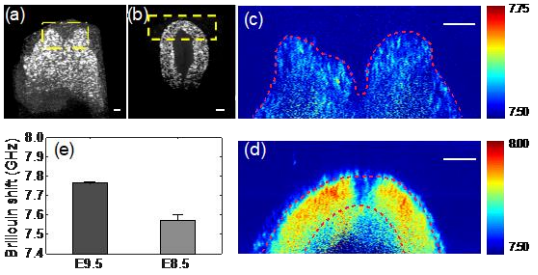

Fig 1. Tissue stiffening of the neural tube during embryonic development. (a) and (b) are OCT cross-sectional images of representative E8.5 and E9.5 embryos. Dashed yellow boxes indicate the imaged region by Brillouin microscope. (c) and (d) are corresponding Brillouin images at the same cross-sections; the red dashed lines indicate the neural folds. (e) averaged Brillouin shift of the neural tube tissues of E8.5 (n=2) and E9.5 (n=2) embryos. All scale bars are 100 μm.

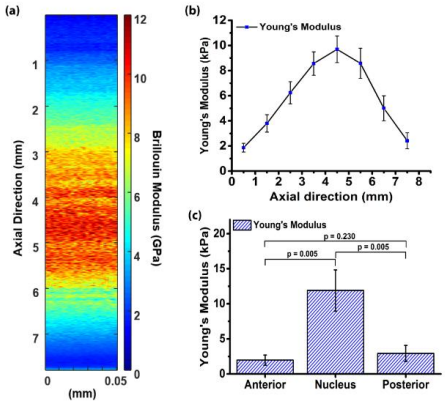

Fig. 2(a) Distribution of the derived Young's modulus from the correlation between Brillouin and Young's modulus along the optical axis. (b) Distribution of the Young's modulus along the optical axis of a typical lens where the error bar is the average over the local 1 mm region of (a). (c) The derived Young's modulus of anterior, posterior and central parts averaged for all 6 lenses used in the study.

Conclusions: Obtained results suggest that OCE and Brillouin microscopy provide complementary information and can be used for quantitative mechanical mapping of tissues.

Acknowledgements: This work is supported, in part, by the National Institute of Health with grants R01HD081216, R01HD083809, P01HD067244, R01HL120140, K25EB015885, R33CA204582, R01HD086765, R01EY022362, R01HD095520, R01EY030063, and P30EY007551.

* *indicates Presenter*

029 **WAVE-BASED OPTICAL COHERENCE ELASTOGRAPHY OF THE ANTERIOR EYE: EXPLORING THE BIOMECHANICS OF LIMBUS.**

Fernando Zvietcovich[1], Achuth Nair[1], Manmohan Singh[1], Salavat R. Aglyamov[2], Michael D. Twa[3], and Kirill V. Larin[1].*

[1]Department of Biomedical Engineering, [2]Department of Mechanical Engineering, [3]College of Optometry, University of Houston, Houston, Texas, USA.

Background: The biomechanical properties of the corneo-scleral limbus when the eye-globe deforms is largely unknown. Previous results using numerical simulations reported that, given the Young's moduli of cornea and sclera, an optimal limbal elasticity can be found to preserve vision quality when the eye is deformed [1]. To the best of our knowledge, there is no experimental evidence that demonstrates this mechanical compensation mechanism of the limbus. Wave-based optical coherence elastography (OCE) has been mostly applied to the study the biomechanics of central cornea [2]. However, OCE of the limbal transitional region between the cornea and sclera presents a difficult challenge due to high mechanical heterogeneity causing back reflection and attenuation of waves, and the presence of smaller and stiffer features such as the limbus.

Aims: The aim of this research is to measure elasticity changes of the anterior eye when subjected to different intraocular pressures (IOP). In addition, elasticity changes of the limbal region with respect to the elasticity variations in the neighboring corneal and scleral regions are evaluated.

Methods: Lamb waves (800 Hz) were mechanically induced in the sclera near the corneo-sclera limbus (Fig. 1a) of in situ porcine eye-globes (n = 4) and imaged using a phase-sensitive optical coherence tomography system (PhS-OCT). Spatially distributed speed maps were calculated along corneal, limbal, and scleral regions when the eyes were subjected to five different IOP-levels (10, 15, 20, 30, 40 mmHg). Finite elements analysis (FEA) of the same regions under the same excitation conditions were conducted for investigating the relationship between elastic (Lamb) wave speed and Young's modulus in the anterior eye.

Results: FEA demonstrated that the Young's moduli of the cornea, sclera, and limbus are strongly related to the phase velocity of the Lamb waves produced at 800 Hz in the anterior eye. 2D speed maps ((Fig. 1b)) revealed a marked heterogeneity and non-linearity of wave speed across the corneal-limbal-scleral region. We report a total change in wave speed in the limbus of Δc ~18.46 m/s greater than in the cornea (Δc ~12.6 m/s) and sclera (Δc ~8.10 m/s) for the same IOP change range. Finally, we found that wave speed in the limbus region surpassed the wave speed in sclera when the IOP increased more than ~25 mmHg (Fig. 1c).

Conclusions: We demonstrated that, when the eye-globe is deformed by an increase of IOP, the limbus is highly non-linear compared to the cornea and sclera, suggesting that the limbus acts as an important support structure between the cornea and sclera.

Acknowledgements: This study was funded, in parts, by the National Institute of Health grants R01EY022362, R01HL130804, R01HD096335, and P30EY007551. F.Z. is supported by the 2020 SPIE-Franz Hillenkamp Fellowship.

References:

[1] M. Asejczyk-Widlicka, D. W. Śródka, H. Kasprzak, and B. K. Pierscionek, "Modelling the elastic properties of the anterior eye and their contribution to maintenance of image quality: the role of the limbus," Eye 21, 1087-1094 (2007).

[2] M. A. Kirby, I. Pelivanov, S. Song, L. Ambrozinski, S. J. Yoon, L. Gao, D. Li, T. T. Shen, R. K. Wang, and M. O'Donnell, "Optical coherence elastography in ophthalmology," J Biomed Opt 22, 1-28 (2017).

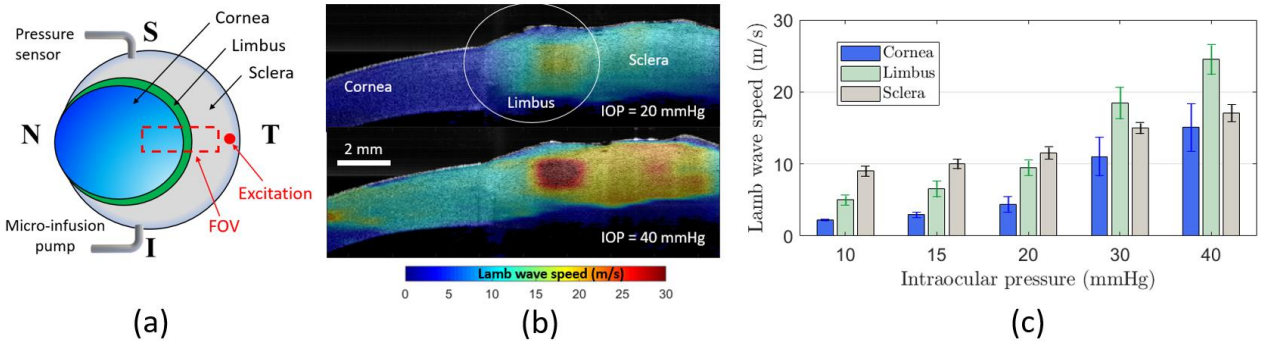

Figure 1. (a) 3D schematic of the scanning field-of-view (FOV) in an ex vivo porcine eye cannulated with two needles for artificial IOP control. N: nasal, T: temporal, S: superior, I: inferior. (b) 2D Lamb wave speed maps of cornea-limbus-sclera transition for IOP levels 20 mmHg (top), and 40 mmHg (bottom). (c) Bar plot representing average Lamb wave speed for all eye measurements (n = 4) versus IOP level. Error bars represent intersample standard deviation.

001 **COMPLEX ELASTIC WAVE PROPAGATION IN MICRO-ELASTOGRAPHY.**

Gabrielle Laloy-Borgna[1], Ali Zorgani[1], Pol Grasland-Mongrain[2], Stefan Catheline[1].*
[1]LabTAU, INSERM, Centre Léon Bérard, Université Lyon 1, Univ Lyon, F-69003, Lyon, FRANCE ; [2]Laboratoire de Physique, Ecole Normale Supérieure de Lyon, CNRS UMR5672, 46 allée d'Italie, F69007 Lyon, FRANCE.

Background: Many techniques have been proposed to measure cell mechanical properties, especially its elasticity. Most need a very accurate model of the cell characteristics but the chosen model may impact the measurement accuracy. Moreover, current measurements take seconds to hours to perform, during which biological processes can modify the cell elasticity, and they necessitate fixing the cell on a substrate. We recently proposed an alternative elasticity measurement technique based on elastic wave propagation within a single cell [1]. The proposed technology was inspired by pioneer works in shear wave elastography developed for organ elasticity imaging [2] [3] [4].

Aims: The aim of this work was to study dispersion of high-frequency shear waves (up to 15 kHz) and to relate it to the medium characteristics. The results might help to improve quantitative mapping elasticity in micro-elastography.

Methods: Shear waves are generated using vibrators from Cedrat Technologies, called APA100M. Waves are captured using an ultrafast camera (Phantom v12.1, up to 46 000 frames per second) and a Leitz optical microscope (x10 lens). The experiments are conducted in controlled elastic solids such as gelatin, Agar and PVA (polyvinyl alcohol). To estimate phase velocity of shear waves, we use Speckle tracking algorithms.

Results: The phase velocity of the shear waves is measured against frequency, and assuming an infinite and homogeneous elastic medium, we can use Voigt model. Fitting Voigt model on experimental data allows us to estimate medium's shear modulus and viscosity.

Conclusions: Using the speed estimation of shear waves in controlled elastic media, we can extract the mechanical properties of the phantoms. It requires to take into account both wave guide effects and viscosity, to allow Voigt model to be used.

Acknowledgements: This work has benefited from support by the Plan Cancer 2018, BPalp.

References: [1] Pol Grasland-Mongrain, Ali Zorgani, Shoma Nakagawa, Simon Bernard, Lia Gomes Paim, Greg Fitzharris, Stefan Catheline, and Guy Cloutier. Ultrafast imaging of cell elasticity with optical microelastography. Proceedings of the National Academy of Sciences, 115(5) :861–866, January 2018.
[2] T A Krouskop. A pulsed Doppler ultrasonic system for making noninvasive measurements of the mechanical properties of soft tissue. Journal of Rehabilitation Research and Development, page 8, 1987.
[3] R Muthupillai, D. Lomas, P. Rossman, J. Greenleaf, A Manduca, and R. Ehman. Magnetic resonance elastography by direct visualization of propagating acoustic strain waves. Science, 269(5232) :1854–1857, September 1995.
[4] Stefan Catheline. Interférométrie-Speckle ultrasonore : application à la mesure d'élasticité. PhD thesis, Université Paris VII, November 1998.

* *indicates Presenter*

015 **ULTRASOUND IMAGE REGISTRATION USING MOMENTUM EQUATION CONSTRAINTS.**

Olalekan A. Babaniyi[1], Michael S. Richards[1].*
[1]Rochester Institute of Technology, 1 Lomb Memorial Drive, Rochester, NY, USA.

Background: Displacement estimation from ultrasound images is an important and challenging problem encountered in ultrasound elastography. Most of the available displacement estimation algorithms are only able to precisely estimate the displacement component along the direction of sound propagation due to the anisotropic ultrasound point spread function (PSF) [1]. This makes it very difficult (and often impossible) to invert for the mechanical properties using direct inversion methods [2].

Aims: The goal of this work is to develop a displacement estimation algorithm that is capable of reconstructing precise estimates of the full displacement vector field from ultrasound images.

Methods: To achieve this goal, we formulate an optimization problem where the goal is to find the displacement field that minimizes the mismatch between ultrasound image sequences acquired as a tissue undergoes deformation. These displacements will be constrained to satisfy the conservation of momentum equations for a 2D elastic solid undergoing quasi-static plane stress deformations using the SPrase Relaxation of Momentum Equations (SPREME) technique [3]. Simulated ultrasound images will be created using a finite element model, with physiological boundary conditions and known displacement fields, and an approximate ultrasound point spread function. Experimental ultrasound image sequences will also be acquired of manufactured tissue mimicking phantoms with known material properties and controlled boundary conditions.

Results: We apply the displacement estimation algorithm to the simulated image data and experimentally acquired ultrasound data from tissue mimicking phantoms and show that we are able to recover precise estimates of the full displacement field from both datasets. We use the displacements in a direct inversion algorithm to reconstruct the elastic modulus field. Reconstructed modulus estimates are compared, visually and quantitatively, to simulated or manufactured values.

Conclusions: We have developed a displacement estimation algorithm that allows us to reconstruct the full displacement field from ultrasound images. These displacement fields can be used in a direct inversion algorithm to efficiently reconstruct the elastic modulus distribution.

References:

[1]. Szabo TL. “Diagnostic ultrasound imaging; inside out.” Kildlington: Elsevier Academic Press; 2004.

[2]. Albocher U, et al. “Adjoint-weighted equation for inverse problems of incompressible plane-stress elasticity.” *Computer Methods in Applied Mechanics and Engineering* 198.30 (2009): 2412-2420.

[3]. Babaniyi OA, Oberai AA, Barbone PE. “Recovering vector displacement estimates in quasistatic elastography using sparse relaxation of the momentum equation.” *Inverse Problems in Science and Engineering* (2016): 1-37.

017 **FRAME RATE OPTIMIZATIONS OF ELECTROMECHANICAL WAVE IMAGING FOR THE MEASUREMENT OF ELECTROMECHANICAL ACTIVATION DURING SINUS RHYTHM.**

Melina Tourni[1], Lea Melki[1], Rachel Webber[1] and Elisa Konofagou[1].*
[1]Columbia University, PS 19-405, 6330 West 168th Street, New York, NY, 10032, USA.

Background: Clinical echocardiograms prioritize high spatial resolution over temporal. This allows for better qualitative diagnosis, yet it restricts the use of time-shifted based techniques such as radiofrequency-based speckle-tracking, which require higher frame-rates. Electromechanical Wave Imaging (EWI) is a high frame-rate ultrasound-based technique relying on axial incremental strain estimation, successfully shown to non-invasively map the transmural electromechanical activation in all four cardiac chambers in vivo [1]. Previous studies have explored the frame rate (FR) limitations upon determining the optimal strain estimation method [2]. However, the impact of the acquisition FR on EWI mapping has not yet been investigated. Exploring EWI frame rate limitations is critical for assessing EWI future integration in the clinic.

Aims: In this study, we investigate the impact of the EWI acquisition frame-rate for the assessment of electromechanical activation during sinus rhythm in healthy humans and evaluate the algorithm's susceptibility to lower frame-rate errors.

Methods: A 2.5-MHz diverging wave pulse excited at 2000 Hz PRF with a Verasonics Vantage system (Verasonics, Redmond, WA), obtained with a P4-2 phased array (ATL/Philips, Andover, MA, USA) was used to image a healthy human heart (26 year old male) in four transthoracic apical echocardiographic views, for 2 seconds per view at a depth of 20 cm. We compute the axial incremental displacement and strains with 1D RF cross-correlation with a window size of 6.2 mm and a 90% overlap followed by a 51-point gaussian window for displacement temporal filtering and a least-squares axial strain estimator of 5mm kernel size. We repeat this process by decimating the RF FR from 2000 Hz to 500 Hz, 250 Hz and 125 Hz. We simultaneously adjust the RF-based cross-correlation axial search range and displacement temporal filtering by the equivalent down-sampling factor. We define the wavefront of the electromechanical activation as the timing of the first sign change of the incremental axial strain after the QRS onset. Multi-2D views are co-registered around the LV longitudinal median axis and corresponding activation times are interpolated around the circumference, to generate 3-D rendered activation maps [3]. Down-sampled EWI activation maps are compared in terms of qualitative and quantitative differences with the 2000 Hz maps which are used as the ground truth. A 15 ms offset from the 2000 Hz selected zero-crossing (ZC) locations is considered to be within an accepted error range for ZC detection with lower FR, whereas any difference larger than that for the same pixel are defined as false positives. Matlab (Mathworks Inc., Natick, MA, USA) was used for all processing steps and Amira 5.3.3 (Visage Imaging, Chelmsford, MA, USA) for 3-D map visualization.

Results: Of the initial pixels used for 2000 Hz EWI isochrone generation, we were able to detect ZCs in 98% of them at 500 Hz, 94% at 250 Hz and 81% at 125 Hz (Fig 1). However, only 92% for 500 Hz, 80% for 250 Hz and 41% for 125 Hz of the initial pixels' ZCs lie within the 15 ms accepted error window and hence were considered true positive ZCs. The 500-Hz map is the most consistent with the 2000 Hz baseline, showing minor differences. The 250 Hz map presents a difference mainly in the RV inferior wall, with 15% of the ZCs falsely detected. The 125 Hz map diverges significantly from the baseline, as observed particularly in the RV inferior wall and the LV lateral wall with an average of 50% of the selected ZCs considered false positives.

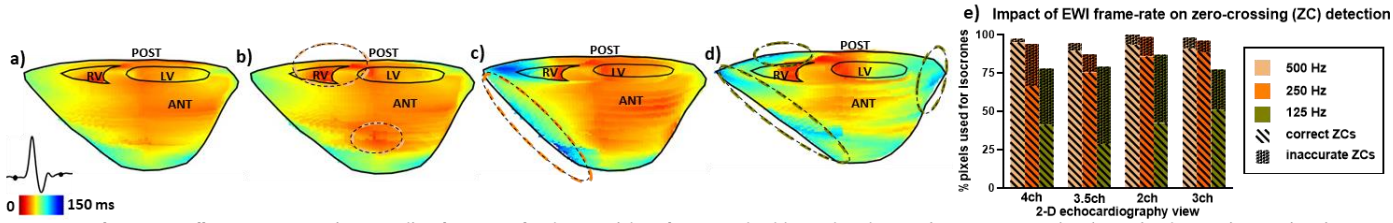

Fig.1: EWI frame-rate effect on zero-crossing sampling frequency for the ventricles of a 26 yo. healthy male volunteer in NSR. 3-D rendered EWI isochrones in anterior view at a) 2000 Hz (baseline), b) 500 Hz, c) 250 Hz and d) 125 Hz. Red represents the earliest activation while blue the latest. e) Proportion of useable pixels at lower frame-rates compared to the 2000 Hz baseline. ZCs are considered correct when contained within a 15 ms range of the initial 2000 Hz ZC temporal locations. LV: Left Ventricle, RV: Right Ventricle, ANT: Anterior, Post: Posterior.

Conclusions: EWI mapping was shown to be quantitatively and qualitatively highly dependent on the acquisition high frame-rate, as expected. These findings indicate that EWI is less reliable at frame-rates lower than 500 Hz, as it can result in misleading electromechanical activation maps, which could interfere with correct diagnosis in a clinical setting.

Acknowledgements: This study was supported in part by NIH - R01 HL140646.

References: [1] Provost et al, Proc. Natl. Acad. Sci. 2011. **[2]** Provost et al 2012 Phys. Med. Biol. 57 1095 **[3]** Nauleau et al, Medical Physics 2017.

* *indicates Presenter*

037 **ULTRASONIC VECTORAL OBSERVATION OF LOW FREQUENCY MECHANICAL WAVE PROPAGATION AND INVERSE PROBLEM APPROACH ON SOFT TISSUE PHANTOM.**

Chikayoshi Sumi[1], Yusuke Kobayashi[1]*
[1]Sophia University, 7-1, Kioi-cho, Chiyoda-ku, Tokyo 102-8554, JAPAN.

Abstract Body Vectoral observations are performed to observe a transverse or shear wave propagation in detail or in a high precision on an ultrasonic soft tissue phantom to be externally vibrated under an uncontrol propagation direction. Simultaneously, a pressure wave is observed via an inverse problem. The results indicate that the vectoral approaches will increase the target tissues and mechanical source types.

Background: We have been developing various high accuracy displacement vector measurement methods. For instance, we applied the 2-dimensional (2D) autocorrelation or cross-spectral phase gradient method to a slowly lateral-compressed soft tissue phantom with a lateral modulation method, a spectral frequency division method, a high-frame-rate beamforming, etc. (e.g., [1,2]). Such a vectoral Doppler observation yielded a more accurate measurement/imaging of strains as well as displacements than when the corresponding 1D methods were used [3]. For various organs, only attachment of a probe onto a target enables us to observe an arbitrary directional displacement. Recently, a transverse or shear wave propagation is generated in a controlled direction by using push beams, which is clinically used with a conventional one-dimensional (1D) Doppler or cross-correlation method. That is, only a propagation of an axial medium displacement is observed.

Aims: In this report, the vectoral measurement/imaging is applied to a dynamically vibrated soft tissue phantom in order to observe a shear wave propagation not under such a directional control, but more in detail and in a higher precision. Since spatiotemporal spectra or the analytic signals have information about the wave propagation direction (wavelength vector), we had developed the multidimensional spectral filtering/division method, which allows (i) separating interference waves including a standing wave, (ii) synthesizing new shear waves and (iii) observing propagation speeds or shear moduli including an anisotropic one with a high accuracy. The approach is compared with our previously developed differential-type inverse problems [4]. Through the inverse approach, waves of a pressure, a curl, an inertia, a strain, a stress and an energy are also observed with a density.

Methods: The 2D autocorrelation or cross-spectral phase gradient method was used to observe axial and lateral medium displacements. A conventional clinical echo equipment (SSD5500, ALOKA, Japan) was used with a linear-array-type probe (7.5 MHz) to acquire echo data. The frame rate was set at 67 Hz. As shown in Figure 1, a cubic phantom (10 mm sides, 30 kPa; a soft inclusion, 10 kPa) was externally vibrated using a large surface vibrator underneath the phantom. The vibration frequency was changed from 10 to 110 Hz.

Results: Figure 1b shows snapshots of lateral, axial and magnitude medium displacements (10Hz). All the propagations of lateral, axial and magnitude displacements were observed dominantly in a lateral direction from the central axis of phantom and however, in a different manner. Median filtering was effective in removing spike-like errors, and Figures 1c and 1d show laterally and axially separated waves (30 Hz). Figure 1e shows a pressure wave (others omitted). The compressive wave propagation had an axial component. Rather than the speed measurement with ignoring the compressive wave (sever soft inclusion artifact [C. Sumi, Proc ITEC2013, ID: 023]), the 2D reconstruction achieved a higher accuracy, i.e., 10.5 vs. 3.8 kPa.

Conclusions: The vectoral approaches were effective in observing a shear wave propagation even under an uncontrol propagation direction. In addition to steered push beams, the approaches will enable us to use various mechanical source types including geometries and sizes to be clinically used for various organs, i.e., dynamic and quasi-static observations for deeply situated tissues and superficial tissues. Spontaneous heart motion or pulsation will also be used. Moreover, the results also indicate that a 3D or 2D inversion may also be performed with a higher accuracy and no pre-separation of interference waves, and even in an anisotropic case. For high frequency imaging, aliasing can be coped with by extrapolating a bandwidth.

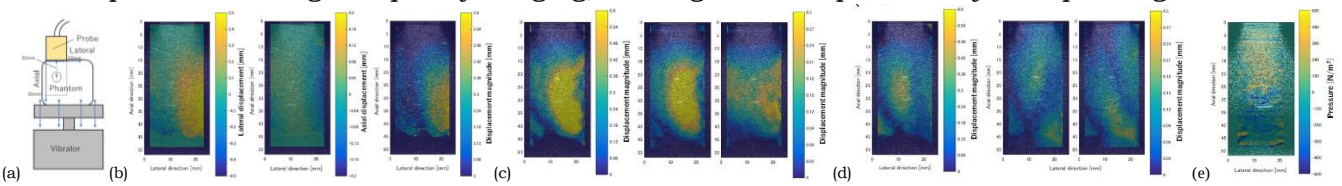

Figure 1. (a) Experimental setup; and observation results: (b) 10 Hz medium displacements, and (c) laterally separated and (d) axially divided 30Hz shear waves; (e) pressure wave.

References: [1] IEEE Trans. UFFC, vol. 55, pp. 2607-2625, 2008. [2] Reports in Medical Imaging, vol. 5, pp. 57-101, 2012. [3] **UMB, vol. 33, pp. 1830-1837, 2007. [4]** Acoustical Science and Technology, vol. 31, pp. 347-359, 2010.

* *indicates Presenter*

002 **REAL-TIME AND HIGH QUALITY ULTRASOUND ELASTOGRAPHY USING CONVOLUTIONAL NEURAL NETWORK BY INCORPORATING ANALYTIC SIGNAL.**

*Ali K.Z Tehrani[1], Mina Amiri[1], Hassan Rivaz[1]**

[1]Concordia University, 1455 Boulevard de Maisonneuve O, Montreal, QC, H3H 2A3, CANADA

Background: Ultrasound Elastography (USE) provides information related to mechanical properties of the tissue. In quasi-static approach, the operator compresses the tissue and the displacement between image before and after compression can be used to obtain relative elasticity.

Although Convolutional Neural Networks (CNN) have been very successful in optical flow problem, they have been rarely used for displacement estimation in USE due to vast differences between ultrasound data and computer vision images. In USE, Radio Frequency (RF) data is needed to obtain accurate displacement estimation. RF data contains high frequency contents which cannot be downsampled without significant loss of information, in contrast to computer vision images.

Aims: Our main goal is to adopt current optical flow CNN to displacement estimation in order to have high quality and real-time displacement estimation. We propose novel inputs to the network to fill the gap between displacement estimation in computer vision and USE.

Methods: We propose to utilize Lite-FlowNet [1] which is a lite and fast optical flow CNN compared to recent networks. For the first time, we propose to use envelope and analytic signal which is composed of Inphase (RF data) and Quadrature (Hilbert transform of RF data) as the inputs of the network.

Results: We compared our method with well-known FlowNet2 optical flow estimation CNN [2] and state-of-the-art Elastography algorithm (GLUE) [3]. The phantom and *in vivo* results are shown in Fig. 1 and Fig. 2. We also computed quantitative results and found that Lite-FlowNet performs comparable to GLUE and substantially better than Flow-Net in terms of CNR. Also, Lite-FlowNet obtains the best results in terms of SR which indicates that this network has a low estimation bias.

Conclusions: In this work, we adopted Lite-FlowNet to USE displacement estimation. In order to reduce information loss due to downsampling, we incorporated analytic signal and envelope as inputs. Results confirm that this method performs on par with state-of-art elastography methods and outperforms FlowNet2 not only in strain quality but also in inference speed.

Acknowledgements: This research is funded by NSERC Discovery Grant RGPIN 04136. The in vivo liver data was collected at Johns Hopkins Hospital. The authors would like to thank Drs. E. Boctor, M. Choti and G. Hager for allowing us to use the data. We also thank NVIDIA for donation of the Titan V GPU.

References:

[1] Hui TW, Tang X, Change Loy C. Liteflownet: A lightweight convolutional neural network for optical flow estimation. InProceedings of the IEEE conference on computer vision and pattern recognition 2018 (pp. 8981-8989).
[2] Ilg E, Mayer N, Saikia T, Keuper M, Dosovitskiy A, Brox T. Flownet 2.0: Evolution of optical flow estimation with deep networks. InProceedings of the IEEE conference on computer vision and pattern recognition 2017 (pp. 2462-2470).
[3] Hashemi HS, Rivaz H. Global time-delay estimation in ultrasound elastography. IEEE transactions on ultrasonics, ferroelectrics, and frequency control. 2017 Jun 21;64(10):1625-36.

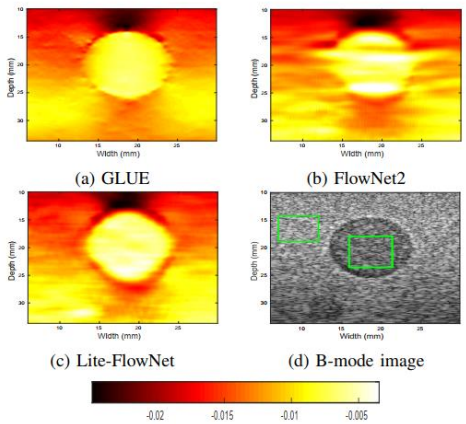

Fig. 1. Strain image of experimental phantom

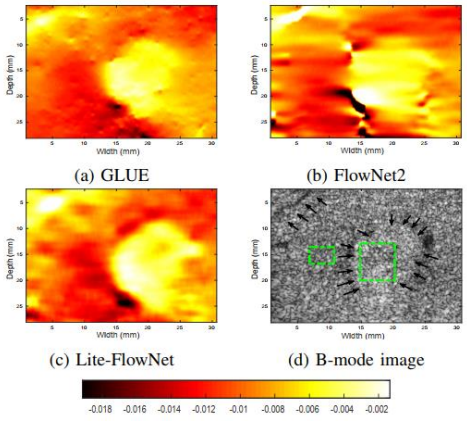

Fig. 2. Strain image of in *vivo data*

* *indicates Presenter*

006 **MULTIPERSPECTIVE 2-D ULTRASOUND STRAIN IMAGING OF PORCINE AORTAS IN AN ABDOMEN PHANTOM.**

Hein de Hoop[1], Niels Petterson[1], Marc van Sambeek[1,2], Frans van de Vosse[1], Hans-Martin Schwab, Richard Lopata[1]*

[1]Eindhoven University of Technology, P.O. Box 513, 5600 MB Eindhoven, The Netherlands; [2]Catharina Hospital Eindhoven, P.O. Box 1350, 5602 ZA Eindhoven, The Netherlands.

Background: Currently, the decision-making for clinical intervention of Abdominal Aortic Aneurysms (AAAs) is based on the maximum diameter of the aortic wall, but does not provide patient-specific information on rupture risk. Ultrasound (US) imaging is a safe and accessible way to regularly assess the geometry and deformation of the aortic wall. However, inherent limitations of this modality, such as the low lateral resolution and poor lateral contrast, degrade the precision of both the geometry and local strain estimates. To tackle these drawbacks, this study introduces a multiperspective scanning sequence, developed on a dual-transducer US system. Using this set-up, high frame rate strain imaging was performed on ex-vivo inflated porcine aortas.

Aims: To investigate the benefits of multiperspective US, i.e. imaging with an additional transducer, as means to improve the image quality, motion tracking, and strain estimation of the abdominal aortic wall.

Methods: Experimental imaging was performed on ex-vivo porcine aortas embedded in a phantom of the abdomen, including a spine and surrounding structures. The aortas were pressurized in a mock-circulation set-up using saline solution. US images were acquired with two curved arrays (C5-2v, Verasonics) using three acquisition schemes: 1) Single perspective conventional focused scanning, 2) single perspective ultrafast imaging, and 3) multiperspective ultrafast imaging. Multiperspective images and axial displacements were incoherently compounded for improved segmentation and tracking of the aortic wall, respectively. The performance between the acquisition schemes was compared in terms of image contrast, motion tracking drift, and strain estimation precision.

Results: In multiperspective images, both lateral resolution and contrast increased in the overlapping wall segments. The compounded multiperspective displacement estimation reduced the mean motion tracking error over one inflation cycle by a factor 7 compared to conventional scanning. Resolution was increased in circumferential (Fig. 1A-C) and radial (Fig. 1D-F) strain images, and circumferential signal-to-noise ratio (SNRe) increased by 16 dB. Radial strain imaging remains cumbersome for the frequency used.

Conclusions: The benefits of multiperspective US imaging include a better visualization of the aortic wall, and improvements in the precision of motion tracking and circumferential strain estimates. Future work will focus on the translation to in-vivo and clinical application, as well as extending the current method to multiperspective 3-D imaging.

Acknowledgements: This work is part of the MUSE project, which has received funding from the European Research Council (ERC) under the European Union's Horizon 2020 research and innovation programme (ERC starting grant 757958).

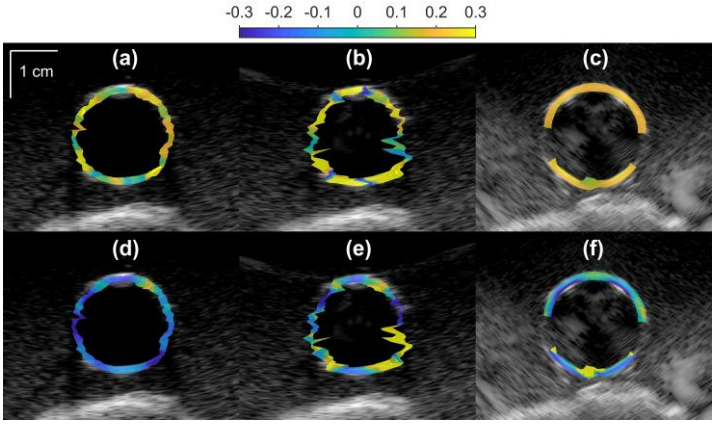

Figure 1. *Circumferential (a-c) and radial (d-f) strain images of the aortic wall in inflation obtained with line-by-line imaging (a, d), ultrafast imaging (b, e), and multiperspective ultrafast imaging (c, f).*

041 **DESIGN OF AN ULTRASOUND PROBE HOLDER TO SECURE THE PROBE FOR REAL TIME IMAGE CAPTURE DURING DYNAMIC LOADING OF THE HUMAN ACHILLES TENDON: A VALIDATION STUDY.**

Gamalendira Shivapatham [1], Wing Keung Cheung [1], Dylan Morrissey [1], Jeffrey C. Bamber [2], Hazel R.C. Screen[1].*

[1]Queen Mary University of London, London, UK; [2] Institute of Cancer Research and Royal Marsden NHS Foundation Trust, London, UK.

Background: The Achilles tendon (AT) connects the triceps surae muscles to the heel bone, and transfers forces during movements that are many multiples of body weight. AT injury is prevalent and highly debilitating. Exploring AT movement and deformation during dynamic loading provides insight into injury mechanisms and management, but it is difficult to mount an ultrasound (US) probe and collect good quality images from a consistent area. Previous studies have utilized custom-made holders [1] but the detailed design is not commonly reported. An analysis of probe movement with two such designs has reported longitudinal rotations of 22.9° and medio-lateral rotations of 0.8° during hopping [2] or longitudinal rotations of 8.1° and medio-lateral rotations of 1.2° relative to the shank during running [3]. Whilst such probe movements can be partially corrected for when tracking global tendon displacement, investigation of intra-tendon shear strain necessitates greater control, hence requiring a probe holder which minimizes relative probe-shank movement during imaging.

Aim: Develop a device to fix an US probe (Analogic L14-5/38) securely over the posterior aspect of the human AT, reducing all rotations relative to the shank to <5°.

Methods: Successful imaging of the AT necessitates use of a standoff pad. Engineering design methods were adopted to develop, prototype and test 5 designs, from which the best was selected using a decision matrix (Fig.1). The final design was 3D printed in Acrylonitrile Butadiene Styrene, then tested on a volunteer performing three exercises (Fig.2) while acquiring US radiofrequency image sequences. Movement of probe and participant were tracked using CODA CX1 system (Charnwood Dynamics Rothley, UK) (Fig.2). B-mode imaging data were also visually checked to confirm image clarity.

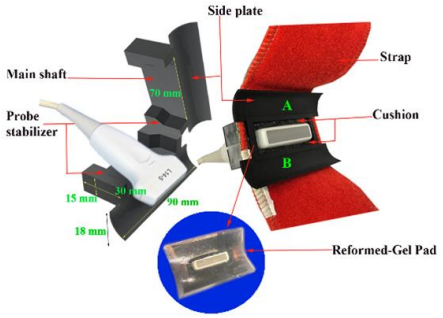

Figure1. Left: design with holder dimensions. Right: US probe within the 3D printed holder. The main shaft is the housing for the probe; the probe stabilizer prevents the probe from pulling backward; the side plate (A&B) is curved to fix securely over the posterior side of the leg. Bottom: an US-gel pad is reformed to securely fit within the side plate area. The strap wraps around the leg.

Results:

Exercise	Seated heal rise with external weight on the thigh (Fig.2b)		Seated eccentric loading of calf muscle. (Fig.2c)		Standing eccentric and concentric loading of calf muscle. (Fig.2d)	
Probe rotation	long	med-lat	long	med-lat	long	med-lat
Mean	5.62	0.47	0.17	0.89	-1.07	3.16
SD	1.38	0.28	0.35	0.056	0.54	0.98

Table.1: Means and standard deviations (over three trials) of longitudinal (long) and medio-lateral (med-lat) probe rotations (deg) during three exercises.

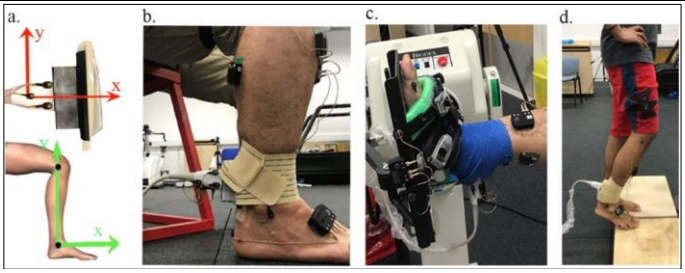

Figure 2. a) The probe secured in the holder with the reformed gel pad, indicating the location of the 3 motion tracking markers, and the probe & shank coordinate systems in red & green, respectively. b), c) and d) The three exercises: seated heel raise, seated eccentric loading of calf muscle and standing eccentric loading of calf muscle, respectively.

Conclusion: The final probe holder design successfully secured the US probe during various exercises, restricting rotations relative to the shank to <6°, and providing improved stability relative to some published performance figures obtained with alternative designs. Stable B-mode movies provided confidence in utilizing this design to determine tendon strains during complex exercises in a research environment.

Acknowledgements: This research was funded by a QMUL research studentship.

References: 1. Franz JR, et al. 2015, Non-uniform in vivo deformations of the human Achilles tendon during walking. Gait & Posture; 41:192-197. 2. Lichtwark GA, et al. 2005, In vivo mechanical properties of the Achilles tendon during one-legged hopping. J Exp Biol; 208:4715-4725. 3. Farris DJ, et al. 2012, The effects of orthotic heel lifts on Achilles tendon force and strain during running. J Applied Biomech; 28:511-519.

042 **TOWARDS THE DEVELOPMENT OF SPECKLE TRACKING FOR VISUALIZING SLIP PLANES IN THE HUMAN ACHILLES TENDON DURING DYNAMIC LOADING; PRELIMINARY RESULTS.**

Gamalendira Shivapatham [1], Wing Keung Cheung [1], Dylan Morrissey [1], Hazel R.C. Screen[1], Jeffrey C. Bamber [2].*

[1]Queen Mary University of London, London, UK; [2] Institute of Cancer Research and Royal Marsden NHS Foundation Trust, London, UK.

Background & Aims: Achilles tendon (AT) injury is common and debilitating, needing improved diagnostics and management. Ultrasound (US) speckle tracking has shown non-uniform strains across the young healthy AT during use [1,2], suggesting that sliding between sub-tendons is fundamental to AT health. To investigate this, methods are needed to detect and quantify AT internal slip-shear. Here, we describe early work towards extending shear-strain methods developed to detect slip-shear at tumor boundaries [3] for eventual detection of sub-tendon sliding, addressing the aligned fibrous structure of tendon and the AT-longitudinal (AT-long) direction of slip-shear. Typically, to employ lateral shear strain to detect high AT-long shear strain, a difference between the AT-long and US-lateral directions would be addressed by rotating an AT-long displacement image calculated from the displacement vector obtained by two-dimensional (2D) speckle tracking. However, 2D tracking window size and shape cannot be optimized for resolution across the tendon, nor for the extended correlation of the echo structure in the AT-long direction. We hypothesized that rotating the US data prior to tracking will improve AT-long shear-strain images, despite the likely speckle decorrelation due to rotation.

Methods: Radiofrequency (RF) speckle tracking of the AT was carried out during plantarflexion (Fig.1A). When tracking before rotation, 2-D block-matching normalized cross-correlation (NCC) was used to determine the displacement vector, and then the AT-L component of displacement, throughout the field of view. The AT-L displacement map was then rotated by the angle (φ) between the sound beam and tendon, so that the vertical axial gradient of lateral displacement reported AT-L shear strain. When tracking after rotation, the RF image was rotated by φ before 2-D RF speckle tracking.

Results: AT-long displacement images obtained after rotation (Fig.1E) and corresponding shear-strain images (Fig.1F) appear to show reduced noise and improved detection of sliding, particularly between the AT and overlying tissues, when compared to those obtained when tracking was performed before rotation (Figs.1C&D). Both methods corroborated published findings of increasing displacement with increasing depth (Fig.1H).

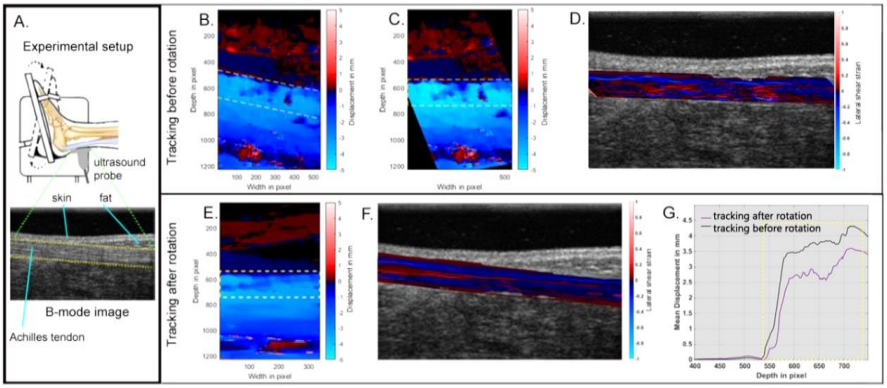

Figure1. A) Example B-scan of the AT (yellow dash lines) acquired during dynamic loading. B) Map of AT-long component of displacement estimated from the displacement vector using 2-D NCC. C) Image B after rotation by angle ϕ (see text). D) AT-long shear-strain map (color) computed from image C and then rotated back by angle ϕ and overlaid on the B-scan. E) AT-long displacement estimated by direct lateral tracking of rotated RF US data. F) AT-long shear-strain map (color) computed from image E and then rotated back by angle ϕ and overlaid on the B-scan. G) AT-long displacement at the end of loading, averaged over the length of the AT, versus depth (distance from the US probe surface) for both methods (yellow box shows the anterior and posterior bounds of the AT).

Conclusions: Previous findings of non-uniform displacement across the AT were confirmed. Estimation of AT-long shear strain from AT-long displacement obtained by tracking rotated RF-data allowed the use of a thin, wide tracking window, addressing the anisotropy of tendon microstructure, appearing to reduce noise and improve resolution for the detection of slip planes. Future work will quantify the improvement relative to loss of speckle correlation, with a view to optimizing the method and deploying it in a clinical study.

Acknowledgements: This research being funded by QMUL research studentship.

References: 1. Bogaerts S, et al, 2017. Evaluation of tissue displacement and regional strain in the Achilles tendon using quantitative high-frequency ultrasound. PloS one, 12(7). 2. Franz JR, et al, 2015. Non-uniform in vivo deformations of the human Achilles tendon during walking. Gait & posture, 41:192-197. 3. Chakraborty A, et al, 2012. Slip elastography: a novel method for visualising and characterizing adherence between two surfaces in contact. Ultrasonics, 52:364-376.

012 **SAFETY ANALYSIS OF SHEAR WAVE ELASTOGRAPHY FOR DYNAMIC CAROTID PLAQUE ELASTICITY ASSESSMENT.**

Angélique D Rog[1,2], Judith T Pruijssen[1], Joosje MK de Bakker[1], Chris L de Korte[1,3], Hendrik HG Hansen[1].*

[1]Radboud University Medical Center, Department of Radiology, Nuclear Medicine and Anatomy, Nijmegen, THE NETHERLANDS; [2]Elisabeth-TweeSteden Ziekenhuis, Department of Medical Physics, Tilburg, THE NETHERLANDS; [3]University of Twente, Physics of Fluids Group, Enschede, THE NETHERLANDS.

Background:

Clinical application of shear wave elastography (SWE) has become widespread with an increasing number of ultrasound systems having an elastography imaging option. These commercial SWE techniques were mainly developed for application in breast and liver. However, multiple studies on the topic of SWE also show promising results for the characterization of unstable plaques in the carotid artery, which rupture is a main initiator of stroke [1]. A drawback of commercially available SWE techniques is the lack of ECG triggering. As a result, it is not possible to estimate elasticity at prespecified time points in the cardiac cycle nor at multiple times per cardiac cycle, while elasticity has been shown to change dynamically [2].

Aims:

This study aims to determine the limitations of dynamic carotid plaque elasticity assessment, in terms of plane wave frame rate (FR) and number of SWE acquisitions per cardiac cycle. Acoustic safety regulations for peripheral vessels and the thermal safety regulations as stated by the food and drug administration (FDA) and the International Electrotechnical Commission (IEC) were taken into account.

Methods:

Acoustic radiation force push pulses and plane waves were transmitted using a SL18-5 transducer connected to an Aixplorer Ultimate ultrasound system (SuperSonic Imagine, Aix en Provence, France). The mechanical index (MI), spatial-peak pulse-average, and spatial-peak temporal-average intensities (I_{sppa} and I_{spta}, respectively) were determined from pressure waveform measurements performed in water with a calibrated 0.2-mm needle hydrophone (Precision acoustics, Dorchester, United Kingdom). The voltage and pulse duration were varied for both sequences to determine the best imaging settings while not exceeding the acoustic output limits. For these settings the maximum allowed number of SWE acquisitions per second was established considering the I_{spta} and temperature limits. One SWE acquisition consisted of a push pulse with a duration of 150 µs followed by a 50 µs pause and then 5 ms of plane wave imaging at a certain, to be determined, FR. Thermal measurements were performed following the IEC-60601-2-37 guideline for the simulated use and the still air test, for which the probe surface temperature rise may not exceed 10°C and 27°C, respectively.

Results:

	Plane wave	Push pulse
Voltage	42V	22V
Apodization	Welch	None
Pulse duration	0.13µs	150µs
Emission frequency	7.5MHz	5MHz
Ratio F/D	-	2
Focal point	-	15mm

Table 1: Settings just below safety limits

Figure 1: Maximum allowed number of sequences per second as a function of the plane wave frame rate

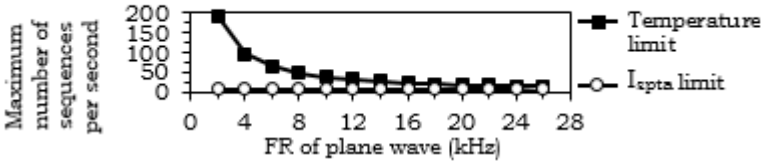

Optimized imaging settings for the plane wave and push pulse not exceeding acoustic output limits can be found in Table 1. The maximum allowed number of sequences per second based on the thermal and I_{spta} limits is shown in Figure 1. Only results for the simulated use test are shown since it is more limiting than the still air test. As shown, the I_{spta} is the limiting factor for the number of sequences per second.

Conclusions:

In literature, a minimum FR of 8 kHz is used for the plane waves to ensure capturing of the shear wave. At this FR and higher, SWE acquisitions can be performed safely 8 times per second without exceeding the acoustic and thermal limits for peripheral vasculature. Thus dynamic vascular elastography can in principle be safely applied. However, caution must be taken when assessing rupture prone, instable plaques. To determine if SWE is safe in these cases, Finite-Element Modeling studies such as [3] are valuable.

References:

[1] K. V. Ramnarine et al., Cardiovascular Ultrasound, vol. 12, nr. 1, 2014.
[2] L. Marais et al., Hypertension, vol. 45, nr. 3, pp. 758-772, 1 3 2019.
[3] J. R. Doherty, et al, Journal of Biomechanics, vol. 46, nr. 1, pp. 83-90, 4 1 2013.

* *indicates Presenter*

022 **ESTIMATION OF SHEAR WAVE ATTENUATION USING THE REVERBERANT SHEAR WAVE ELASTOGRAPHY (R-SWE) APPROACH.**

J Ormachea[1], Richard G. Barr [2], KJ Parker[1].*
[1]University of Rochester, Rochester, NY, USA 724 Computer Studies Building, Box 270231, Rochester, NY 14627, USA. [2]Northeastern Ohio Medical University and Southwoods Imaging, Youngstown, OH, USA.

Background: Different approaches to measure the viscoelastic properties of the liver are becoming available to clinicians, many involving shear waves. Shear wave attenuation (SWA), an independent parameter, is important because it could add information about the tissue pathology [1]. For example, steatosis adds a viscous (lossy) component to the liver, which increases the SWA.

Aims: This work estimates SWA, in addition to the shear wave speed (SWS), using the innovative R-SWE approach, in which multiple shear waves propagate in many directions [2,3].

Methods: Tissue viscoelastic characterization was obtained by measuring SWS and SWA derived from the real and imaginary parts of autocorrelation profiles from the particle velocity field, respectively. A Verasonics (Vantage-128™) ultrasound system was used to track the induced displacements in a low and high viscous CIRS phantoms by applying vibrations at 150 Hz. Additionally, phantom results (SWS and SWA) were compared with another acoustic radiation force (ARF)-based technology implemented in an ultrasound system (RS85, Samsung Medison). Finally, SWS and SWA were assessed in deep *in vivo* human liver tissue, including obese patients, using a custom-made clinical bed with multiple embedded vibration sources to generate the reverberant shear wave field.

Results: Using R-SWE, SWA were 39.2±6.9 Np/m and 89.7±10.9 Np/m, at 150 Hz, for the low and high viscous CIRS phantoms, respectively. A reasonable agreement with the ARF-based system was obtained for both calibrated phantoms, these alternative SWA estimates were 40.5±12.2 Np/m and 87.2±7.8 Np/m, at 150 Hz, for the low and high viscous phantoms, respectively. SWA shows better differentiation between low and high viscoelastic materials than SWS alone. The preliminary *in vivo* liver measurements show that R-SWE could be used to achieve an accurate viscoelastic characterization *in vivo*. SWA in a thin normal patient was 79.0±1.4 Np/m at 150Hz; on the other hand, a higher SWA value was obtained in an obese patient case, 101.8±24.9 Np/m at 150Hz.

Conclusions: The R-SWE approach shows the potential to obtain an improved viscoelastic characterization of *in vivo* tissue by measuring both SWS and SWA from the complex reverberant field.

Acknowledgements: We are grateful for support from Elastance Imaging LLC for the loan of equipment.

References: [1] Parker K J, et al. 2018 Analysis of Transient Shear Wave in Lossy Media Ultrasound Med Biol. [2] Parker K J et al.2017 Reverberant shear wave fields and estimation of tissue properties Phys Med Biol. [3] Ormachea J et al. 2019 An initial study of complete 2D shear wave dispersion images using a reverberant shear wave field Phys Med Biol.

016 HIGH FRAME RATE PULSE WAVE IMAGING IN STROKE PATIENTS IN VIVO.

Grigorios M. Karageorgos[1], Changhee Lee[1], Salah Mahmoudi[1], Rachel Weber[1], Randolph Marshall[2], Joshua Z. Willey[2], Eliza Miller[2] and Elisa E. Konofagou[1,3].*
[1] Department of Biomedical Engineering, Columbia University, New York, USA;
[2] Department of Neurology, Columbia University Medical Center, New York, USA;
[3] Department of Radiology, Columbia University Medical Center, New York, USA.

Background: Arterial wall stiffness and blood flow patterns are considered to be key factors in vascular disease progression, and have been associated with risk of cardiovascular events such as ischemic stroke. Pulse Wave Imaging (PWI) is a non-invasive, ultrasound imaging technique which can estimate regional Pulse Wave Velocity (PWV) of an arterial segment and simultaneously image 2-D vector flow field at high temporal and spatial resolution.

Aims: To employ PWI information to investigate arterial wall stiffness and blood flow patterns in the carotid arteries of stroke patients in vivo.

Methods: Twenty-three (N=23) carotid artery disease patients diagnosed with low degree of stenosis (<40%) were recruited, and were divided into three age matched groups: Patients with history of stroke (N=11, 66-89 y.o.); patients experiencing Transient Ischemic Attack (TIA) (N=6, 64-83 y.o.); Asymptomatic patients (N=6, 63-86 y.o.). A Verasonics Vantage 256 system was used to perform 2-D ultrasound scans of a longitudinal view of the common carotid artery (CCA). An acquisition sequence involving the transmission of 3 plane waves at angles -10°, 0° and 10°, and pulse repetition frequency of 10 kHz was employed, at a center frequency of 5 MHz. The acquired RF signals were properly filtered and a 2-D cross correlation algorithm was employed to obtain the flow velocity vectors ($\boldsymbol{v}$) at each point location in the field of view. With the same RF signals, PWI methodology was performed to estimate axial wall velocities and PWV.

Subsequently, two markers were calculated to analyze the flow patterns: 1) flow velocity magnitude ($\overline{|v|}$) and 2) standard deviation of vector flow angles (STD($\boldsymbol{v_{arg}}$)) averaged inside the lumen and throughout the systolic phase. The latter quantity serves as a marker of flow turbulence.

Results: Figure 1-A) shows an example frame of the PWI imaging sequence. Figure 1-B) illustrates the PWV versus $\overline{|v|}$ in each subject, along with the logistic regression boundary separating the datapoints corresponding to stroke patients, from the TIA and asymptomatic groups. It can be observed that stroke patients were characterized by higher PWV combined with low $\overline{|v|}$. Figure 1-C) shows a comparison of the ratio of PWV over $\overline{|v|}$ among the three groups. One-way ANOVA with Holm-Sidak correction revealed that PWV/$\overline{|v|}$ was significantly higher in stroke patients, as compared to TIA (0.46 ± 0.20 vs 0.22 ± 0.08, p<0.01) and asymptomatic (0.46 ± 0.20 vs 0.17 ± 0.05, p<0.01) subjects. Finally, STD($\boldsymbol{v_{arg}}$) was significantly higher in stroke patients, compared to TIA (19.74° ± 5.49° vs 13.01 ± 3.65°, p < 0.05) and asymptomatic (19.74° ± 5.49° vs 11.28° ± 1.82°, p<0.01) groups. Those results suggest that stiffer arterial wall combined with diminished and/or turbulent flow may be associated with stroke occurrence.

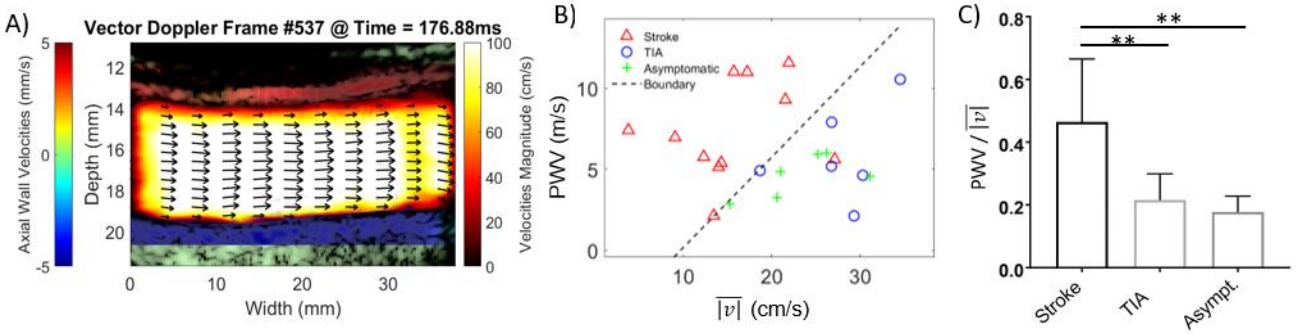

Figure 1: A) Frame illustrating the PWI sequence, with the axial wall velocities and flow velocity vector field overlaid onto the B-mode. B) Plot of PWV versus $\overline{|v|}$. C) Bar-plot with the ratio of PWV over $\overline{|v|}$ in each group.

Conclusions: This study demonstrated the feasibility of PWI to provide additional insight in carotid artery wall-fluid dynamics, which could potentially aid in stroke prognosis and monitoring by differentiating stroke from TIA patients and between symptomatic and symptomatic subjects.

Acknowledgements: This study was funded in part by the National Institutes of Health: R01HL135734.

011 **MULTI-PLANE ULTRASOUND ELASTOGRAPHY OF HEALTHY ABDOMINAL AORTAS IN VIVO.**

Larissa C. Jansen[1,2], Hans-Martin Schwab[1], Marc R.H.M. van Sambeek[1,2], Frans N. van de Vosse[1], Richard G.P. Lopata[1].*

[1]Eindhoven University of Technology, Eindhoven, Noord-Brabant, THE NETHERLANDS; [2]Catharina Ziekenhuis Eindhoven, Eindhoven, Noord-Brabant, THE NETHERLANDS.

Background: Ultrasound (US) elastography is a method for estimating strains. These can provide insights in the mechanical behavior of abdominal aorta tissue. Recently, a 2D + t US elastography study showed that circumferential strains in abdominal aortic aneurysm (AAA) patients are reduced compared to healthy volunteers [1]. As the Field-Of-View (FOV) of 2D US is limited, only a single cross-section can be evaluated. Moreover, US elastography has a limited performance in regions where image contrast and resolution are reduced. With 3D + t US a larger FOV can be achieved. However, in some cases the aneurysm cannot fully be captured. Furthermore, motion estimation is limited by the relatively low volume rate of current 3D + t US imaging [2].

Aims: The aim of this study is to achieve multi-plane US elastography imaging with sufficient frame rates (~20Hz) and within a large FOV by extending 2D US imaging with probe tracking. Furthermore, an automatic segmentation algorithm is developed to enhance robustness of motion estimation in regions where speckle tracking performance is reduced.

Methods: Twelve healthy volunteers participated in this study. Radio Frequency (RF) data were collected with a curved array probe (Mylab70, ESAOTE EUROPE, Maastricht, NL) at multiple locations along the length of the aorta. At each location, the probe's orientation was sensed by an electromagnetic probe tracker (Curefab Technologies, München, Germany). Postprocessing was performed offline in Matlab (Mathworks Inc., Natick, MA, USA). An automatic 2D star-Kalman and snake algorithm was applied to segment the lumen-wall border. In addition to a coarse speckle tracking iteration on envelope data, coarse displacements were computed from frame-to-frame segmented contours (Fig. 1). The coarse displacements from both methods were averaged and followed by two speckle tracking iterations on RF data; each at a finer resolution and limited search window. Thereafter, circumferential strains were calculated from the displacements using least squares strain estimation. Next, strains were mapped in 3D space according to the probe's orientation (Fig. 2).

Results: 2D US imaging was extended with probe tracking for multi-plane elastography in a FOV of interest (Fig. 2). The addition of automatic segmentation for displacement estimation improved frame-to-frame tracking in the side wall regions compared to solely using speckle tracking. As well as that, it reduces inter-observer variability and allows for automatic selection of frames of a heart cycle. In most regions, the circumferential strains have the expected patterns of healthy aorta strains (Fig. 3) As expected, strains are best estimated in regions where the insonification direction is closely aligned with the strain direction (Fig. 2-3).

Conclusions: Multi-plane US elastography in combination with automatic segmentation is a promising tool for measurement of tissue properties at multiple locations along the length of the aorta. Compound US elastography might further improve strain estimation in upper and lower wall regions (Fig. 3).

Acknowledgements: This work is part of the NWO Perspectief Project Ultra-X-treme.

References: [1] Taniguchi R. *Ann. Vasc. Dis.*, Vol. 7, No. 4, p.p. 393-398, 2014; [2] van Disseldorp E. *Eur J Vasc Endovasc Surg*, Vol. 59, No. 1, p.p. 81-91, 2020.

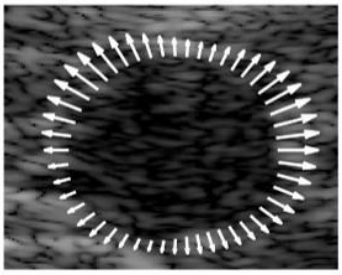

Figure 1. Vectors indicating displacements calculated from automatically segmented contours.

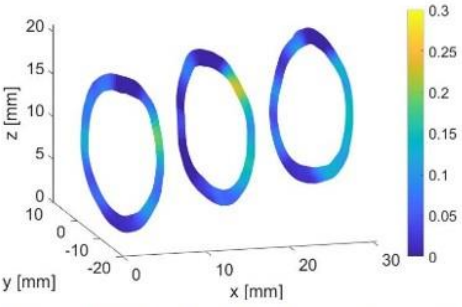

Figure 2. Multi-plane US elastography showing circumferential strains at end systole at multiple locations along the length of the aorta.

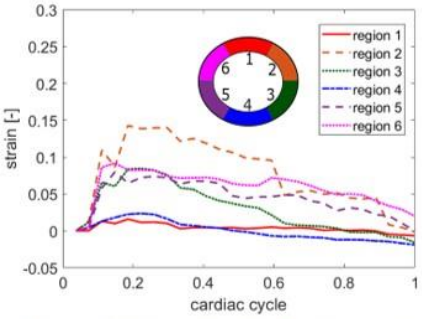

Figure 3. Circumferential strain at one 2D imaging location averaged over six regions in the vessel wall.

003 **ROBUST DATA FUNCTION IN GLOBAL ULTRASOUND ELASTOGRAPHY.**

Md Ashikuzzaman[1], Hassan Rivaz[1]*

[1]Concordia University, 1455 Boulevard de Maisonneuve O, Montreal, QC, H3H 2A3, CANADA.

Background: Time delay estimation (TDE) between pre- and post-deformed radio-frequency (RF) frames is a critical task in ultrasound elastography. TDE by optimization of a regularized cost function consisting of a data term and a spatial [1,2] or temporal [2] regularization term usually leads to low variance TDEs. The data term considers only the sample intensities, and similarity of gradients of RF data has not been exploited yet. In addition, RF data sometimes suffers from large outlier errors that can create large artifacts if they are not handled.

Aims: Herein, we propose a novel ultrasound elastography technique where the data term takes both intensity and gradient similarities into account. Adaptively weighted linear combination of similarities in pixel intensity and spatial components of the image gradient formulates our new data term. The second contribution of the proposed technique is to make elastography robust to outliers.

Methods: Let $I_1(i,j)$ and $I_2(i,j)$ denote two RF frames acquired before and after tissue deformation. First, we calculate the initial estimate of the displacement field between I_1 and I_2 using Dynamic Programming (DP) [3]. To refine the DP initial estimate, we devise a novel highly non-linear cost function: $C=\sum\sum\theta(i,j)D_I(i,j)+(1-\theta(i,j))D_{\nabla I,y}(i,j)+(1-\theta(i,j))D_{\nabla I,x}(i,j)+R$. Here, $D_I(i,j)$, $D_{\nabla I,y}(i,j)$ and $D_{\nabla I,x}(i,j)$ are defined as follows: $D_I(i,j)=[I_1(i,j)-I_2(i+a_{i,j}+\Delta a_{i,j}, j+l_{i,j}+\Delta l_{i,j})]^2$, $D_{\nabla I,y}(i,j)=\gamma[\nabla I_{1,y}(i,j)-\nabla I_{2,y}(i+a_{i,j}+\Delta a_{i,j}, j+l_{i,j}+\Delta l_{i,j})]^2$ and $D_{\nabla I,x}(i,j)=\gamma[\nabla I_{1,x}(i,j)-\nabla I_{2,x}(i+a_{i,j}+\Delta a_{i,j}, j+l_{i,j}+\Delta l_{i,j})]^2$. γ denotes a matching parameter and ∇ indicates the discrete gradient operator. R represents the spatial regularization terms which are the same as [1]. $\theta(i,j)$ is a data-driven weight map to adaptively control the contributions of intensity and gradient similarities to the total cost. Inspired by [4], we calculate $\theta(i,j)$ using: $\theta(i,j)=1/(1+e^{\lambda(D_I(i,j)-D_{\nabla I,y}(i,j)-D_{\nabla I,x}(i,j))})$ where λ is tuned to obtain a proper weight distribution. We optimize the aforementioned cost function to iteratively compute the fine-tuning displacement field and $\theta(i,j)$. Finally, a robust and spatially smooth time-delay estimate is obtained by adding the refinement field to the DP initial estimate. Since our technique introduces a robust data function, we call it rGLUE.

Results: We have validated our technique against a simulation phantom and *in vivo* liver data. Both of the experiments show that our technique is more robust to outliers than GLUE [1] (Figs. 1, 2 and 3).

Conclusions: A novel data function for regularized optimization based ultrasound elastography consisting of adaptively weighted intensity and gradient similarity terms has been proposed in this work. Simulation and *in vivo* liver experiments prove the technique's robustness to outliers.

Acknowledgements: We thank Drs. E. Boctor, M. Choti and G. Hager for allowing us to use the *in vivo* data.

References:

[1] Hashemi, H S. and Rivaz, H, "Global time-delay estimation in ultrasound elastography," IEEE Trans UFFC, vol. 64, no. 10, pp. 1625–1636, 2017.

[2] Ashikuzzaman, M. et al., "Global ultrasound elastography in spatial and temporal domains," IEEE Trans UFFC, vol. 66, no. 5, pp. 876–887, 2019.

[3] Rivaz, H. et al., "Ultrasound elastography: a dynamic programming approach," IEEE Trans Medical Imaging, vol. 27, no. 10, pp. 1373–1377, 2008.

[4] Xu, L. et al., "Motion detail preserving optical flow estimation," IEEE Trans PAMI, vol. 34, no. 9, pp. 1744-1757, 2012.

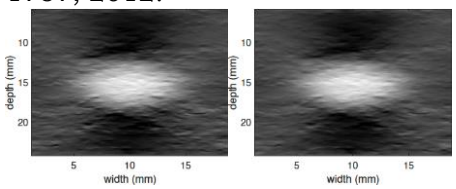

Fig. 1 Simulation: GLUE strain, rGLUE strain

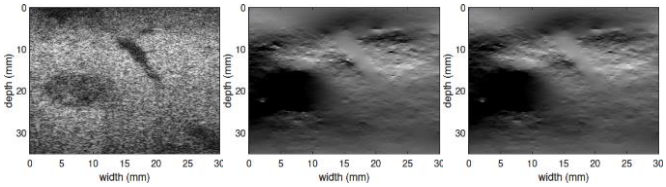

Fig. 2 *In vivo*: B-mode image, GLUE & rGLUE strains

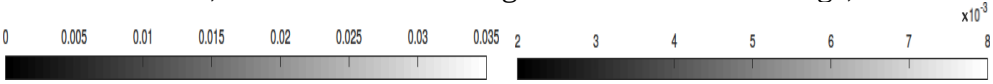

Fig. 3 Color bar: Simulation data, *in vivo* data

014 **LIVER ELASTOGRAPHY REVISITED: CAN PORO-ELASTIC THEORY EXPLAIN IN VIVO DISPERSION?**

Johannes Aichele[1], Stefan Catheline[1].*
[1]INSERM - University of Lyon, Lyon, France.

Background: In transient elastography elasticity is inferred from shear wave speed using elastic theory. The method is now widely applied for non-invasive liver fibrosis detection. However, the observed dispersion of the shear wave speed in vivo measurements shows a mismatch with purely elastic and visco-elastic theory.

Aims: Using a laboratory phantom experiment and revisiting in vivo studies of liver elastography we show that modeling the liver as a poro-visco-elastic solid is more appropriate than assuming linear elasticity or a visco-elastic model.

Methods: We use a Verasonics Vantage ultrafast ultrasound scanner to measure shear wave dispersion in a highly porous melamine foam saturated by water and a Xanthan solution. We compare the experimental results to the analytic results of Biot's theory[1,2] of poro-visco-elastic wave propagation for both cases. We then use the same theory to model shear wave dispersion in the liver, using literature values for porous and elastic parameters.

Results: The shear wave dispersion of the the water saturated foam and the Xanthan saturated foam are well modeled by Biot's theory using a viscosity of 0.47 mPas for water at 40°C and an apparent viscosity of 0.76 mPas for the Xanthan solution at 40°C. The experiment exemplifies that fluid viscosity must be taken into account for proper modeling of the shear wave dispersion in soft porous materials. The same model explains a wide range of shear wave dispersion curves in the liver reported in the literature which is inconsistent with linear elasticity and visco-elasticity.

Conclusions: Validity of Biot's theory for a soft porous phantom has been show. Application of the model on the liver is consistent with reported in vivo dispersion measurements. Inversion for porous parameters and improved inversion for elastic parameters, which are altered by liver diseases, is thus feasible. Furthermore, the theory might find application in elastography imaging of other porous organs such as the brain and the lung.

Acknowledgements: This project has received funding from the Plan Cancer 2014-2019 of the Institut National de Cancer through the BPALP project.

References: [1] Biot, M. a. (1956). Theory of propagation of elastic waves in a fluid saturated porous solid. I. Low frequency range. Journal of the Acoustical Society of America, 28(2), 168–178. https://doi.org/10.1121/1.1908239
[2] Biot, M. A. (1962). Generalized Theory of Acoustic Propagation in Porous Dissipative Media. The Journal of the Acoustical Society of America, 34(9A), 1254–1264. https://doi.org/10.1121/1.1918315

018 **AMPLITUDE-MODULATION FREQUENCY OPTIMIZATION FOR HARMONIC MOTION IMAGING (HMI).**

Niloufar Saharkhiz[1], Hermes A. S. Kamimura[1], Md Murad Hossain[1], Elisa E. Konofagou[1,2].*
[1]Columbia University, PS 19-405, 6330 West 168th Street, New York, NY, 10032, USA; [2]Columbia University Medical Center, 161 Fort Washington Avenue, Suite 648, New York, NY, 10032, USA.

Background: Harmonic motion imaging (HMI) assesses tissue viscoelastic properties by generating amplitude-modulated (AM) acoustic radiation force (ARF) within the medium. The amplitude of the induced displacements is inversely proportional to the tissue stiffness. In our previous studies, a low AM frequency (25 Hz) could provide inclusion contrast and characterize tissues using conventional frame rates.

Aims: Investigate to what extent using different AM frequencies in HMI can improve characterization of tissue inhomogeneity and determine whether tailored AM frequency can increase the contrast-to-noise ratio (CNR) for inclusions with different mechanical properties

Methods: *In silico*: The AM-modulated ARF and the resulting HMI displacements were simulated in the K-wave package in MATLAB (Fig. 1(a-b)). First, the ARF was generated by a focused ultrasound (FUS) transducer with a center frequency of 4 MHz. The propagation of the acoustic waves was simulated to compute the spatial distribution of the ARF in 2-D. The force AM frequency was linearly increased from 25 to 150 Hz (2 cycles of each). Then, the elastic wave propagation was simulated to calculate the particle velocities and HMI displacements based on the output of the previous stage. The Young's moduli (E) were 5, 17, 40 and 60 kPa to mimic homogenous acoustic media with different stiffnesses. The speed of the compressional waves was purposely set to 100 ms^{-1} to overcome the computation memory limitations. *In vitro:* The HMI setup consisted of two confocally aligned transducers: a 4-MHz FUS transducer (H-215; Sonic Concepts Inc. Bothell, WA, USA) that generated periodic oscillations at the focal region (f_{AM}: 25, 50 and 100 Hz), and a 2.5-MHz phased array imaging transducer (P4-2; ATL/Philips, Andover, MA, USA) that tracked the induced displacements. A CIRS elasticity phantom with the background Young's modulus of 5 ± 1 kPa and an embedded cylindrical inclusion (diameter 10.4 mm, Young's modulus 60±10 kPa) was used for data acquisition. The transducer assembly was moved in a point-by-point raster scan to image the entire region of interest. At each point, RF frames were acquired using a Verasonics Vantage system at a frame rate of 1000, 2000 and 4000 Hz (40times the AM frequency). The channel data was converted to RF data using delay-and-sum (DAS) beamforming, and the axial displacements were estimated using a 1-D normalized cross-correlation. The CNR was calculated as $|\mu_b - \mu_i|/\sigma b$ where, μ_b and μ_i are the mean displacement of the background and inclusion, respectively and σ_b is the standard deviation of the HMI displacement of the background.

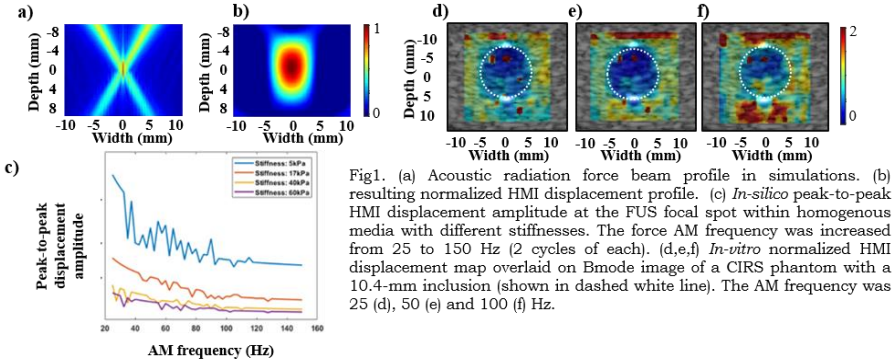

Fig1. (a) Acoustic radiation force beam profile in simulations. (b) resulting normalized HMI displacement profile. (c) *In-silico* peak-to-peak HMI displacement amplitude at the FUS focal spot within homogenous media with different stiffnesses. The force AM frequency was increased from 25 to 150 Hz (2 cycles of each). (d,e,f) *In-vitro* normalized HMI displacement map overlaid on Bmode image of a CIRS phantom with a 10.4-mm inclusion (shown in dashed white line). The AM frequency was 25 (d), 50 (e) and 100 (f) Hz.

Results: *In silico*: The peak-to-peak HMI displacement amplitude decreased with increasing the AM frequency for all the media (Fig1.c). In addition, the maximum difference between HMI displacement amplitudes for soft (5 kPa) and hard (17, 40 and 60 kPa) media was found to occur at lower AM frequencies. *In vitro:* The HMI displacement amplitude decreased by increasing the AM frequency (mean peak-to-peak HMI displacement of 8.5+0.4, 2.6±0.1 and 1.0±0.1 μm for AM frequencies of 25, 50 and 100 Hz, respectively, within the background). However, the 50-Hz AM frequency was found to provide the highest CNR among the other frequencies (21.2 vs. 12.3 and 5.6 for AM frequencies of 25 and 100 Hz) (Fig.1(d-f))

Conclusions: Lower AM frequencies may lead to high inclusion-to-background displacement ratio. However, they may not lead to homogenous displacement maps and, therefore, result in low CNR. Future work will include investigation of the effect of inclusion geometry and viscosity on the AM frequency optimization in order to improve inclusion contrast, using multi-frequency acquisitions.

Acknowledgements: Supported in part by National Institutes of Health (R0ICA228275)

Please Fill Out Both Pages

Conference Evaluation and Questionnaire

OVERALL CONFERENCE

	Poor		Mid		Excellent
Overall Conference Evaluation	1	2	3	4	5
General comments/suggestions:					

SCIENTIFIC PROGRAM

	Poor		Mid		Excellent
Quality of the Presentations	1	2	3	4	5
Relevance of Presentations to the Conference's Theme	1	2	3	4	5
Time Allotted for Presentations	1	2	3	4	5
Time Allotted for Discussion	1	2	3	4	5
Poster Session	1	2	3	4	5
Tutorial	1	2	3	4	5
Student Participation	1	2	3	4	5
Equipment Exhibit	1	2	3	4	5
Additional comments/suggestions:					

CONFERENCE MATERIALS

	Poor		Mid		Excellent
Proceedings Book	1	2	3	4	5
Other Registration Materials	1	2	3	4	5
Additional comments/suggestions:					

CONFERENCE FACILITIES AND SOCIAL PROGRAMME

	Poor		Mid		Excellent
Virtual environment	1	2	3	4	5
Virtual Registration Desk	1	2	3	4	5
Virtual Chat Rooms	1	2	3	4	5
Joining Instructions	1	2	3	4	5
Audio–Visual: Visual material legibility	1	2	3	4	5
Sound audibility	1	2	3	4	5
Presentation transition	1	2	3	4	5
Presentation and session preparation	1	2	3	4	5
Host Internet Connectivity	1	2	3	4	5
Additional comments/suggestions:					

Please Fill Out Both Sides

Conference Evaluation and Questionnaire

CONFERENCE ADMINISTRATION

	Poor		Mid		Excellent
Website	1	2	3	4	5
Registration off–site	1	2	3	4	5
Administrative staff	1	2	3	4	5
Correspondence	1	2	3	4	5
Additional comments/suggestions:					

GENERAL INFORMATION

I am a Returning Delegate	Yes		No
I plan to attend the next conference in 2021	Yes	Perhaps	No
and present a paper(s) / poster(s)	Yes	Perhaps	No
Other(s) from my lab would attend the next conference	Yes	Perhaps	No
and he/she / they would present a paper(s) / poster(s) / tutorial(s)	Yes	Perhaps	No
How did you learn of this conference? (Check all that apply)	☐ Email Announcement		
☐ Internet	☐ Website		
☐ Other	☐ Colleague		
Tutorial Topic Suggestions or Offers for next year:			
Additional Comments/suggestions:			

If you would be willing to host the Conference in your city, please give your name to the Conference Staff.
Questions or comments are welcome at any time at <secretariat@elasticityconference.org>
Thank You!